UNIVERSITÉ DE SHERBROOKE
Faculté de génie
Département de génie mécanique

RÉDUCTION DES PERTES DE CHALEUR PAR CONVECTION AUX PAROIS DE LA CHAMBRE DE COMBUSTION DES MOTEURS À HYDROGÈNE GRÂCE À LA COMBUSTION STRATIFIÉE PAR VORTEX

REDUCED CONVECTIVE COMBUSTION CHAMBER WALL HEAT TRANSFER LOSSES OF HYDROGEN-FUELED ENGINES BY A VORTEX-STRATIFIED COMBUSTION PROCESS

Thèse de doctorat
Spécialité : génie mécanique

David OH

Jury : François CHARRON (rapporteur)
Jean-Sébastien PLANTE (directeur)
Martin BROUILLETTE (co-directeur)
Luc FRÉCHETTE
Roger RIOUX
Mathieu PICARD
Riccardo SCARCELLI

Sherbrooke (Québec) Canada août 2016

Tous les cieux proclament combien Dieu est glorieux, l'étendue céleste publie l'œuvre de ses mains. Un jour en informe un autre, une nuit à l'autre nuit en transmet la connaissance.

- Psaumes 19 : 2-3

RÉSUMÉ

Un procédé de combustion stratifié par vortex est introduit pour les moteurs à combustion interne et permet d'augmenter leur efficacité thermique en réduisant les pertes de chaleur par convection. Cette thèse explique tout d'abord l'état de l'art de cette nouvelle approche. Ensuite, le processus expérimental et les phénomènes au sein d'un moteur optiquement accessible à deux-temps à injection directe d'hydrogène sont étudiés en détails. Il est également présenté les observations des images strioscopiques, les résultats des mesures en zéro-dimension de pression du cylindre et de dégagement de chaleur. Les simulations sont confrontées aux essais expérimentaux pour deux types de configurations de chambre à combustion : la première permet de réaliser un mélange homogène sans mouvement de l'écoulement selon une direction particulière qui représente l'état existant des moteurs à allumage par étincelle, alors que la seconde est l'approche du type stratifié par vortex. Enfin, une étude comparative CFD à deux-dimensions (2-D) en mode transitoire a permis de mettre en évidence un potentiel de réduction d'environ 50% du flux de chaleur convectif de pointe lors de l'utilisation du procédé stratifié par vortex.

Les observations expérimentales et résultats de simulation montrent que la réduction de flux de chaleur lors de l'utilisation du procédé stratifié par vortex est le résultat de la combinaison de deux effets : (1) Le temps du mélange diffusif est plus long que le temps de remplissage d'air pur lorsque l'air est rempli le long de la circonférence de la paroi de la chambre de combustion dû à l'effet Coandă. Il en résulte une stratification de la charge radiale distincte pendant la préparation du mélange lors de la course de compression ; le combustible est donc concentré au centre alors que l'air essentiellement pur est à la périphérie ; (2) Le second phénomène observé est la ségrégation forcée durant le processus de combustion, provoquée par les forces de volume dues à l'accélération gravitationnelle du mélange des gaz avec des densités différentes en rotation rapide. Il n'y a alors pas de combustion en périphérie et la propagation de la flamme se fait vers le centre de la chambre de combustion.

Mots-clés : Moteur à combustion interne, hydrogène, pertes de transfert de chaleur aux parois, écoulement vortex, charge stratifiée, strioscopie.

ABSTRACT

A vortex-stratified combustion process for hydrogen-fueled reciprocating internal combustion engines is introduced to increase the thermal efficiency by reducing the convective heat transfer losses to the surrounding walls during combustion. This dissertation explains the theoretical background of this novel approach. It investigates the process experimentally in a fired, optically accessible, 2-stroke, hydrogen-fueled, direct-injected engine, presenting the schlieren observations, the results of zero-dimensional cylinder pressure indication and apparent heat release measurements comparing two combustion chamber designs – one that actualizes a homogeneous mixture without specific charge motion directionality representing current spark ignited engine practice and another with the here-introduced vortex-stratified approach. Then, a comparative, transient 2-D CFD analysis finds an approximately 50% reduction in the peak convective flux with the vortex-stratified process compared to the reference non-vortex design.

The experimental observations and simulation results show that the reduced heat flux of the vortex-stratified approach is driven by the combination of two effects:

(1) The first is finite-time diffusive mixing getting outpaced by the replenishment of pure air being introduced preferentially along the circumference of the combustion chamber due to the Coandă effect. This results in a distinct radial charge stratification during mixture preparation in the compression stroke with a fuel-concentrated center and essentially pure air at the periphery;

(2) The second effect is the forced-segregation of different density reactants during the course of the combustion process caused by large body forces that result from the gravitational acceleration of the rapidly rotating charge, which inhibit combustion at the periphery and causes the propagating flame to curl away from the walls toward the center.

Keywords: Internal combustion engine, hydrogen, wall heat transfer losses, vortex flow, stratified charge, schlieren.

ACKNOWLEDGMENTS

I would like to thank my doctoral advisor Prof. Jean-Sébastien Plante for all his guidance during the duration of my studies. He has been an intellectually stimulating source of inspiration for ideas, as well as encouragement and motivation when they were much needed. I am glad not only to call him my teacher, research director and advisor, but also my friend. I would also like to thank very much my co-director Prof. Martin Brouillette, who has been a tremendous source of insight and has illuminated new and better paths for my research. I am also grateful to Prof. Luc Fréchette, Roger Rioux, Prof. François Charron, Prof. Mathieu Picard, Prof. Alain Desrochers and Dr. Riccardo Scarcelli who, altogether, have come on board as jurors at various times and guided me faithfully and kindly in the over six-year journey of my doctorate.

A work of this magnitude is not the product of one person or only a few. I sincerely thank the financial patronage of the Centre de technologies avancées (CTA) – Bombardier Recreational Products (BRP) – Université de Sherbrooke and the support of the staff past and present – specifically Jerome Wubbolts, Maxime Desjardins-Goulet, Gilbert LeFrançois, Pascal Ranger, Josiane Simon, Samuel Roy, Jean-Yves Doyon, Marc Viens, Jean-François Vachon, Stéphane Deschênes, Patrick Bisaillon, Sylvain Blanchard, Claude Gagnon and Ghislain Robert.

This dissertation would not have been possible without the Natural Sciences and Engineering Research Council of Canada (NSERC) Collaborative R&D grant 434914-12.

I acknowledge for their help people who over the years have contributed in varied, meaningful ways to this final product: Dr. Thomas Wallner, Dr. Melisa Hatat, Benoit Dupont, Anna Sophie Schmitt, Gabriel Pouliot, Yee Hern Tan, Gary Patterson, Arman Pouragha, Shane Kirksey, Alexandre-Landry Blais, Prof. Emin Isaakhanian, Mihai Rasidescu, Steve Langlais and Gerry DeWit. I would also like to thank my research colleagues at CAMUS and Guifré Julio.

Thanks to Benoit Simard, who inspired and persuaded me to come to pursue my doctorate in Québec at the Université de Sherbrooke – who has been an esteemed colleague and trusted friend – and Dr. Anick Petitpas. Thank you, my colleagues and friends in Sherbrooke for your friendship and support over the years: William and Anna-Lina Bombardier; Garrett Morgan and Heather MacKay; Anthony Bélair and Audrey Campeau.

Thank you, my dear friends at Oasis Christian Centre and the Quebec House of Prayer for your intercession and agape: Prof. Jim and Doreen Benson; Larry, Andrée and Julie Davis; Jonathan and Nathalie Anderson; Brian and Tanya Allatt; Gerald, Mary and Stephen Goddard; Celia Mayne, Prof. Joanne Kingsley, Nicole Schlichter, Nathalie Hostetler, Shelly Mushtaler, and not least Jay and Laura Sims (who have encouraged me to “keep my hands on the plow” to complete this dissertation). I certainly would not have been able to do this without all of you.

Last but certainly not least, thank you, mom, dad and Dennis, who have encouraged me to pursue my dreams to the greatest possible extent and prayerfully endured this journey through many years of living in different countries and continents. Thank you, my “second family” – Ed, Kathie and Paul Lambert – and “grandma” Joan Marshall. I love you all.

TABLE OF CONTENTS

LIST OF FIGURES

LIST OF TABLES

LIST OF SYMBOLS

Symbol	Definition
A	Surface area [m^2]
a_c	Centripetal acceleration [m/s^2]
c	Concentration [$kmol/m^3$]
C_p	Specific heat capacity at constant pressure [$kJ/(kg \cdot K)$]
d	Cylinder bore diameter [m]
D	Diffusive coefficient [m^2/s]
D_T	Turbulent diffusive coefficient [m^2/s]
h	Convective heat transfer coefficient [$W/(m^2 \cdot K)$]
J	Diffusion flux [$kmol/(m^2 \cdot s)$]
k	Conductive heat transfer coefficient [$W/(m \cdot K)$]
k-ε	Turbulence model, with k denoting turbulent kinetic energy [m^2/s^2] and ε denoting turbulent dissipation rate [m^2/s^3]
l	Length scale parameter [m]
l_I	Integral length scale [m]
l_M	Taylor micro length scale [m]
m	Mass [kg]
M	Molar mass [kg/kmol]
M	Moment, or torque [$N \cdot m$]
n	Number of cylinders
n	Polytropic coefficient
Nu	Nusselt number
p	Pressure, or partial pressure [Pa]
P	Power [W] or [kW]
Pr	Prandtl number
r	Radius [m] or [mm]
R	Radius of cylindrical combustion chamber [m] or [mm]
Re	Reynolds number
Re_T	Turbulent Reynolds number [-]
R_G	Universal gas constant [$kJ/(kmol \cdot K)$]
s	Stroke length [m]
S_l	Laminar flame speed [m/s]
T	Temperature [K]
u	Fluctuating component of velocity [m/s]
u'	RMS of turbulent velocity fluctuations [m/s]

u_I	Integral velocity scale [m/s]
U	Velocity [m/s]
$\overline{U}$	Mean velocity [m/s]
v	Velocity [m/s]
V	Volume [m³]
v/v	Volume ratio [-]
x	Mole fraction [-]
γ	Specific heat ratio, or isentropic exponent coefficient [-]
δ	Distance between the wall and the limiting combustible charge or flame extent [m] or [mm]
η	Efficiency [%]
λ	Air-fuel ratio related to stoichiometric [-]
μ	Dynamic viscosity [kg/(m·s)]
ν	Kinematic viscosity [m²/s]
π	Pi (3.14159265…), also purity ratio
ρ	Density [kg/m³]
ϕ	Fuel-air equivalence ratio [-]
ω	Angular velocity [rad/s]

LIST OF ACRONYMS

Acronym	Definition
AHRR	Apparent heat release rate
AMR	Adaptive mesh refinement
BMEP	Brake mean effective pressure
BSFC	Brake specific fuel consumption
BSNOx	Brake specific NOx
BTE	Brake thermal efficiency
CA	Crank angle
CAD	Computer-aided design
CARB	California Air Resources Board
CDI	Capacitive discharge ignition
CFD	Computational fluid dynamics
CFR	Cooperative Fuel Research
CI	Compression ignition
CO	Carbon monoxide
CoV	Coefficient of variance
DI	Direct injection
DNS	Direct Numerical Simulation
DoE	Design of experiments
DR	Delivery ratio
EOC	End of combustion
EOI	End of injection
FPGA	Field-programmable gate array
FPS	Frame per second
GH2	Gaseous hydrogen
H2	Hydrogen gas
H2-DI	Hydrogen direct injection
HC	Hydrocarbons
HCCI	Homogeneous-charge compression ignition
HiL	Hardware-in-the-loop
HPC	High-performance computing
ICE	Internal combustion engine
ICOMIA	International Council of Marine Industry Associations
IDI	Indirect injection
IMEP	Indicated mean effective pressure
IO	Input-output

ISFC	Indicated specific fuel consumption
ISNOx	Indicated specific NOx
ITE	Indicated thermal efficiency
LDA	Laser-Doppler anemometry
LED	Light emitting diode
LES	Large Eddy Simulation
LFL	Lower flammability limit
LIF	Laser-induced fluorescence
LPDI	Low-pressure direct injection
LTC	Low temperature combustion
MBT	Minimum advance for best torque
MFB	Mass fraction burned
NO	Nitrogen monoxide
NOx	Oxides of nitrogen
NTP	Normal temperature and pressure
O2	Oxygen gas
OEM	Original equipment manufacturer
PIV	Particle image velocimetry
PPC	Partially premixed combustion
RANS	Reynolds-averaged Navier-Stokes
RCCI	Reactivity-controlled compression ignition
RoHR	Rate of heat release
RPM	Revolutions per minute
SI	Spark ignition
SOC	Start of combustion
SOI	Start of injection
TDC	Top dead center
WOT	Wide-open throttle

CHAPTER 1 INTRODUCTION

1.1 Context and Motivation

The internal combustion engine has been the ubiquitous energy conversion device for transportation and power generation for over a century, while being simultaneously subjected to continued development. This period has seen many variations of fuels, combustion processes employed, detailed design, manufacturing refinements and the ever increasing use of analog electric and digital electronic systems for sensors, controllers and actuators with ever-increasing complexity. Nevertheless, a state-of-the-art engine placed side-by-side to one of its century-old ancestors will still show distinct commonalities in the basic design.

Driven in part by concerns of climate change, increasingly stringent environmental regulations, as well as dramatic price and supply shocks of primary energy sources, the past five decades have seen the internal combustion engine simultaneously achieve both astonishing reductions in pollutant emissions and improvements in fuel conversion efficiency. Continued regulatory tightening, the serious implications of anthropogenic carbon emissions, declining fossil fuel reserves, as well as the imperative to reduce the emissions of other harmful pollutants, represent existential challenges to the viability of conventional internal combustion engines in applications as diverse and far-reaching in the modern economy and daily life as small household implements like lawn trimmers, motorized scooters, motorcycles, passenger automobiles, buses, trucks, locomotives, ships, electric generators, as well as pipeline oil pumps and gas compressors. Some of these applications are seeing competition from electric propulsion – themselves imperfect solutions due to the present challenges of simply moving primary energy conversion from the point of use to distant, centralized powerplants with their associated pollutants (except renewables), transmission losses, limited local energy storage density and simultaneously higher energy-specific costs.

While no single ideal solution exists, it is clear that continued viability of the internal combustion engine and its sustainable development require holistic approaches that include significant and ongoing efficiency improvements at each step from the primary energy “well”

to the end point of use, as well as diversified primary energy sources that, in the immediate term, need to include a mix of fossil fuels, nuclear and renewables, with a plan fully toward the last as quickly as possible.

1.2 Research Project Definition

Recognizing that, in the best case, only about one-half of the latent chemical energy in the fuel burned in an internal combustion engine is converted to useful work and the rest rejected into the environment as heat, this research project is premised upon the pursuit of improving the efficiency of engines, one along several energy conversion processes mentioned in the previous paragraph from the primary energy well to the end point of use. The literature is replete with diverse methods toward this objective. The present work is borne out of the same goal of efficiency improvement, set in the framework of a specific area of application – namely reciprocating internal combustion engines for recreational vehicles – and specifying hydrogen as the energy carrier. Work that began simply to convert a production-based two-stroke gasoline marine outboard engine to hydrogen fuel operation presented several development challenges, not all of them directly germane to efficiency improvement. Nevertheless, using proven approaches to increasing the efficiency, like raising the compression ratio and employing direct injection, it became apparent that a technological barrier has been reached from being able to extract further efficiency improvements in conventional engine design. Overcoming this barrier would require new solutions to reduce the losses responsible for this diminished efficiency. In a way, the approach taken in this research is in reverse to traditional practice; the conventional method is to find some novel discovery or means to achieve an improved efficiency – such as a new engine architecture or thermodynamic cycle – as a focus and an end in itself. This research considers that there are upper bounds to the efficiency of engines dictated by the laws of thermodynamics and caused by various factors, and comes to a solution by systematically trying to reduce the most important factor causing the diminished efficiency.

1.3 Research Objectives

The objectives of this research are thus:

1. To survey the literature of hydrogen-fueled internal combustion engines, particularly current practices of achieving high thermal efficiency and the challenges of further improving the thermal efficiency thereof;
2. Determine an area of opportunity not found in the literature to improve the efficiency of hydrogen-fueled engines;
3. Conceive and develop a solution based on this new approach to improve the efficiency;
4. Build a working prototype engine that demonstrates this new approach;
5. Quantify and evaluate the efficiency improvement potential represented in this solution.

1.4 Original Contributions

Engine concepts with marketing monikers like “vortex combustion” or “stratified charge” will be shown in the following chapter to be not new. Even the basic premises underlying the work in this dissertation are well documented in the literature, such as combustion under the influence of very high centripetal accelerations within a rotating flow. Experiments have been performed in non engine-related fundamental studies, and variations of confined vortex flows for thermal insulation have been proposed for applications like gas turbines and rockets, but to the extent that is known to date, the idea of a hyperacceleration vortex-stratified combustion process presented in this dissertation is the first to be realized in a reciprocating internal combustion engine, with a functional prototype demonstrating the principle and a comparative numerical analysis performed.

Also to the extent that is known to date, the experimental work covered in this dissertation is the first to perform schlieren imaging on a fired, optically accessible engine at speeds of up to 5000 RPM.

1.5 Organization of this Dissertation

Chapter 2 shall present the underlying technical motivation for this dissertation – that is, improving the efficiency of hydrogen-fueled engines – by way of the first of 3 journal papers, the conclusions of which underscore the importance of wall heat transfer losses and thus form the genesis for the need for the systematic mitigation thereof.

Chapter 3 extends the defined problem statement at the conclusion of Chapter 2; that is, the systematic reduction of wall heat transfer losses, and begins with a thought experiment to illustrate the problem and imagine a solution, which leads to an introduction to the concept of vortex-stratified flows. Pertinent history and fundamentals of internal combustion engine technology – focusing upon the stratified charge variant or that employ some claimed form of a vortex flow in the working process – shall be reviewed. Thereinafter throughout this dissertation, references will be made comparing and contrasting the "vortex" or "vortex-stratified" concept being introduced in this work with a "non-vortex" counterpart, the latter which represents current spark ignition engine practice without any particularly ordered flow motion or mixture stratification.

Chapter 4 shall present the second paper, which reviews the literature that further supports the importance of reducing wall heat transfer losses as the key factor of improving the thermal efficiency of hydrogen-fueled engines. A theoretical framework is presented that forms the scientific basis that underpins the premises and hypotheses of the vortex-stratified combustion process. The results of experimental investigations performed on a fired, optically accessible, 2-stroke, hydrogen-fueled, direct-injected, spark-ignited prototype research engine are also presented. The set-up of the test cell rig will be described, followed by presentation and description of crank angle-resolved schlieren images and results of zero-dimensional measurements of cylinder pressure indication and apparent heat release.

Chapter 5 shall present the third and last paper, which elucidates the fundamentals of convective wall heat transfer losses in the context of the desired objective toward its reduction in a hydrogen-fueled engine. First-order analytical calculations will support the premise of limiting the extent of the flame from reaching the combustion chamber walls and estimate the

theoretical potential reduction of wall heat flux. The results of numerical analyses on geometrically similar CFD models of the combustion chamber designs introduced in Chapter 4 shall then be presented and discussed, illustrating the vortex-stratification of gas species in greater detail than is possible from observation of uncalibrated experimental schlieren images from Chapter 4 alone. The numerical analyses also quantify the total wall surface heat flux between the vortex-stratified and non-vortex homogeneous concepts; the former is found to have a peak value that is about 50% less than the latter counterpart with injection timing and all other model parameters remaining equal.

Chapter 6 shall discuss the results of the preceding chapters, with a focus on their implications on engine efficiency. This shall be followed with a discussion of outlooks for future work.

This dissertation ends with a summary of concluding remarks in Chapter 7.

1.5.1 List of publications

This dissertation is based on the journal articles listed in Table 1.1. They are aimed to be read as chapters inserted in-line as-published or as-submitted for publication within this document to form one unified, coherent work. Each article shall occupy a dedicated chapter and be preceded with an introductory foreword page highlighting the article details and a translation of the abstract in French. The articles are written and submitted to different journals over a period separated over several years. While they are intended to be complementary within the framework of the overall topic of this dissertation, nevertheless they are also required to be able to stand alone individually. Therefore, some tangency and repetition of certain key concepts, figures, tables and references are inevitable. However, these are minimised to the greatest extent possible with the overarching objective to balance the stated needs of each paper to be standalone works yet be part of a coherent dissertation. For the same reason, the literature review is also split among the different chapters where they are most relevant rather than being all consolidated in one place at the beginning of the dissertation as per usual practice.

Table 1.1: List of publications referred-to in this dissertation.

Paper No.	Appears in Chapter	Reference
I	2	Oh, D., Plante, J., "A Highly Efficient Small-Displacement Marine Two-Stroke H2-DI Engine with Low Emissions," ASME. J. Eng. Gas Turbines Power, **135**(8):082001-082001-10, 2013, doi:10.1115/1.4023752.[1]
II	4	Oh, D., Brouillette, M., Plante, J., "Reduced Convective Combustion Chamber Wall Heat Transfer Losses of Hydrogen-Fueled Engines by Vortex-Stratified Combustion – Part 1: Background and Optical Engine Observations," SAE Int. J. Engines, 16JENG-0020, 2016.[2]
III	5	Oh, D., Brouillette, M., Plante, J., "Reduced Convective Combustion Chamber Wall Heat Transfer Losses of Hydrogen-Fueled Engines by Vortex-Stratified Combustion – Part 2: Numerical Analysis," SAE Int. J. Engines, 16JENG-0021, 2016.[3]

[1] Submitted November 19, 2012, revised February 14, 2013, published online June 24, 2013.
[2] Submitted April 14, 2016.
[3] Submitted April 14, 2016.

CHAPTER 2 BACKGROUND

Foreword

Authors and affiliation:

David Oh: Doctoral candidate, Université de Sherbrooke, Faculty of Engineering, Department of Mechanical Engineering.

Jean-Sébastien Plante: Professor, Université de Sherbrooke, Faculty of Engineering, Department of Mechanical Engineering.

Date of acceptance: February 14, 2013

Status of acceptance: Final published version

Journal: ASME Journal of Engineering for Gas Turbines and Power.

Reference:

Oh D., Plante J., "A Highly Efficient Small-Displacement Marine Two-Stroke H2-DI Engine With Low Emissions," ASME. J. Eng. Gas Turbines Power **135**(8):082001-082001-10, 2013, doi:10.1115/1.4023752.

Titre français : Un moteur marin deux-temps à faible déplacement et à injection directe d'hydrogène avec un haut rendement et de faibles émissions.

Contribution to the document:

This article provides a background context for the need to improve of the efficiency of hydrogen-fueled engines. It presents design measures and results of a gasoline two-stroke engine converted to operate with hydrogen. It is found that the thermal efficiency improves with later fuel injection, which infers greater charge stratification. However, an upper limit of efficiency is reached on existing technology; the article concludes with identifying from the literature that wall-heat transfer losses is the predominant factor that limits the achievable thermal efficiency, and that further improvement will require novel approaches at reducing these losses. Therefore, the systematic mitigation thereof – employing experimental optical observation and CFD analysis – by imposing designed regimes of charge- and flow motion stratification in the combustion chamber for reduced thermal convection is the subject of further work and are respectively covered in separate articles in subsequent chapters.

Résumé français :

Un moteur deux temps à hydrogène de 9,9 CV (7,4 kW) basé sur un moteur marin hors-bords fabriqué en série est présenté. Bien que la puissance nominale du moteur à hydrogène corresponde à celle de l'original, un meilleur rendement thermique indiqué de 42,4% est atteint selon le mode opérationnel d'ICOMIA Mode 4, correspondant respectivement à 80% et 71,6% de la vitesse et du couple nominale. L'efficacité thermique au frein à la puissance nominale est 32,3%. Les mesures sur les gaz d'échappement suggèrent que le moteur pourrait répondre aux exigences les plus strictes de « CARB 5-Star » pour moteurs marins à allumage par étincelle, qui limitent les émissions de HC+NOx a 2,5 g/kWh et ceux sans aucun post-traitement. Les essais ont été réalisés sur un moteur 2 temps avec un système à injection directe d'hydrogène gazeux de basse pression et sans l'utilisation de pompe d'alimentation additionnelle. Ces pièces de ce système sont adaptées de composants fabriqués en série.

Par la suite, il a été déterminé qu'une injection tardive d'hydrogène peut améliorer l'efficacité thermique du moteur mais provoque une augmentation des émissions de NOx ; et lorsque poussée à l'extrême, augmente alors la variation de travail par cycle aussi. Il apparait donc des liens reliant la durée de combustion, la concentration en NOx et la variation d'IMEP dues à une augmentation de la stratification de la charge lorsque l'injection est retardée. Plusieurs stratégies d'alimentation en carburant, des simulations par GT-POWER, d'alimentation d'huile, les problèmes liés à la lubrification lors de l'utilisation de l'hydrogène et enfin des essais de calibration sont présentés. Par la suite suivent des essais sur les performances dynamométriques en état stationnaire, des mesures de pression dans les cylindres, des mesures de NOx et des analyses de dégagement de chaleur. Tous ces résultats valident le fait qu'une injection tardive du combustible et une charge stratifiée implique de faire un compris entre des rendements élevés et des émissions de NOx.

2.1 Abstract

A hydrogen-fueled two-stroke prototype demonstrator based on a 9.9 horsepower (7.4 kW) production gasoline marine outboard is presented, which, while matching the original engine's rated power output on hydrogen, achieves a best-point gross indicated thermal efficiency (ITE) of 42.4% at the ICOMIA Mode 4 operating point corresponding to 80% and 71.6% of rated engine speed and torque, respectively. Brake thermal efficiency (BTE) at rated power is 32.3%. Preliminary exhaust gas measurements suggest that the engine could also meet the most stringent CARB 5-Star marine spark-ignition emission standards limiting HC+NOx emissions to 2.5 g/kWh without any after-treatment. These are realized in a cost-effective concept around a proven two-stroke base engine and a low-pressure, direct-injected gaseous hydrogen (LPDI GH_2) system, which employs no additional fuel pump and is adapted uniquely from volume production components.

Later fuel injection is found to improve the thermal efficiency at the expense of increased NOx emissions and, at the extreme, increased cyclic variation. These observations are hypothesized and supported by phenomenological inferences of observed trends of combustion duration, NOx concentration and IMEP variance to be due to increasing charge stratification with the later timings. This work outlines the pathway – including investigations of several fuel delivery strategies with limited success – leading to the current status including design; modeling with GT-POWER; delivery of lube oil; lubrication issues using hydrogen; and calibration sweeps. Experimental results comprising steady-state dynamometer performance, cylinder pressure traces, NOx emission measurements, as well as heat release analyses, support the reported numbers and the key finding that late fuel injection timing and charge stratification drive the high efficiencies and the NOx trade-off; this is discussed and forms the basis for future work.

2.2 Introduction

The two-stroke gasoline engine has been a mainstay for small recreational vehicle- and motorcycle applications for nearly a century due to its high power density and – by virtue of the lack of a valvetrain and pressurized gallery lubrication system – mechanical simplicity, lightweight and low manufacturing cost compared to four-stroke counterparts. The mass-

specific power density is furthermore greater since two-strokes have twice as many combustion events per crankshaft revolution. However, it has been blighted by very high unburned hydrocarbon (HC) emissions that, as a result of ever more stringent regulations, have caused it to be almost entirely forced out of the market in favor of four-stroke engines. This is due to raw, externally premixed fresh charge comprising air, fuel and lube oil being short-circuited into the exhaust during the scavenging process. The lost available energy also results in poor off-design point fuel efficiency. Both problems are addressed in part with gasoline direct injection, but are only decisively eliminated (apart from trace emissions from the lube oil) using hydrogen as the energy carrier.

Using hydrogen in internal combustion engines predates even Diesel (1892), Akroyd-Stuart (1890), Otto (1876) and Beau de Rochas (1862), with the work of Rivaz dating to 1807 [1]. Research into hydrogen two-stroke engines was a topic of great interest in the 1970s, notably with the extensive work by Furuhama and collaborators [2, 3, 4]. The premise of this combination of technologies was clear: the already-recognized high HC emissions of the two-stroke engine would be substantially reduced, while the banes of hydrogen-fueling – namely knocking tendency, high NOx emissions with rich and/or stratified charge strategies and low power density – would be respectively addressed by the combination of lower mean effective pressure for a given power output, inherent internal residual gas content and more frequent power strokes. However, as on-road emissions regulations tightened globally and meeting them with conventionally fueled two-stroke engines became too onerous for all but small recreational vehicles and large railroad-, genset- and marine Diesels, research activity in hydrogen-fueled variants in tandem waned beyond the mid-1980s. Therefore, the literature on the subject has been very scant ever since, as the trend has moved toward four-strokes and advanced by several research groups, among them [5, 6, 7, 8] and even achieving limited volume production by major OEMs [9, 10]. The progresses made on four-stroke hydrogen-fueled engines, with heretofore unavailable modern fuel systems in volume production quantities, inspired reinvestigating the two-stroke H2 concept as a mid-term production-viable solution for a clean, efficient propulsion unit for recreational marine applications with modest power requirements.

The motivations for targeting this segment are manifold. For one, the CARB-established limit of HC+NOx emissions in the 7.4 kW rated power class represents a 92% reduction in the current Tier 4 (4 Star) regulations from Tier 1, from 67 to 5 g/kWh. A presently voluntary 5 Star designation would further halve that limit to 2.5 g/kWh. This has forced almost all two-stroke gasoline marine outboards out of the market. Even with the move to four-stroke engines, additional complexity will be necessary – possibly exhaust after-treatment – in order to fully meet the regulations. This will incur significant extra costs that are proportionally highest yet least tolerable in the lowest power rating segments. The second motivation is a purely pragmatic one, since a modest output powerplant will also have concomitantly modest needs for hydrogen storage to achieve a targeted range between refueling – here defined as 2 hours on the ICOMIA duty cycle, which is shown in Table 2.1 [11].

Table 2.1: ICOMIA marine test cycle.

Mode	Engine Speed*	Brake Torque*	Normalized Time Factor
1	Idle	0	0.4
2	0.4	0.253	0.25
3	0.6	0.465	0.15
4	0.8	0.716	0.14
5	1	1	0.06

* As a fraction of engine rating

Furthermore, in many jurisdictions, boats with outboard engines below 10 HP (7.46 kW) are exempt from vessel registration and operator licensing [12], thereby removing one regulatory barrier for the market introduction of a novel alternative-fuel powerplant.

The constraints of cost, space and weight for hydrogen storage in a low-power watercraft underscore the imperative of maximizing fuel efficiency through engine-side measures. This paper outlines the design evolution, numerical modeling, experimental investigations including test bench calibration work and their results, which demonstrate gross ITE exceeding 42%. This is a significant achievement given the very small engine swept displacement (123 cm^3 per cylinder) and the adapted low-cost, volume-production components employed for the H_2 LPDI

system. Measurement data show that the key enabler for the high attained efficiencies is late fuel injection forming a stratified charge. In spite of the trade-off of increased NOx emissions, it is foreseeable that the most stringent emissions regulations can still be respected.

2.3 Design

The base engine is a series-production 2009 model year two-stroke carbureted gasoline marine outboard with 9.9 HP rating, the basic geometrical specifications of which are listed in Table 2.2. The original magneto capacitive-discharge ignition (CDI) system is replaced with an inductive-type with both mapped and test bench-adjustable spark timing. In preparation for hydrogen fueling, cold spark plugs, NGK CR10E, are employed in place of OEM-specified ones.

Table 2.2 : Base engine specifications

No. of cylinders and layout	2 inline, 180° crankshaft
Bore x stroke (displacement)	56 x 50 mm (246 cm^3)
Connecting rod length	90 mm
Compression ratio	6.8:1 (trapped)
Scavenging type	Crankcase
Porting arrangement	Loop, Schnuerle
Lubrication type	Fuel-oil premix, 100:1 v/v
Induction	Carburetor, reed valves
Port height (transfer/exhaust)*	41/33 mm

* Measured from piston TDC position

Initial investigations employ gas injectors from Hoerbiger GmbH nominally operating at 5 bar gravimetric pressure. These are mounted on a gas rail attached to the engine block that communicates with one of two transfer ports per cylinder in a “semi-direct injection” scheme. Hydrogen is first injected into the transfer ports and then admitted into the cylinders once the ports are uncovered. The orientation of the injectors allows the spray jets to have a straight line-of-sight path through the open transfer port angled upwards toward the combustion chamber of

each cylinder, thus avoiding direct fuel short-circuiting into the exhaust. The carburetor is retained for functional compatibility of the reed valve block and to give the same restriction characteristics of the original engine, but the throttle angle can be independently manipulated from the test bench. Investigations are also done employing the same injector type upstream of the carburetor to achieve external mixture preparation or indirect injection. The cylinder head is modified to accept transducers for pressure indication measurements.

However, tests of both semi-direct and indirect injection prove unsatisfactory. Despite sweeps of injection- and ignition timings as well as throttle angles, baseline power output cannot be achieved, being hampered by abnormal combustion events such as knocking, pre-ignition and backfiring; these are made worse with increasing engine load. As a result, indirect- and semi-direct injection strategies are abandoned and the focus directed upon a cost-effective direct-injection system.

The important boundary conditions of low system cost and production viability preclude exotic hydrogen storage and one-off fuel delivery solutions. Compressed gaseous hydrogen at 350 bar is thusly the chosen technology to the exclusion of others. Medium- and high-pressure (50-300 bar) injection systems are also similarly rejected. A search for available hydrogen direct injectors found nothing in volume-production. Based on work by Caley and Cathcart (2006) to adapt injectors from an air-assisted DI gasoline system to natural gas fueling [13], injectors manufactured by Synerject used in a volume-production recreational watercraft are adapted for hydrogen in this current work. The outward-opening, poppet-valve, solenoid-actuated gas injectors are originally specified for 5.5 bar gravimetric supply pressure. The large pressure difference between the tank and at the injectors dispenses with the need for a separate pump; only a pressure-regulating system and fuel rail are needed. This reduces the fuel system cost and simplifies the overall package for the spatial constraints within the envelope of an outboard engine and in the boat.

Incorporating hydrogen direct injection (H2-DI), as well as the objective to maximize thermal efficiency, necessitates a new cylinder head yielding an increased compression ratio. The chosen geometry is a hemispherical bowl-in-head that is offset away from the exhaust ports

with approximately central vertical positioning of the injectors and closely located sparkplugs. Generous squish promotes charge turbulence near TDC for rapid mixing and short combustion duration; the latter defined by the 10-90% mass fraction burned (MFB). The geometric compression ratio is variable from 12 to 14.5:1 using metal head gaskets of varying thicknesses. The remaining components of the engine – pistons, porting and crankcase, bearings, exhaust, etc. – are carried over from production.

2.4 Lubrication

The original engine employs total-loss premixed gasoline and oil at a 100:1 volume ratio as the means of lubrication. Without liquid fuel being used, lubrication is supplied via an external reservoir and a 12V electric diaphragm pump. Drillings are made into the crankcase through which oil is conveyed at pulsed intervals and distributed by scavenge air motion and moving components. With the oil volume per pulse as given, the frequency is calculated to supply the desired quantity rate and stored in a map as a function of engine load and speed. The total quantity of supplied lube oil is kept in the same order as the original engine on an equal g/kWh basis based on the known fuel-oil ratio and estimates of the baseline gasoline specific fuel consumption.

An off-the-shelf, synthetic-blend, TCW3-rated two-stroke engine oil proves unsatisfactory operating after a short order with hydrogen fuel, as observations of the crankcase and cylinder reveal severe sludge and varnish formation. As Figure 2.1 shows, the sludge manifests differently in separate parts of the engine; accumulations on the piston crown and combustion chamber are a deep black color with a consistency of pitch, suggesting carbonizing oxidation of the lube oil, while in the crankcase and ports are a foamy, white, substance indicative of aqueous emulsion and/or hydrogenation with some component of the base oil or additive package. Hard varnish and rust also form on the cylinder liner and piston ring pack, eventually causing noticeably increased resistance to crank the engine and greater measured difference between indicated- and brake mean effective pressures due to friction. Prolonged running time under these conditions result in scuffing of the liner; increasing lube oil rates and adjusting the regulated engine-out coolant temperature do not alleviate the problem but exacerbate sludge formation.

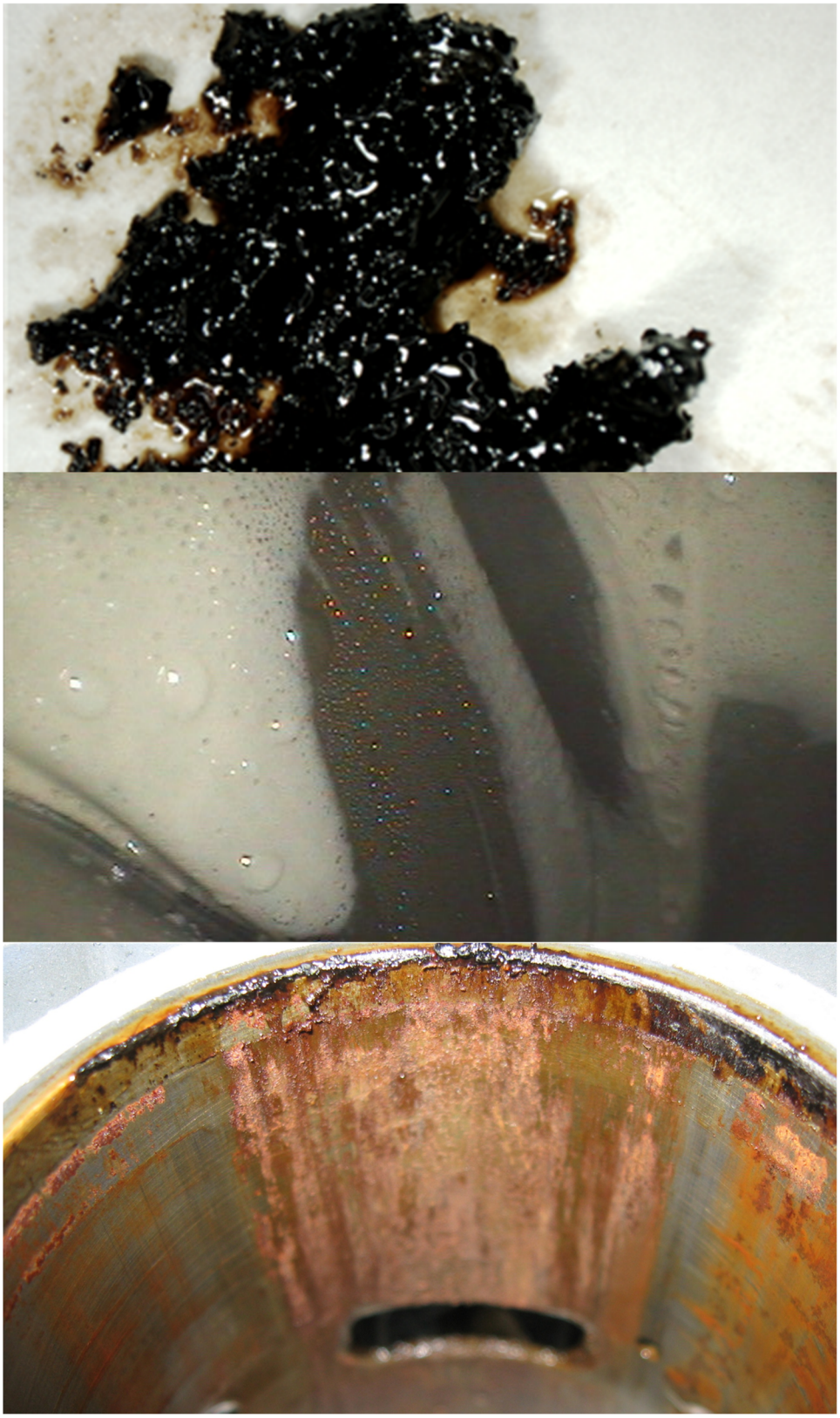

Figure 2.1: Top - black sludge collected from cylinder head; middle – white foamy sludge in crankcase; bottom - varnish and rust formation on cylinder liner.

The solution to this problem is found by testing lube oil samples with known, controlled base stock types and eliminating the variables of the additive package and reaction potentials with hydrogen or its byproducts. It is hypothesized that hydrogenation and varnish formation are minimized with a base stock that contains minimal unsaturated bonds. As a result, unadditized Group III (severely hydro-processed) oil is used. With this lubricant, all formation of varnish and sludge throughout the engine cease and despite the lack of an additive package, even after accumulating hundreds of hours of operation, no bearings or other engine components have failed, exhibited accelerated wear or shown increased deposit formation. As a torture test, lube oil injection rates are further reduced by between 25-50% below the equivalent 100:1 gasoline/oil mixture with no ill effects, supporting the findings of Ambler and Zocchi (2001) in a 50cc two-stroke engine with direct gasoline injection converted from premixed lubrication to oil injection [14].

Because lube oil is transported by the scavenge charge in a total-loss scheme, minimizing the consumption rate is important from the standpoint of reducing exhaust HC emissions; while burning hydrogen in itself produces no HC, the combined HC+NOx emissions are limited by regulation. More critically, engine oil vapors carried in suspension with the charge air ignite and give rise to carbonaceous hotspots that exacerbate abnormal combustion with hydrogen.

2.5 Numerical Modeling

A simulation model is done using GT-POWER to correlate predicted engine performance and efficiency with the results of the experimental work, as shown in Figure 2.2. This is to fulfill the objective of using the validated model to evaluate the effects of future changes to the porting design and combustion process on engine performance and efficiency. To this end, two important parameters are the relationship of delivery- and purity ratios for two-stroke engine scavenging detailed by Blair (1999) [15] and the apparent heat release rate (AHRR).

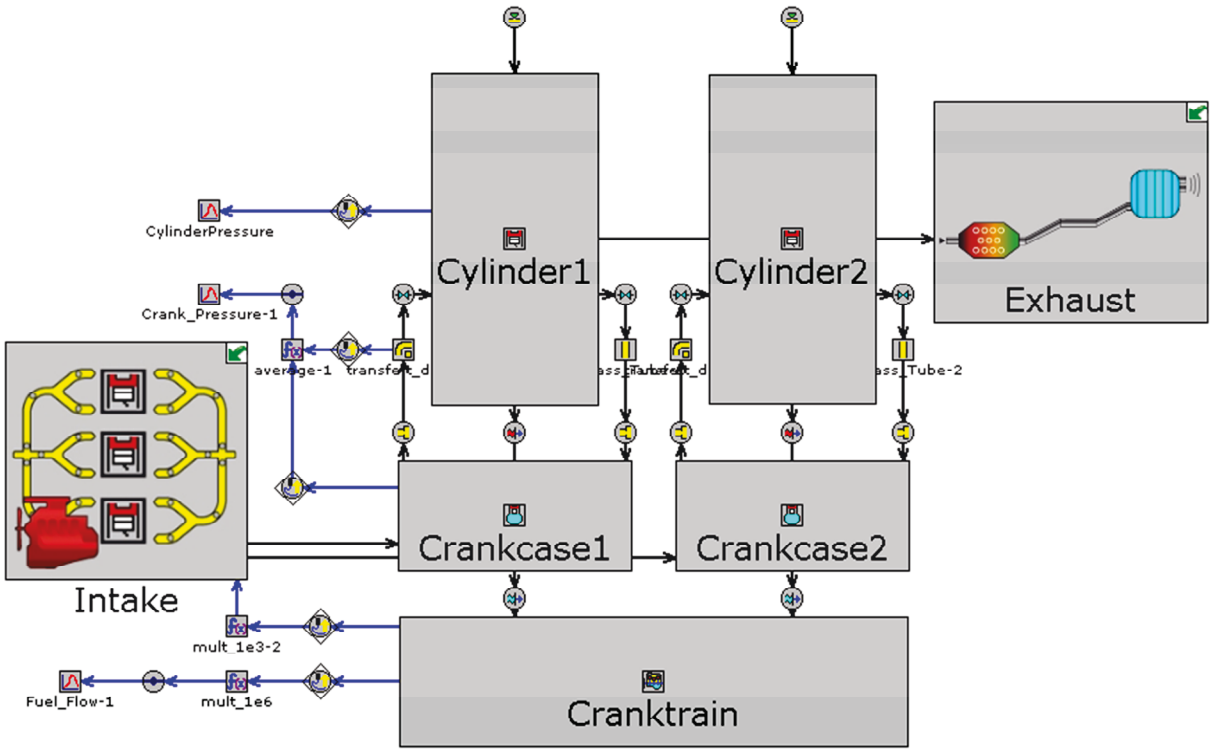

Figure 2.2: GT-POWER model map.

The delivery ratio, DR, is defined as the total air mass supplied to the engine, m_{total}, divided by the reference mass, m_{ref}, required to fill the cylinder swept volume, V_{swept} under prevailing atmospheric density, ρ_{atm}. It can be determined experimentally through the measured total air mass flow rate, $\dot{m}_{total}$, by:

$$DR = \frac{\dot{m}_{total}}{m_{ref}}\left(\frac{60}{RPM}\right), \text{ where} \tag{2.1}$$

$$m_{ref} = \rho_{atm} V_{swept} \tag{2.2}$$

The purity of the trapped charge, π, is defined as the mass ratio of the air trapped in the cylinder before combustion, m_{ta}, to the total mass of the cylinder charge, m_{tr}, the latter of which is composed of the sum of the masses of the fresh trapped charge, m_{tas}, exhaust gas, m_{ex}, and any air remaining unburned from the previous cycle, m_{ar}:

$$\pi = \frac{m_{ta}}{m_{tr}}, \text{ where} \tag{2.3}$$

$$m_{ta} = m_{tas} + m_{ar} \tag{2.4}$$

$$m_{tr} = m_{tas} + m_{ex} + m_{ar} \tag{2.5}$$

Experimental determination of the charge purity is difficult since the actual in-cylinder gas compositions, particularly the residual burned exhaust gas and unreacted air from the previous cycle are needed; these cannot be inductively determined from external measurements, but require direct in-cylinder fast gas sampling or optical methods that are beyond the scope of this work. However, the literature from Blair (1999) [15] and Heywood and Sher (1999) [16] show that large numbers of investigated two-stroke engines in a wide displacement range tend to have characteristics that cluster within scatterbands as sketched qualitatively in Figure 2.3 generally between the envelopes of the perfect mixing and perfect displacement models, according to the scavenging- and porting strategies employed, whether they be crankcase- or blower scavenged; use reed-, rotary-, piston- or poppet valving; and uniflow-, cross-, loop- or other design.

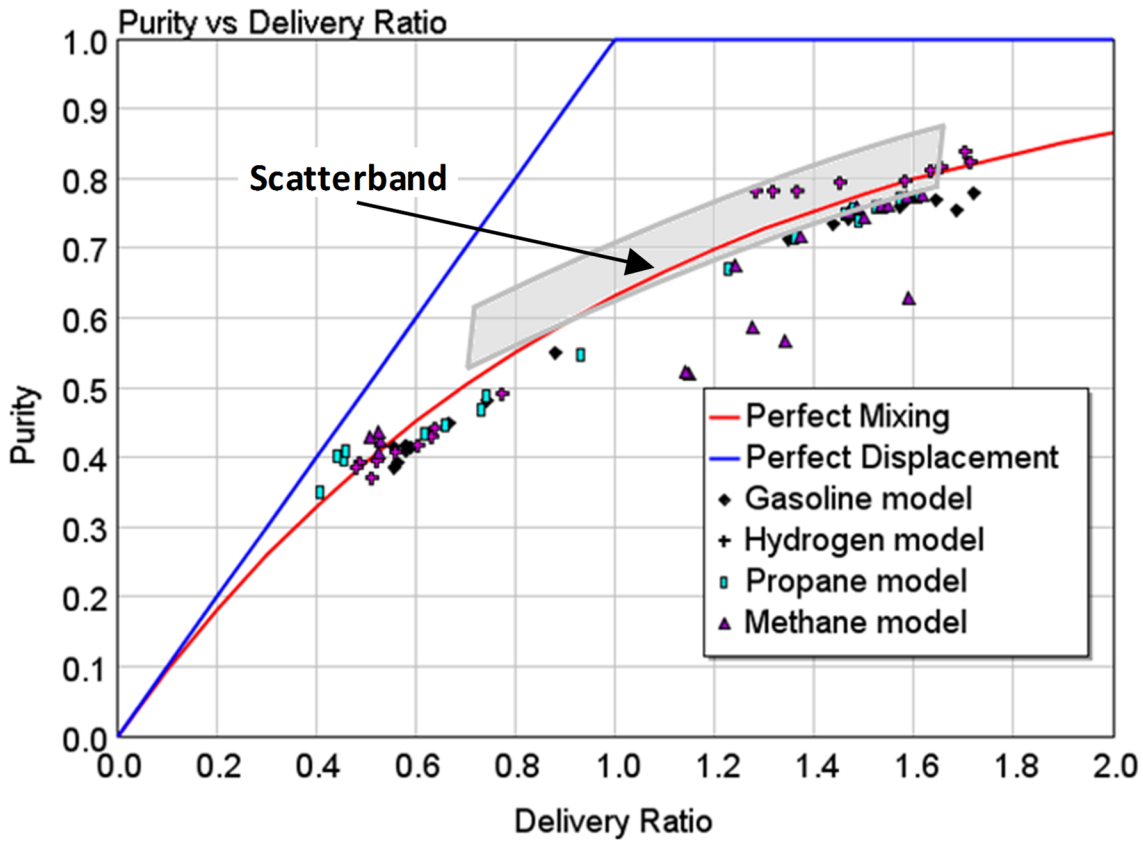

Figure 2.3: Purity and delivery ratios with scatterband sketched.

The delivery ratio and charge purity are thus determined in the GT-POWER model using a 1-D gas flow model with the geometrical properties, port cross-sectional areas and fuel used

of the actual engine. Parameters such as the imposed forward- and reverse port flow coefficients and purity are defined in arrays and adjusted using design of experiments (DoE) to within plausible scatterband ranges of values found in the aforementioned literature that give agreement on the measured air mass flow rate, IMEP, as well as pressure indications in-cylinder and in both the transfer- and exhaust ports.

For the operating point corresponding to rated power conditions at 4500 RPM, the pressure trace of the GT-POWER model is compared against experimental results in Figure 2.4.

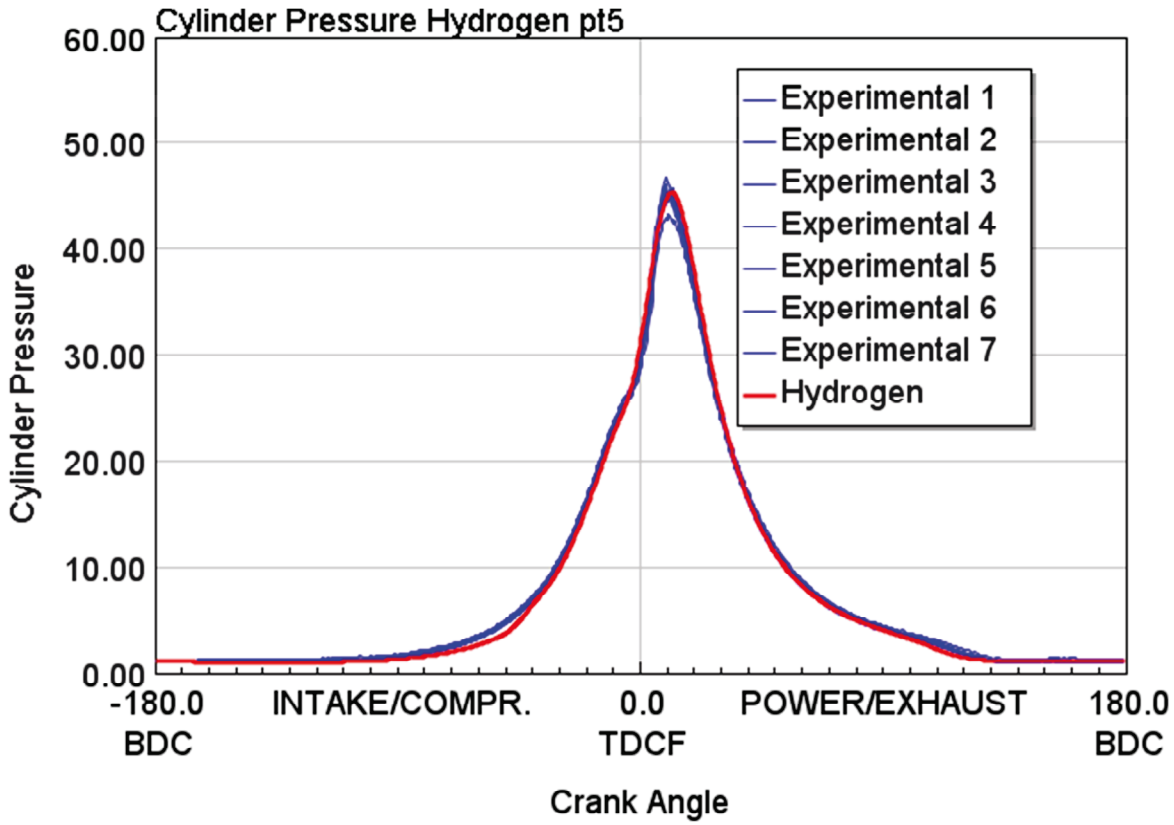

Figure 2.4: Comparison of simulation and experimental cylinder pressure traces.

The AHRR is extracted from cylinder pressure indication data derived from the First Law of Thermodynamics and curve-fit to the so-called Wiebe or Vibe function after I. I. Vibe (1956) [17], the parameters of which include combustion start, θ_{SOC}, delay, $\Delta\theta_d$, and duration, $\Delta\theta_b$:

$$dQ = \frac{\gamma}{\gamma-1} p dV \frac{1}{\gamma-1} V dp \tag{2.6}$$

$$MBF\ (\theta) = 1 - e^{-a\left(\frac{\theta-\theta_{SOC}}{\Delta\theta}\right)^{m+1}} \tag{2.7}$$

$$m = \frac{ln\left(\frac{ln(1-0.1)}{ln(1-0.9)}\right)}{ln(\Delta\theta_d) - ln(\Delta\theta_d + \Delta\theta_b)} - 1 \tag{2.8}$$

$$a = -ln(1-0.1)\left(\frac{\Delta\theta}{\Delta\theta_d}\right)^{m+1} \tag{2.9}$$

$$\Delta\theta \approx 2\theta_d + \theta_b \tag{2.10}$$

$$\Delta\theta_d \equiv 0 - 10\%\, MFB \tag{2.11}$$

$$\Delta\theta_b \equiv 10 - 90\%\, MFB \tag{2.12}$$

In addition to the aforementioned combustion start, delay and duration, another important parameter for the heat release is the center of combustion (50% MFB). Since the heat release curve is normalized rather than absolute, it reaches an ultimate value of unity and gives no information about the actual total quantity of released energy. A second-law analysis, beyond the scope of the present work, can quantify absolute energy release on the ordinate and also split sources of exergy losses in the cycle due to, for example, wall-heat transfer, incomplete combustion, non-ideal heat release and leakage.

The heat release curves are plotted in real-time by the cylinder pressure indication system described in the following chapter. These curves can then be approximated as Vibe functions described by parameters calculated from the measured values such as combustion start, delay and duration.

The specific fuel consumption and thermal efficiencies are calculated by the relationship of the measured fuel mass flow rate, $\dot{m}_F$, lower heating value, Q_{LHV}, and engine power, P, substituting and throughout each equation consistently using indicated- or brake values (here denoted with the indices I and B, respectively) where appropriate. Integration of the in-cylinder pressure acting on the displaced volume over the cycle gives the analogous gross IMEP (neglecting pumping work in the lower crankcase), with the relationship to indicated power, $P_{(I),gross}$, in a two-stroke engine given as:

$$P_{(I),gross} = I\,MEP\left(\frac{RPM}{60}\right)\pi\left(\frac{d}{2}\right)^2 s\,n \tag{2.13}$$

where d denotes bore diameter, s is the stroke and n is the number of cylinders. The brake power can be calculated by substituting the BMEP (where known) in place of the IMEP using Equation 2.13 above, or from the brake torque, M, measured at the dynamometer from:

$$P_{(B)} = \left(\frac{RPM}{60}\right)2\pi M \tag{2.14}$$

The brake- or indicated thermal efficiencies, $\eta_{th,(B)/(I)}$, or written respectively as BTE or ITE elsewhere, are given by:

$$\eta_{th,(B)/(I)} = \frac{P_{(B)/(I)}}{\dot{m}_F Q_{LHV}} \tag{2.15}$$

and the specific fuel consumptions are related to the thermal efficiencies by:

$$(B)/(I)SFC = \frac{1}{\eta_{th,(B)/(I)} Q_{LHV}} \tag{2.16}$$

In all calculations and for the determination of gasoline energy-equivalent specific fuel consumptions, the lower heating values are taken to be 43 MJ/kg for gasoline and 120 MJ/kg for hydrogen.

2.6 Experimental Setup

The engine control system is realized in Simulink® for the software and actuated using Opal-RT for the hardware-in-the-loop (HiL) platform. The system controls ignition- and injection timing events, lube oil injection rate and throttle opening, synchronized to crank position with an AVL crank angle calculator (CAC). Fuel- and air mass flow measurements are by Micro Motion (coriolis type) and SuperFlow sensors, respectively. A Borghi-Saveri eddy-current dynamometer is employed and the test cell uses the entire outboard mounted in a water tank to simulate realistic operating conditions (since the exhaust backpressure is affected by the exhaust pipe being partially submerged under water). The propeller is replaced with a mechanical connection to the dynamometer. Cylinder pressure measurement is accomplished with the AVL Indicom/Indismart suite. Exhaust gas measurements employ a Horiba MEXA-720NOx. The D2T Morphee2 system is used for test bench controls and data acquisition.

Experimental measurements are conducted both by sweeping across engine loads at various constant RPMs and at the five discrete operating points defined by the ICOMIA cycle.

2.7 Results

Figure 2.5 shows the ITE in sweeps of engine load and speed in the baseline hardware and calibration trim at MBT spark timings. The plots are characterized by high efficiency over broad ranges of load at each investigated engine speed. Indicated efficiencies tend to rise with engine speed, that is, mean piston speed, due to decreasing importance of heat transfer per cycle [18]. The exception is at 5000 RPM, where the short cycle period (12 ms), requires relatively longer injection pulse widths in crank angle degrees to supply the necessary fuel flow and thus force earlier SOI (start of injection) timings, which will be shown to have deleterious effects on efficiency. As previously stated, however, more relevant to marine applications is the ICOMIA duty cycle involving discrete loads and speeds corresponding to points along the propeller law curve. Therefore, the results going forward will be presented at specific ICOMIA operating modes.

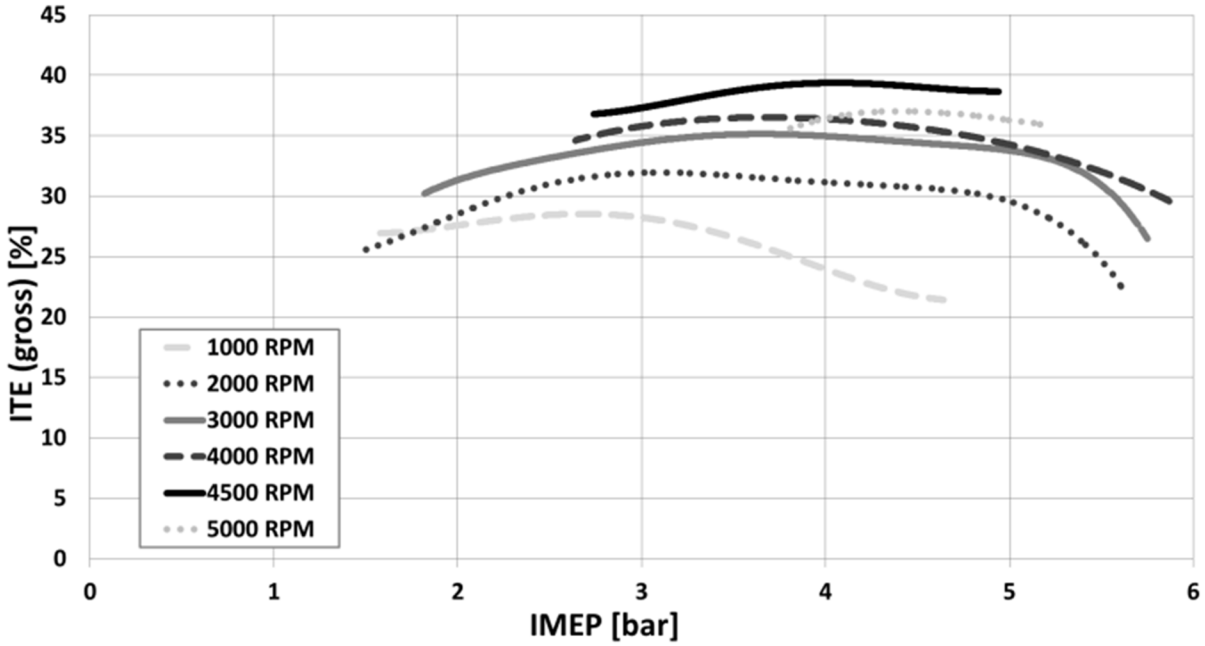

Figure 2.5: Indicated thermal efficiency vs. indicated mean effective pressure (MBT spark timings).

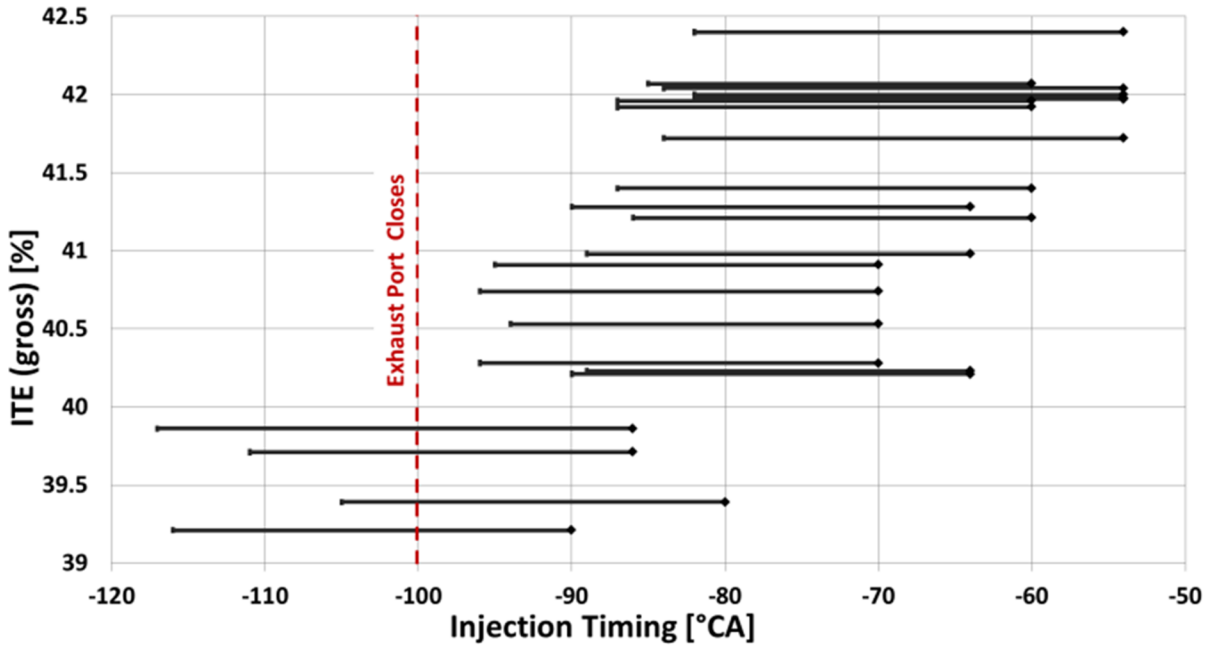

Figure 2.6: Effect of injection timing on indicated thermal efficiency, constant gas mass flow, ICOMIA mode 4, MBT ignition timing.

A key enabler for high ITE is observed to be late injection timing as Figure 2.6 shows. It can be clearly understood that one effect of early injection in two-stroke engines on ITE is implicated by fuel lost to the exhaust while that port is open. A different explanation, however, is required in the observed trend of increasing ITE with even later injection where short-circuiting due to open exhaust ports play no role. The hypothesis is that later injection increases charge stratification at constant bulk trapped air-fuel ratios. This stratification leads to locally richer mixture zones than the prevailing mean. It is further hypothesized that this stratification increases the overall rate of heat release (RoHR) due to increasing laminar flame velocity from lean conditions toward the vicinity of stoichiometric as shown by White et al. (2006) [19].

Furthermore, these locally rich zones would result in higher flame temperatures. Therefore, the stratification hypothesis via these phenomena can be inferred by examining the combustion duration and engine-out NOx emissions, the latter since thermal NOx formation is well-understood via the Zeldovich mechanism to be a strong function of temperature:

$$N_2 + O \rightarrow NO + N \quad (2.17)$$

$$N + O_2 \rightarrow NO + O \quad (2.18)$$

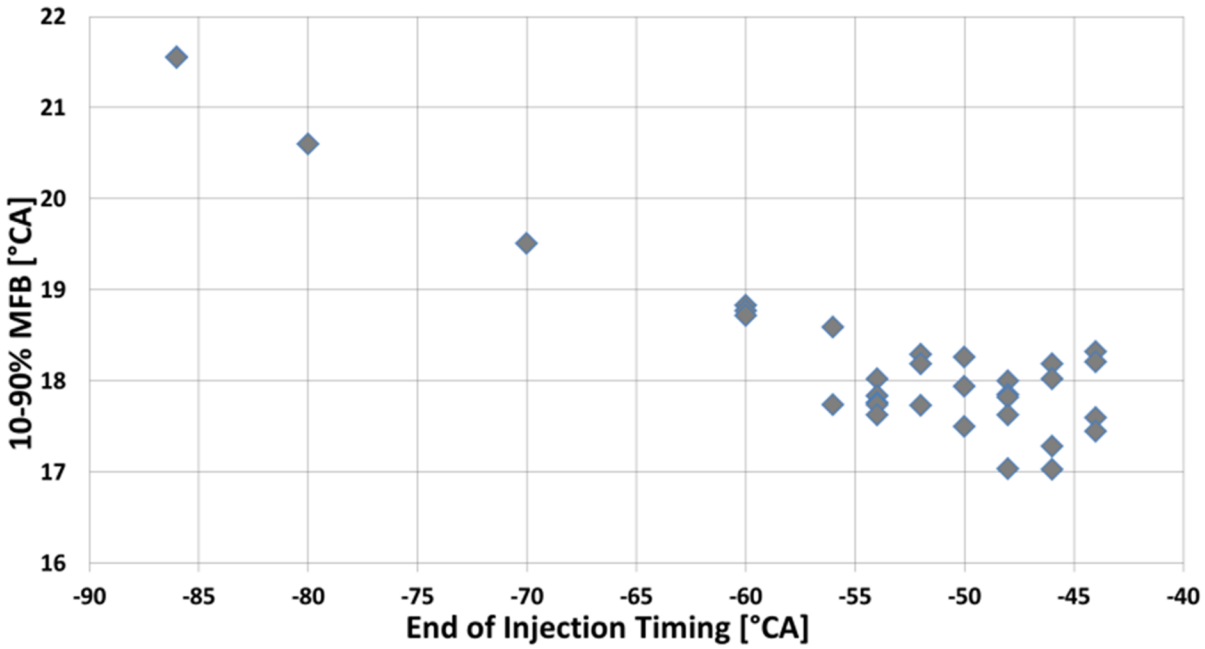

Figure 2.7: Effect of end-of-injection timing on burn duration at ICOMIA Mode 4, MBT ignition timing.

Increased stratification, i.e., higher occurrence of fuel-rich mixture zones, should be manifest through more rapid heat release and higher NOx emissions at constant engine load/speed points compared to a homogeneous mixture at the same overall trapped fuel-air equivalence ratio. Faster heat release raises the ITE because the thermodynamic cycle approaches a constant volume heat addition process that is optimal for a fixed given geometric compression ratio; however, this would be tempered with diminishing returns by increased thermal losses. Verhelst and Wallner (2009) show that wall heat transfer is the dominant source of efficiency loss in an $H_{2\text{-}D}I$ single-cylinder research engine and nearly twice than that operating on gasoline at the same loads and speed [8].

Figure 2.7 shows that burn duration indeed declines with later injection, suggesting a correlation of later injection, i.e. greater charge stratification, with more rapid combustion rates. Figure 2.8 confirms that NOx emissions also increase with later injection, in agreement with prediction. These therefore affirm the hypothesis of the effects of increased charge stratification on the RoHR, NOx emissions and ITE.

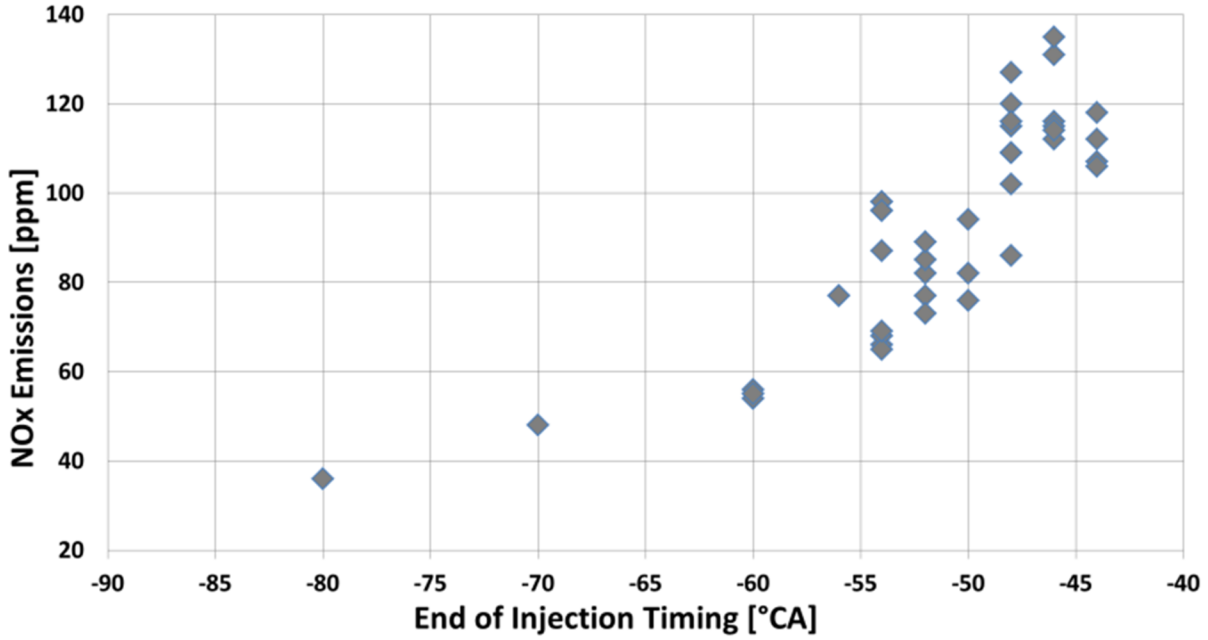

Figure 2.8: Effect of end-of-injection timing on NOx concentration at ICOMIA Mode 4, MBT ignition timing.

Further adjustment toward very late injection timings result in increasing combustion instability (CoV of IMEP), as shown in Figure 2.9. This can also be explained through the stratification hypothesis since, just as richer-than-mean mixture zones are being set-up with later injection, leaner zones also form elsewhere as a consequence. While hydrogen possesses the unique properties of being able to ignite with very low ignition energies and lean mixtures, both do not manifest simultaneously. White et al. (2006) show that minimum ignition energies range almost two orders of magnitude between the lean and rich ignition limits and, at very lean relative air fuel ratios, exceeds that of methane-air and heptane-air mixtures close to their respective stoichiometric values [19]. The cycle-to-cycle spatial volume fractions and the stochastic nature of the location distributions of these stratified zones in the combustion chamber, particularly in relation to the sparkplug at the time of ignition, determine the robustness of flame kernel formation and, in interaction with in-cylinder charge motion and turbulence, the cyclic time rate of flame front propagation through the charge and combustion stability as a result. It can also be reasoned that the proximity of rich zones relative to the combustion chamber walls will have a significant effect on heat transfer, even more so given the small quenching distance of hydrogen flames compared to that of hydrocarbon fuels.

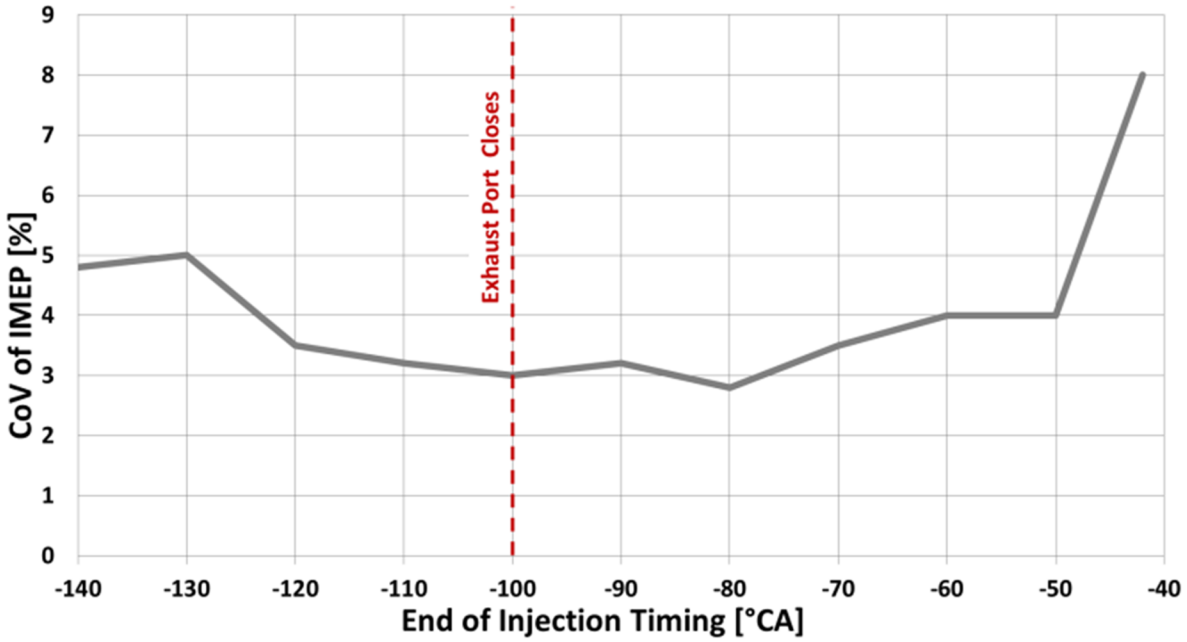

Figure 2.9: Coefficient of variance of IMEP vs. injection timing, 3000 RPM, 0.1 g/s gas flow, MBT ignition timing.

Due to the low operating pressure of the hydrogen fuel injection system, the extent to which the injection timing can be phased later in the compression stroke is limited by the necessary pressure gradient between the supplied fuel and the surroundings to which it is injected. Above the critical pressure ratio of 0.53 for hydrogen in air, the flow across the throat of the injector ceases to be sonic and the mass flow rate becomes decoupled from the opening time until no more hydrogen can be injected when the pressure gradient disappears or reverses.

Figure 2.10 shows the raw heat release rate plots directly inferred from the cylinder pressure indication of 50 sequential cycles at the operating point corresponding to maximum rated engine power and speed. Figure 2.11 shows the cumulative or integral heat release of 50 cycles at the same operating point. A 300-cycle ensemble average curve with respective 10-, 50- and 90% MFB points labeled are also highlighted. In both figures, the cyclic variation can be observed, and two outlier cycles clearly stand out in Figure 2.10 with their late peaks compared to the majority of the others.

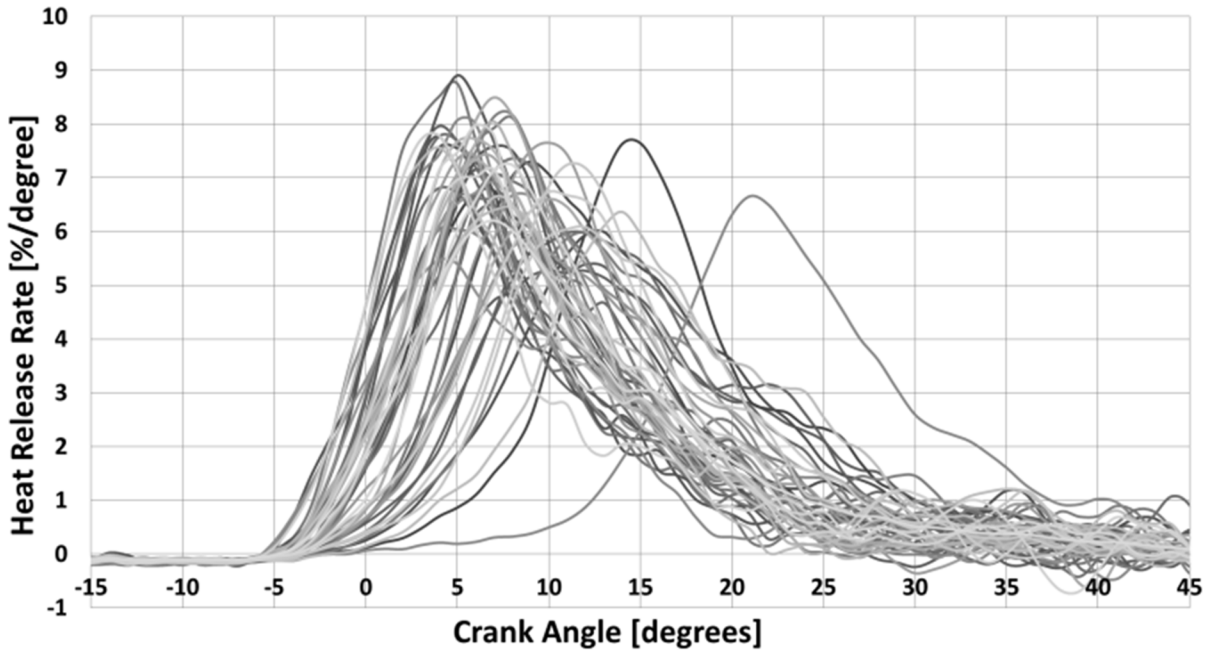

Figure 2.10: Raw instantaneous apparent heat release rate plots of 50 sequential cycles, ICOMIA Mode 5.

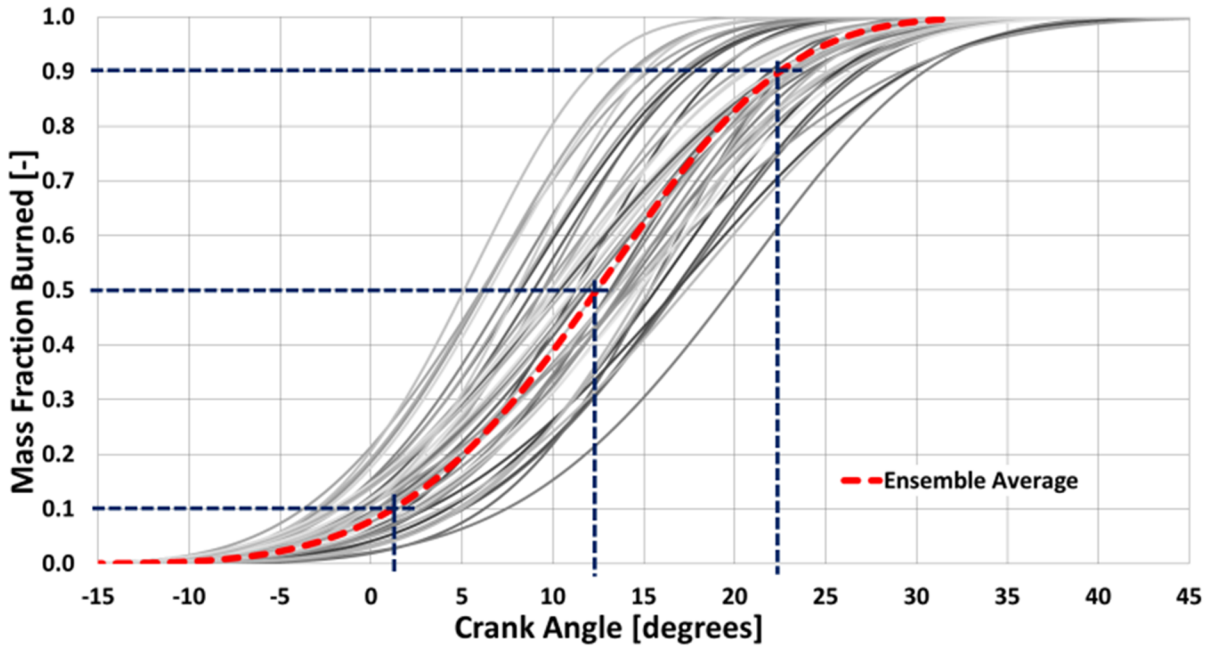

Figure 2.11: Cumulative heat release Vibe curve-fits of 50 sequential cycles and 300-cycle ensemble average, ICOMIA Mode 5.

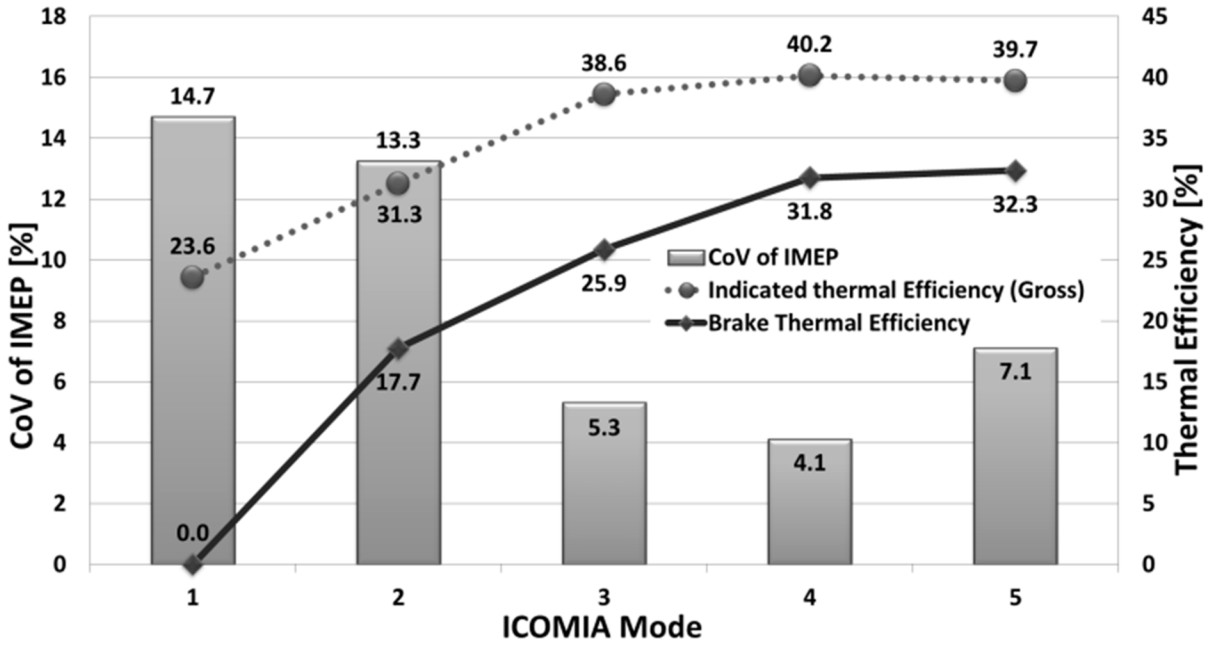

Figure 2.12: Coefficient of variance of IMEP and thermal efficiencies over each mode of the ICOMIA cycle.

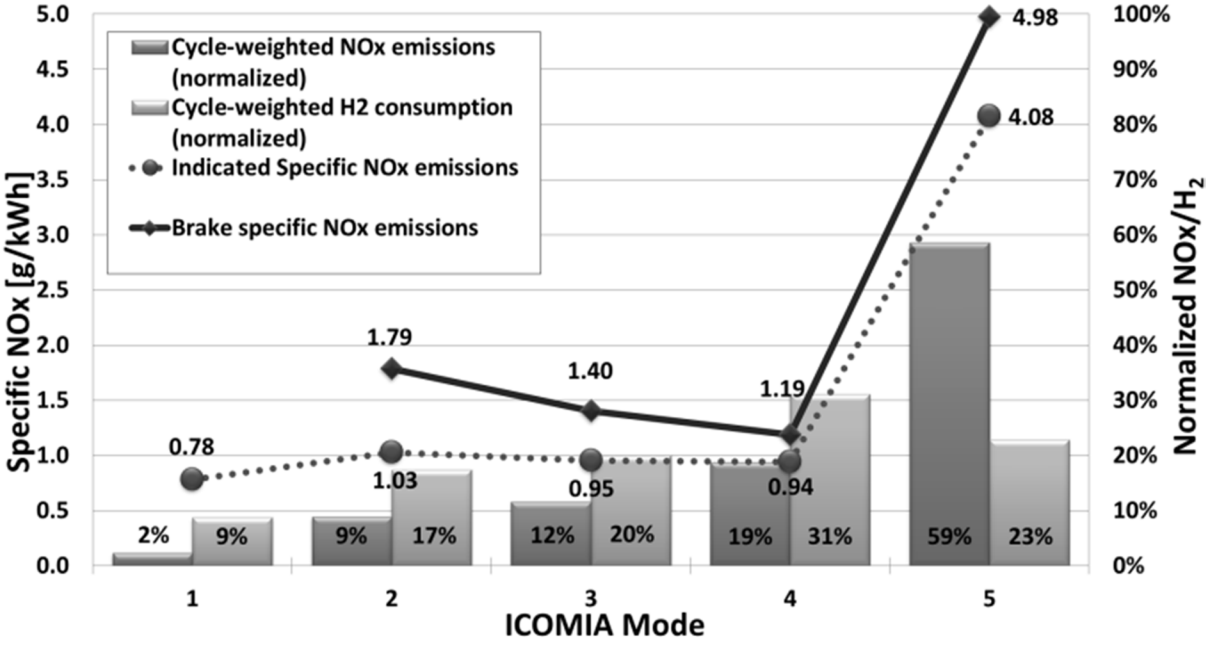

Figure 2.13: ICOMIA cycle NOx emissions and hydrogen consumption, efficiency-optimized calibration.

The cumulative heat release curves in Figure 2.11 are Vibe curve-fits and only employ the statistics of each cycle as described by Equation 2.7. Despite what appears to be significant cyclic variation from a view of the heat release curves, it is not excessive for this type of engine. Figure 2.12 summarizes the measured CoV of IMEP and efficiencies under one calibration setting and hardware setup for each of the ICOMIA operating points. In the relative context of small, two-stroke engines, the CoVs represent very good values and are corroborated by excellent subjective assessments of running smoothness.

The efficiency-optimized NOx emissions corresponding to each operating point are summarized in Figure 2.13. The cycle-weighted brake specific NOx is 2.46 g/kWh. The figure shows that although operation at Mode 5 (full-rated power and RPM) accounts for only 6% of the ICOMIA cycle duration, it generates 59% of the full-cycle NOx emissions. On the other hand, this point accounts for 23% of consumed hydrogen, compared against 9, 17, 20 and 31% for modes 1 through 4, respectively. Therefore, design and calibration optimization should be focused upon modes 4 and 5. Calibration sweeps showed that in this design, BSNOx emissions can be reduced by 18% (to 2.01 g/kWh) with a trade-off 3.3% increase in fuel consumption. As a side effect, the NOx-optimized CoV is lower due to earlier fuel injection timings and less stratification.

The test cell setup in the present work is such that the brake measurements at the dynamometer encompass the entire outboard drivetrain, plus churning losses of the exposed rotating components under water and the belt transmission from the prop shaft axis to the dynamometer input shaft. Therefore, expressing brake efficiencies alone will magnify losses and will make the engine appear to perform at worse efficiencies. It could also give the illusion of higher brake specific emissions.

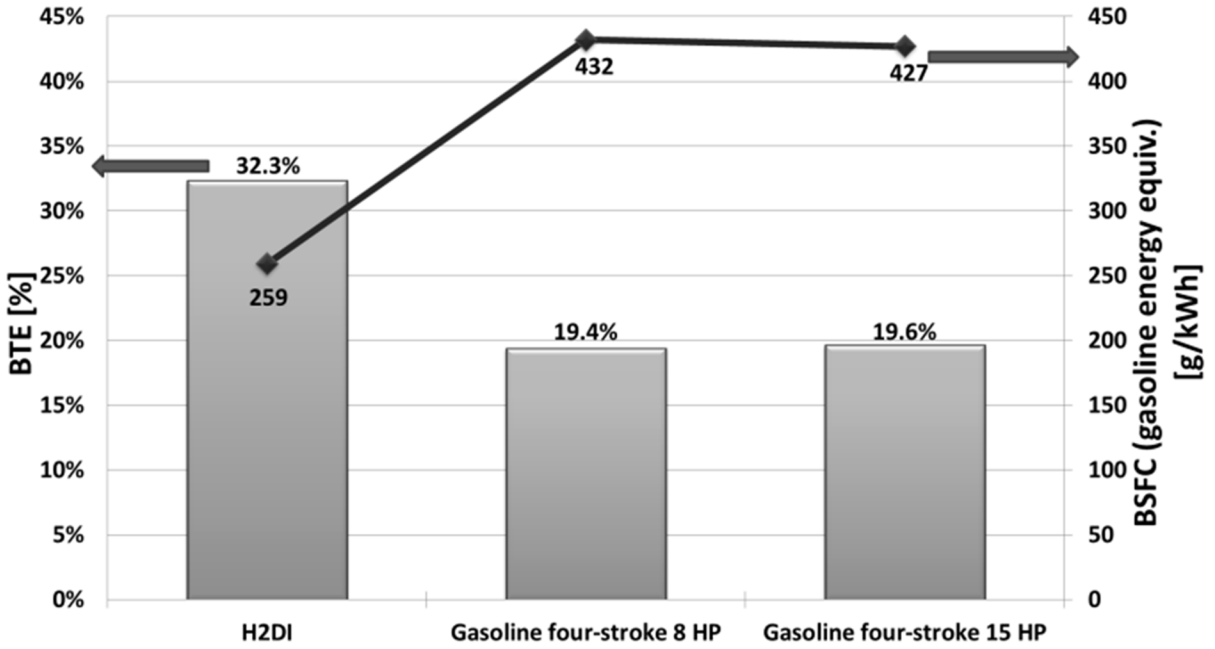

Figure 2.14: Comparison of brake thermal efficiency and specific fuel consumption at rated power (ICOMIA Mode 5), hydrogen vs. gasoline engines (energy-equivalent basis); gasoline engine data from [21].

The present results are contrasted to comparable low-output outboard engines found in literature. Murillo et al. (2003) reported the rated power BSFCs of 8 and 15 HP (6 and 11.2 kW) four-stroke Yamaha outboard engines as 432 and 427 g/kWh [20], corresponding to brake thermal efficiencies of 19.4 and 19.6%, respectively. In the present work, the gasoline energy-equivalent BSFC, also at rated power, is 259 g/kWh, or a brake thermal efficiency of 32.3%. These results are summarized in Figure 2.14.

To put this in context, the achieved brake thermal efficiency at rated power represents a 65% improvement, resulting in a 40% reduction of fuel consumption, compared to gasoline outboard engines of similar outputs.

2.8 Summary

A prototype small-displacement, two-stroke, direct-injected hydrogen engine has been designed and constructed with a priority placed upon achieving high fuel efficiency and low emissions, while pursuing a cost-optimized strategy and mid-term market feasibility using a fuel system adapted from volume production-available components. While matching the rated power of the original gasoline engine, the achieved best-point gross indicated thermal efficiency is 42.4%. The brake thermal efficiency at rated power is 32.3%. The ICOMIA cycle-weighted gross indicated thermal efficiency is 36.3%; brake thermal efficiency is 25.5%; and brake specific NOx emissions is 2.46 g/kWh, the majority of which is in the Mode 5 (maximum rated power) operating point that accounts for only 6% of the duty-cycle time. Late fuel injection is observed to be the key driver in raising the thermal efficiency, but at the expense of increased NOx emissions. The hypothesized cause of this is increasing charge stratification, which is supported by phenomenological inference of the effects of injection timing sweeps on combustion duration, NOx emissions and cyclic variations.

The low injection pressure limits the extent of realizable late timings. Furthermore, it is unlikely that the compression ratio can be further raised without increasing the tendencies for abnormal combustion and NOx emissions. Additional simultaneous efficiency improvement and NOx reduction will require substantial redesign after detailed determination of the sources of thermodynamic losses and novel approaches to their minimization. Wall-heat transfer is inferred as the predominant loss factor, combining the small engine dimensions, very high compression ratio and the peculiarities of hydrogen combustion with its small quenching distance and high flame speed. The systematic mitigation thereof – employing experimental in-cylinder optical observation, wall surface heat flux measurements and CFD analysis – by imposing designed regimes of charge- and flow motion stratification in the combustion chamber for reduced thermal convection is the subject of further work,. A gross indicated thermal efficiency of 45% and engine-out, cycle-weighted indicated specific NOx emissions of 1 g/kWh are targeted.

CHAPTER 3 FRAMEWORK FOR VORTEX-STRATIFIED COMBUSTION

3.1 Preface

The previous chapter found a correlation between increased thermal efficiency and late fuel injection timing, achieving diminishing returns and reaching an upper bound of the former due to increasing cyclic variation and NOx emissions. This correlation was traced to charge stratification by phenomenological inference of measured trends of combustion duration as well as the aforementioned cycle-to-cycle variance of IMEP and exhaust NOx concentration, since the degree of charge stratification is not known a priori. However, the inductive reasoning that made this correlation implicates the stochastic nature of the cycle-to-cycle location distributions of fuel-rich stratified zones in the combustion chamber; these zones, inferred by the NOx emissions, are responsible for high local gas temperatures. It can therefore be reasoned that the proximity or contact of these rich zones – with their attendant high temperatures – to the combustion chamber walls will have a significant effect on heat transfer.

Without some means of controlling the very location of the fuel-rich mixture in the combustion chamber, consistently from cycle-to-cycle, any kind of conceptual solution premised around a stratified charge would encounter the same limiting efficiency ceiling encountered in Chapter 2 and will not address the identified important need to reduce wall heat transfer losses as a key for further efficiency improvements. A conventional stratified charge combustion process for hydrogen-fueled engines is therefore expressly not the approach pursued in this dissertation; rather, a different concept is prescribed.

3.2 Thought Experiment – Homogeneous vs. Vortex-Stratified Combustion

The fundamental premise of this dissertation – the systematic reduction of wall heat transfer losses – is introduced by means of a thought experiment. Consider a closed chamber of arbitrary geometry filled with a prepared homogeneous fuel-air mixture and having a spark plug at some location. The mixture is ignited at the spark plug and a flame kernel initiates at this location and

propagates over a finite period of time across the chamber until the unburned charge is consumed. The flame will quench at some distance near the walls – the actual value varies according to the fuel and prevailing pressure and temperatures of the gas and at the wall. The thermal flux "experienced" at the walls surrounding the chamber is then some function of:

1. The burned gas temperature;
2. The temperature and thermal properties of the wall surface;
3. The flow conditions adjacent to the boundary layer;
4. The proximity of the source of the burning event from the walls.

It is useful to introduce here the heat transfer equation, where $\dot{Q}_{wall}$ is the wall heat transfer rate or flux, h is the heat transfer coefficient, A is the surface area and $\left(T_{gas} - T_{wall}\right)$ represents the temperature gradient between the gas and wall. This will be discussed in greater detail in Section 5.3.1 but for the present purposes, it suffices only to inspect intuitively the parameters that affect the heat flux.

$$\dot{Q}_{wall} = h \cdot A \cdot \left(T_{gas} - T_{wall}\right) \tag{3.1}$$

The first, second and fourth items in the above list all affect heat transfer through the temperature gradient between the gas to the wall, while the third affects h. Increasing one or more of the coefficient h, the surface area and/or the temperature gradient will all increase heat transfer. With the objective of reducing the heat transfer losses to the surroundings while taking the wall surface properties as a given, the solution then is one or a combination of:

1. Reducing the combustion temperature;
2. Modifying the flow or fluid properties to reduce h;
3. Constraining the distance of the burning away from the walls.

Humans are personally familiar with these phenomena when sitting around a campfire or inside a sauna. A blazing fire is hotter than an extinguished one or spent ashes. One will feel subjectively hotter if there is a velocity of the hot air over one's skin – whether by a breeze of wind or by blowing from one's breath – than if the surroundings were stationary or quiescent. Similarly, in the case of a sauna, one will feel an intense sensation of heat upon throwing some

water on the rocks, although the thermometer reading does not simultaneously change by a noticeable amount or may even fall slightly. This is because in evaporating the water on the surface of the rocks, the ambient humidity suddenly rises, thus raising the heat transfer coefficient between the air and one's skin. If one sits close to the campfire or the heat source in the sauna, one will also feel subjectively hotter than to step further away.

The first approach of reducing the burned gas temperature has been investigated extensively in lean-burn and so-called "low-temperature combustion" schemes under many different names. The focus has primarily been with the objective of reducing emissions of nitrogen oxides (NOx) since formation follows the well-known Zeldovich mechanism as mentioned in Chapter 2. Second, like the analogy of the enhanced heat transfer due to the increased wind velocity over a surface, much design effort is spent in engine development for an optimum amount of in-cylinder charge motion and turbulence – sufficient that good fuel-air mixing and a rapid rate of combustion are achieved, but not excessively so that heat transfer losses negate efficiency gains from the other areas. The last approach of confining the burning to some distance away from the walls is more difficult to realise in a reciprocating internal combustion engine, because it implies imposing some means of stopping the flame from reaching close to the walls. This must be achieved without artificially extinguishing the flame and thereby forfeiting the available chemical energy in the unburned reactants while doing this in an unsteady flow regime with intermittent combustion events.

3.3 Historical Review of "Vortex" and "Stratified Charge" Internal Combustion Engines

For precision, it is first important to define the choice of the term "vortex" to describe the process to be presented in this work. Yilmaz et al (2003) [21] give a succinct summary of definitions for the classification of "swirl flow," the descriptive term for a fluid flow in which the tangential component of the main stream velocity is a significant contribution to the resultant velocity. Swirl flows may be classified into three groups depending upon characteristic velocity profiles: curved, rotating and vortex flows. These velocity profiles are different, depending upon the particular flow geometry and swirl generation methods:

1. Curved flow is produced by a stationary boundary, causing a continual bending of the local velocity vector, and complex secondary flows with an appreciable velocity component normal to the instantaneous osculating plane are generated. Curved flows can be generated by inserting coiled wires, twisted tapes and helical vanes into the pipe, by coiling the tube helically or by making helical grooves in the inner surface of the duct;
2. Rotating flow is generated by a rotating boundary, either confining the flow (as for a rotating tube) or locally influencing the flow field (as for a spinning body in a free stream);
3. Vortex flow is also called a "free vortex" or "decaying swirl flow." These are generated by the use of tangential entry swirl generators and guided vane swirl generators. Tangential entry of the fluid into a duct stream can be achieved by using a single tangential inlet duct or more than one tangential entry.

At this juncture, it is clear from the above listing, especially from what it is not – the first two definitions – that the flow of interest is properly called a vortex, in which case the question then arises:

> *What is its novelty compared to previous so-called vortex-type combustion processes such as have been trademarked by Honda as CVCC™ (Compound Vortex Controlled Combustion), as well as in stratified charge and Diesel engines – both divided-chamber and direct-injected variants – employing some form of swirl flow that have been tried since the 1920s?*

In reciprocating internal combustion engine parlance, swirl has a slightly variant definition from the preceding and is distinguished by the axis on which the bulk charge motion takes; "swirl" then refers to the rotation of the fluid along the centerline axis of the cylinder, while "tumble" represents rotation orthogonal to this.

Technical flows in engine combustion chambers are not characterised by perfect biaxial swirl and tumble but rather are very complex and stochastic, varying both spatially and temporally; at various points in the process there may be rotational flows over multiple centers

and at different scales. Tumble can take place at any azimuthal angle normal to the cylinder or swirl axis, so that a "cross-tumble" is defined as flow rotation at some angle from a reference Cartesian axis orthogonal from the cylinder axis, which may be defined as parallel to the crankshaft axis by convention or some other axis about which the flow dominates. Similarly, cross-swirl is a deviation from the cylinder axis that can best imagined like the changing tilt of the Earth's poles relative to its orbiting plane during the course of a solar year or a spinning top gyrating as its rotation slows down. Swirl by the above definition is traditionally associated with direct-injected CI engines and tumble with SI engines [22, 23, 24].

The answer to the above question about the novelty of the present vortex combustion process is that the operating principle proposed in this dissertation is ambivalent to the directional axis of rotation; the more generic term "vortex" is employed throughout, with swirl, tumble and their cross-counterparts stated only when specifically warranted. The principle being introduced here will be shown to exploit much higher tangential velocities – and centripetal accelerations by consequence – to achieve the fuel-air charge and thermal stratifications. In addition, although the current study is done with hydrogen as the fuel and investigations are performed on a spark-ignited, two-stroke, reciprocating engine, the vortex-stratified combustion principle is fuel-flexible; applicable to spark- or compression ignition engines; and is ambivalent to engine architecture, e.g. two- or four-stroke, piston-based or rotary.

Another question that needs to be answered is:

What is the problem that engines operating on a stratified charge principle – indeed any combustion process – is trying to solve, and it is successful in this regard?

Stratified charge SI engines were initially proposed as a solution to the widespread early problem caused by fuels of the day having poor ignition characteristics, i.e. having insufficient octane rating, or scarcity due to two World Wars that necessitated substitution with lower quality fuels. Knocking combustion is the result, caused by shock waves generated by high rates of pressure rise of colliding flame fronts, one propagating radially outward from the spark plug and one or more fronts caused by spontaneous ignition of the end-gas ahead of the normally propagating one. Knocking is characterized by an audible sound during the combustion process,

which is caused by excitations of the engine structure surrounding the combustion chamber resulting from the impact of these high pressure shock waves. The effect on in-cylinder pressure can be seen in the comparison of cylinder pressure trace diagrams of a normally operating engine cycle with knocking ones of varying degrees, as shown in Figure 3.1 [25].

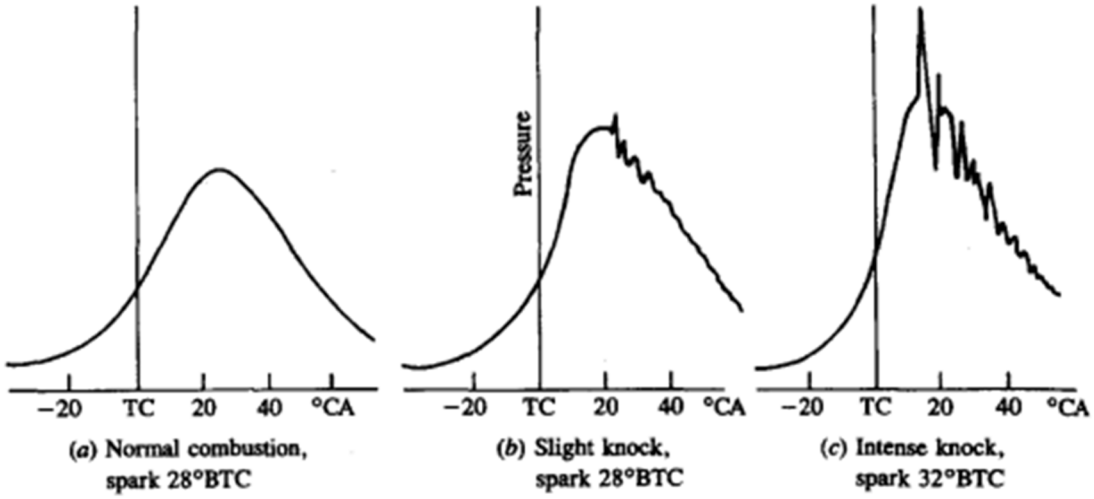

Figure 3.1: Cylinder pressure traces showing normal combustion and varying degrees of knocking. From Heywood (1988), p. 454.

In contrast to the smooth progress of cylinder pressure after firing TDC of normal combustion (Figure 3.1, left), the pressure trace with slight knock (middle) shows ripples. The left and middle pressure traces are result from the same operating point at the knock-limited spark timing; the onset of knock occurs in certain cycles as a result of cyclic variation. As the spark timing is further advanced, intense knock results. This is characterized by a highly jagged pressure trace with large fluctuations and peak amplitudes at high frequencies (Figure 3.1, right). Left uncontrolled and unmitigated, knocking is not only unpleasant to hear, but in serious cases is damaging to engine parts such as pistons.

A unified analytical model of knocking has not yet been developed, but the contributing mechanisms to its causes and control are broadly understood. Knocking is exacerbated by using fuel of too low octane rating, high temperatures and pressures of the prepared mixture at the beginning of ignition (too high compression ratio), early spark timing, high loads, low engine speeds and too low flame speed. Low flame and engine speeds allow greater residence time in

the unburned zone ahead of the normal flame front from being quickly consumed before forming a spontaneously igniting end-gas [26].

Eliminating knock – often though erroneously interchanged with the term detonation – absent suitable fuels, involved measures that diminished engine performance and efficiency by:

1. Reducing the maximum output before incipient knock;
1. Reducing the thermodynamic efficiency by forced reduction of the compression ratio[4];
2. Increasing pollutant emissions and further increasing fuel consumption by requiring enrichment of the fuel-mixture beyond the stoichiometric equivalence ratio.

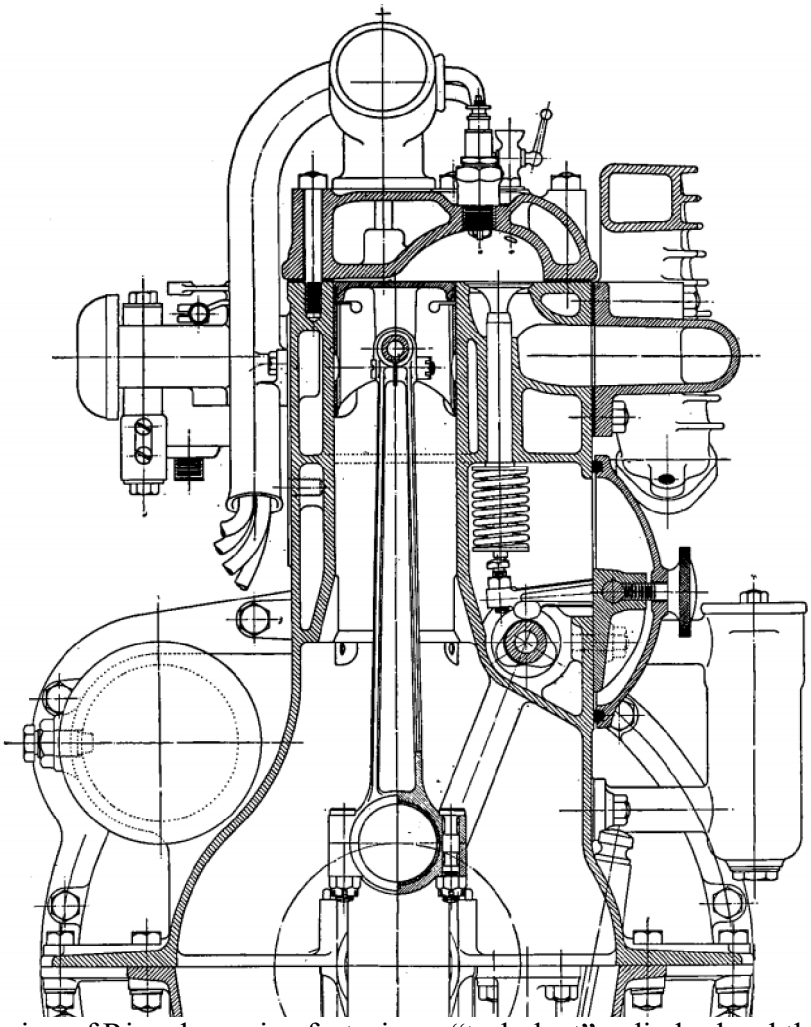

Figure 3.2: Drawing of Ricardo engine featuring a “turbulent” cylinder head that promoted a vortex flow. From Ricardo (1931), p. 103.

[4] In the early days of the internal combustion engine, compression ratios were limited to the order of 5 – 6 for spark ignited engines, whereas values twice or more of these are commonplace today.

Ricardo (1931) [27] found that knocking could be suppressed by appropriate design of the combustion chamber using some empirically observed rules. He patented a form of cylinder head, shown in Figure 3.2., that came to be known as the "turbulent head," and became widely used for many years. The claimed primary objectives aimed in this design of head were:

1. To create additional turbulence during the compression stroke in order to:
    a. Increase the rapidity of burning and so obtain both a greater effective expansion ratio and, at the same time, render the engine much less susceptible to ignition timing;
    b. Scour away as far as possible the layer of gas which normally clings to the cool surfaces of the combustion chamber and is therefore chilled to such an extent as to escape complete combustion either entirely or until so late in the expansion stroke as to be of little value;
    c. Reduce the tendency to detonate by keeping the unburnt gas in rapid motion, thus enabling it the more readily to get rid of the heat of compression by the oncoming flame front and, at the same time, to break up the flame front;
2. To reduce the length of flame travel from the sparking plug to the farthest point in the combustion chamber by rendering inoperative, so far as detonation is concerned, the part of the combustion chamber over the farthest side of the piston. This was accomplished by bringing the piston into such close contact with the head that the gas between these two relatively cool surfaces was so chilled as to avoid detonation;
3. To keep the flame travel as short as possible by placing the sparking plug in a central position;
4. To reduce, to the minimum, the surface/volume ratio and therefore the heat loss during combustion, though this latter is relatively small.

Further quoting Ricardo:

> *The above were the intentions of the design at the time it was first produced; by such means it was found possible to obtain from a side-valve engine a power output and economy at least as good as those previously obtainable from an overhead valve engine of equal dimensions, with the added advantage of a reduction both in the tendency to detonate and in the "sensitiveness" to ignition timing.*

The above-listed objectives, particularly the fourth one, were roundabout actually presaged in theory by Beau de Rochas in his 1862 French patent that correctly outlined the conditions under which maximum efficiency in an engine could be achieved without having reduced these ideas into practice by building a working prototype [28]. These were:

1. The largest possible cylinder volume with the minimum boundary surface;
2. The highest possible working speed;
3. The greatest possible expansion ratio;
4. The greatest possible pressure at the beginning of expansion.

All 4 conditions describe the necessity of a thermodynamic process with the minimum of heat losses (1 and 2); the maximum expansion – and by extension, compression – ratio (3); and heat addition to take place as quickly as possible to exploit the maximum pressure at the beginning of expansion (4).

For SI engines the key objectives in the years following Ricardo's pioneering investigations into in-cylinder turbulence and stratified charge combustion until post-World War II were knock suppression, tolerance for low-quality fuels, and the ability to operate with a variety of fuels other than gasoline. However, two major events shifted the focus:

1. The worsening air pollution problem in Los Angeles and regions, cities and industrial centers in the United States prompted passage of the Clean Air Act (1963) with subsequent amendments, e.g. the Motor Vehicle Air Pollution Control Act of 1965 [29] that as a result spurred research into reducing vehicle and particularly engine emissions.
2. Steep increases in the price of crude oil in a volatile market, triggered by the Arab oil embargo in 1973 and the outbreak of the Iranian Revolution in 1979 [30], with the resulting shortages and rationing in the West, prompted concerted efforts by the automotive industry to reduce fuel consumption.

Stratified charge engines and related research were well-positioned for these new areas of focus. Better fuel conversion efficiency was promised by enabling the stratified charge engine to operate with overall mixtures lean of stoichiometric, regardless of compression ratio as shown in Figure 3.3.

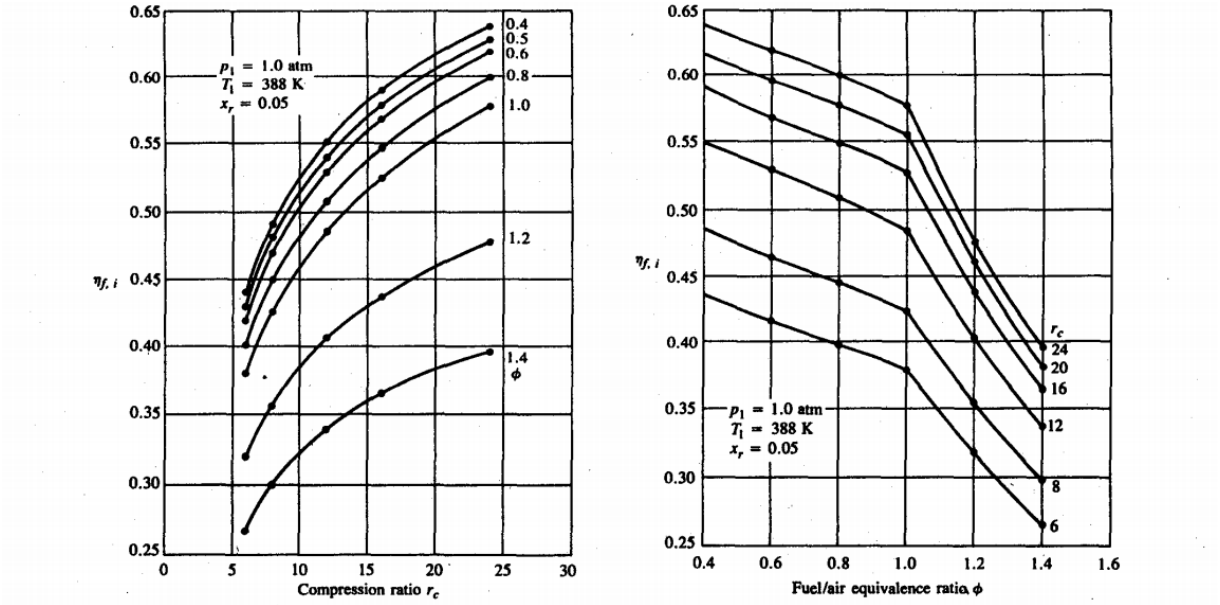

Figure 3.3: Fuel-air cycle results for indicated fuel conversion efficiency as a function of compression ratio and equivalence ratio. From Heywood (1988) p. 182.

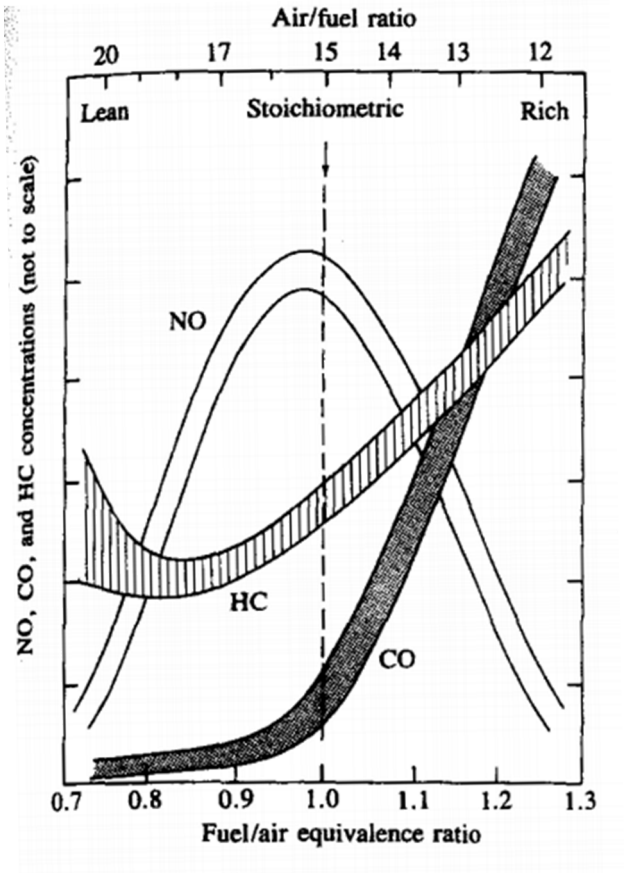

Figure 3.4: Variation of HC, CO and NO concentration in the exhaust of a conventional spark-ignition engine with fuel-air equivalence ratio. From Heywood (1988), p. 571.

During the nascent period following enactment of emission control regulations in the United States and elsewhere, automobile manufacturers considered stratified charge engines to be a solution to permit eliminating or at least delaying the need for exhaust aftertreatment, at the time still immature technology with very high costs. By virtue of lean overall fuel-air equivalence ratios, stratified charge engines permit reduction of raw, engine-out emissions of the three main regulated pollutant species, namely nitrogen oxide (NO), unburned hydrocarbons (HC) and carbon monoxide (CO) compared to stoichiometric operation, as shown in Figure 3.4.

One vehicle model to reach the market on this wave of promise of the stratified charge engine was Honda with its Civic featuring the CVCC™ engine [31]. Meanwhile, stratified charge engines remained of research interest, particularly in markets like Japan and Europe through the 1990s [32, 33].

An extensive review of these myriad engine types dating back nearly a century is not recounted here, but the reader is referred to the book chapter by Weaving (1990) [34] as well as many texts that cover the subject, such as that by Heywood (1988) [25]. The importance here is to distinguish these pre-existing designs in their objectives and means with those of the present work. Doing this requires parsing the different approaches into broad classifications and comparing them to the vortex combustion process featured in this thesis. These classifications encompass compression ignition (CI, usually Diesel-fueled) and spark ignition (SI, usually gasoline-fueled) engines; divided combustion chambers or direct-injected; and whether or not an ordered swirl flow is set-up. One complicating factor is that there have been very numerous designs proposed in the past century and among all these approaches are considerable variation and overlap, such that comparisons in turn are difficult, but fortunately are not important to get an appreciation of the distinctions to the proposed process.

For Diesel engines, Ricardo developed a divided chamber in the 1930s using a swirl motion of the air[5,6]. Another earlier approach proposed by L'Orange was a divided chamber

[5] Ricardo first proposed exploiting rotational air motion in the combustion chamber for more thorough and rapid mixing with fuel in a design was granted US Patent 1,622,885 in 1927.
[6] The contemporary swirl chamber, called "Comet," was granted US Patent 2,113,711 in 1938.

connected to the main cylinder via one or more orifices with no ordered bulk rotational motion[7]. Both cases were devised because Diesel engines from their first successful operation in 1897 were for comparatively low speed operation in marine and stationary applications. The use of low volatility fuel oil precluded sufficiently rapid evaporation, mixing and combustion within the short available window of time within each cycle at higher engine speeds, where the fuel was injected directly into the open combustion chamber at pressures –and atomization quality by extension – that were limited by the technological capabilities of the day. Both forms of divided chamber – where air is forced into it by increasing cylinder pressure thus developing for the respective approaches high angular velocity or turbulence – permit fuel, injected at relatively modest pressures and less stringent requirements for atomization quality, to be rigorously and rapidly mixed. The respective swirl and pre-chamber indirect-injection (IDI), as these approaches have come to be known, enabled a whole new class of high-speed Diesel engines capable of speeds of up to 5000 RPM and application into passenger cars [35]. With continued development and numerous design evolutions, both the approaches as shown in Figure 3.5 remained in production cars until the late 1990s and at least the former swirl chamber type still remains in use for very small Diesel engines in lawn tractors and portable generators.

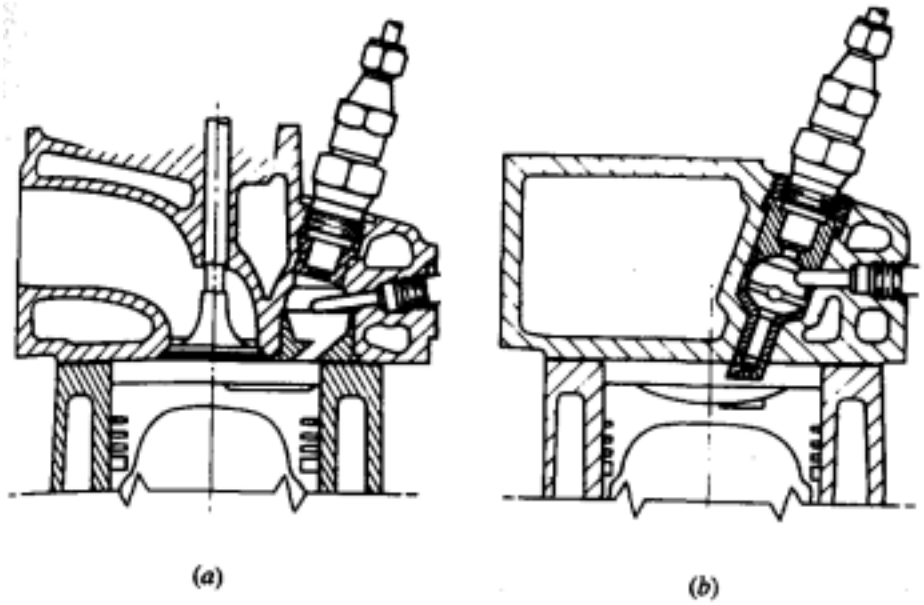

Figure 3.5: Two common types of small indirect-injection Diesel engine combustion system: a) swirl prechamber; b) turbulent prechamber. From Heywood (1988), p. 495.

[7] The earliest US patent for the divided chamber by L'Orange bearing the principles recognizable in contemporary implementations is No. 949,951, granted in 1910 after his German patent no. 230517 granted in 1909.

Recently, direct injection has largely displaced divided swirl and pre-chamber designs in Diesel engines due to its higher thermal efficiency; a 15-20% reduction of fuel consumption is reported [36]. The difference in efficiency is caused by pressure and heat losses caused by the narrow connections of the divided chambers to the main cylinder, with the attendant high flow velocity/turbulence leading to increased convective thermal flux to the walls. The application of direct injection in passenger cars have only been made possible by separate measures taken to reduce combustion noise.

Outside of internal combustion engines, thermal insulation or film cooling exploiting a vortex containment or confinement approach has been an area of active research in steady-flow devices like gas turbines [37], liquid-fuel rockets [38] and nuclear rockets [39, 40].

3.4 Proposed Approach

The application of a stratified charge and vortex-type combustion, as well as the eclectic inspiration for thermally insulating gas turbines and rockets, led to the idea to attempting to a flame containment approach in a hydrogen-fueled reciprocating internal combustion engine, with the primary objective of reducing the heat transfer losses to the combustion chamber walls and ultimately to the surrounding environment. These losses reduce the available energy for the gas to perform useful work in the engine. The reduction of wall heat transfer is premised in this thesis upon confining the burning of fuel-air mixture to some distance away from the walls, leaving a layer in-between of gas that does not participate in combustion. A proof-of-concept was realised and a design was conceived using the base engine described in Chapter 2. The desire to observe this phenomenon during real-time engine operation led to designing the experimental prototype to have optical access into the combustion chamber that can be observed using the schlieren approach and recorded in a high-speed digital camera. These investigations are described in the next chapter.

CHAPTER 4 EXPERIMENTAL INVESTIGATIONS

Foreword

Authors and affiliation:

David Oh: Doctoral candidate, Université de Sherbrooke, Faculty of Engineering, Department of Mechanical Engineering.

Martin Brouillette: Professor, Université de Sherbrooke, Faculty of Engineering, Department of Mechanical Engineering.

Jean-Sébastien Plante: Professor, Université de Sherbrooke, Faculty of Engineering, Department of Mechanical Engineering.

Date of submission: April 14, 2016

Journal: SAE International Journal of Engines

Reference:

Oh D., Brouillette, M., Plante J., "Reduced Convective Combustion Chamber Wall Heat Transfer Losses of Hydrogen-Fueled Engines by Vortex-Stratified Combustion – Part 1: Background and Optical Engine Observations," SAE Int. J. Engines 16JENG0020, 2016.

Titre français : Réduction des pertes de chaleur par convection aux parois de la chambre de combustion des moteurs à hydrogène grâce à la combustion stratifiée par vortex – Partie 1 : Contexte et observations d'un moteur optique.

Contribution to the document:

This article first reviews the contemporary research that has found that wall heat transfer losses represent the most important factor influencing the thermal efficiency of hydrogen-fueled internal combustion engines. After an explanation of the theoretical framework for the physical mechanisms that feature in the vortex-stratified process, it presents the design of the combustion chamber geometry. The setup of the experimental test bench and results of the optical and thermodynamic investigations are then presented and discussed.

Résumé français :

Un procédé de combustion stratifié par vortex pour les moteurs à combustion interne à hydrogène est introduit afin d'en améliorer le rendement thermique en réduisant les pertes de chaleur par convection aux parois lors de la combustion. Ce procédé implique un champ rotationnel ordonné de la charge dans une chambre à combustion séparée, transversale et cylindrique qui est lui-même connecté à la chambre principale qui comprend le cylindre du moteur et le piston. Le combustible à l'état gazeux est directement injecté lors de l'étape de compression pendant que l'air entre dans la chambre de combustion de façon tangentielle et préférentiellement le long de la circonférence à cause de l'effet Coandă. Les deux flux s'entrainent donc mutuellement et favorisent la formation d'un vortex puissant grâce aux géométries de la chambre et des conduits. Durant le mélange, le combustible est confiné radialement en raison de la combinaison de diffusion en temps fini dépassée par la reconstitution de l'air de la périphérie, et le champ centripète formé par l'écoulement agissant du mélange de gaz de différentes densités. Lors de la combustion, la flamme suit d'abord la circulation du fluide mais également traverse en direction du centre de la chambre cylindrique. Cet article examine ce procédé dans un moteur optiquement accessible à deux-temps à injection directe d'hydrogène aux vitesses jusqu'à 5000 1/min. Cet article explique la théorie et présente les observations strioscopiques. De plus, une étude comparative des résultats en zéro-dimension de pression du cylindre et de dégagement de chaleur est menée pour deux configurations de chambre de combustion, soit la chambre à vortex et une chambre de référence sans vortex.

Note : À la suite des corrections demandées par les membres du jury, le contenu de cet article peut différer de celui qui sera accepté.

Following the corrections requested by members of the jury, the content of this article may differ from the one that will be accepted.

4.1 Abstract

A vortex-stratified combustion process for hydrogen-fueled reciprocating internal combustion engines is introduced to increase the thermal efficiency by reducing the convective heat transfer losses to the surrounding walls during combustion. The process imposes a highly ordered rotational field upon the charge in a separate, transverse, cylindrically shaped combustion chamber by means of channels that connect with the main chamber enclosed by the engine cylinder and piston. Gaseous hydrogen is injected directly during the compression stroke, while air enters into the combustion chamber tangentially and preferentially along the circumference due to the Coandă effect. The two streams entrain one another and develop into a vigorous vortex by virtue of the chamber and channel geometries. As mixing proceeds, the fuel is confined radially from the combination of finite-time diffusion being outpaced by the replenishment of pure air at the periphery, and the centripetal field formed by the rotating flow acting on the different density gas mixture. Combustion takes place with a flame propagation that initially follows the rotation of the bulk flow but also curls radially inward toward the center. This work investigates the process in a fired, optically accessible 2-stroke hydrogen-fueled direct-injected engine tested at up to 5000 RPM. This paper, the first of two parts, explains the theoretical background, presents the schlieren observations and the results of zero-dimensional cylinder pressure indication and apparent heat release measurements comparing two combustion chamber designs – one that actualizes a homogeneous mixture without specific charge motion directionality and another with the here-introduced vortex-stratified approach.

4.2 Introduction

With the spark-ignited reciprocating ICE being under constant development and improvement for over a century, it has become apparent that a technological barrier has been reached from being able to extract further efficiency improvements. Doing so will necessitate novel approaches to reduce thermodynamic losses, namely incomplete and real combustion, wall heat transfer, pumping losses and friction, as shown in Equation 4.1:

$$\eta_{th,brake} = \overbrace{\underbrace{\eta_{th,ideal cyc.} - \Delta\eta_{inc.comb.} - \Delta\eta_{real comb.} - \Delta\eta_{wall\ heat}}^{\eta_{th,ind,net}} - \Delta\eta_{pumping}}^{\eta_{th,ind,gross}} - \Delta\eta_{friction} \qquad (4.1)$$

Of these, Verhelst and Wallner (2009) [8], Eichlseder et al (2003) [41], Wimmer et al (2005) [42], Shudo (2007) [43] and several other researchers [44, 45, 46, 47, 48] identified wall heat transfer as the predominant factor of reduced efficiency in hydrogen-fueled engines, and a key factor to its improvement, because heat transfer contributes to the largest magnitude lost. For example, Verhelst and Wallner (2009) showed that wall heat losses accounted for some 10 percentage points of thermal efficiency for an H2-DI engine, double that of a gasoline counterpart at the same operating point and much more consequential for diminishing the indicated thermal efficiency than all other factors listed in Equation 4.1 [8]. Oppenheim (2002) proposed an air-blast atomizer to direct the combustible charge away from the walls, thereby preventing contact of hot combustion products therewith and reducing heat transfer losses [49]. Heitland et al (1998) [50] showed several concepts of confining the combustion in a fireball surrounded by a layer of residual gas using air blast valves similar to those proposed by Oppenheim in an earlier work. Shudo and Oba (2009) [47] also stressed the importance of reducing heat transfer from the burning gas to the combustion chamber wall for improving the thermal efficiency in hydrogen engines. They found that the cooling loss fraction with hydrogen was about double that of methane (both operating stoichiometrically) over a range of tested ignition timings and employed a split-injection technique to direct high equivalence ratio mixtures at a desirable position such as the spark plug and slow the diffusion toward the walls in order to control the spatial distribution of the mixture for achieving cooling loss reduction and thermal efficiency improvement in hydrogen combustion engines.

Therefore, the main overall objective of this work is the systematic mitigation of wall heat transfer losses by some means of imposing a designed regime of charge and flame extent stratification in the combustion chamber for reduced thermal convection. Here it is proposed to achieve this by a novel method of confining the fuel-concentrated charge in the geometric center, bounded in-between with an insulating layer of essentially pure air at the periphery adjacent to the walls that is substantially maintained during combustion. In this chapter, a theoretical framework describing the flow dynamics of the proposed system is provided. Schlieren observations from an experimental optically accessible engine are presented. The visualizations demonstrate the effectiveness of the vortex-stratified concept in setting up the vigorous rotational flow field that forms a radial density gradient of the prepared charge mixture

before ignition, which indicates a gas species stratification. The following chapter provides an understanding of the basis for heat transfer loss reduction by correlating the experimental observations presented here with CFD analysis that illustrates the vortex-stratification of gas species in greater detail than is possible from schlieren images alone. It also quantifies the peak heat flux, which is found to be 50% less compared to a referencecombustion chamber design that actualizes a homogeneous mixture without specific charge motion directionality, with injection timing and all other model parameters remaining equal.

4.3 Background

4.3.1 Wall heat transfer losses

In the absence of appreciable bulk motion, turbulence, mixture composition non-uniformity and local temperature variations in the unburned charge, a premixed, spark-initiated flame front expands roughly spherically from the point source of ignition with a thin reaction sheet at the laminar flame speed S_l. Increased turbulence levels cause a wrinkling and convolution of the flame front and greatly enhances the burning rate [25]. The flame front propagates throughout the combustion chamber until extinguished by one or more factors such as oxygen depletion, fuel availability within combustible limits, or by quenching. Norton and Vlachos (2003) state that flames are quenched because of two primary mechanisms: thermal and radical [51]. Thermal quenching dominates here and occurs when sufficient heat is removed through the walls that combustion cannot be self-sustained.

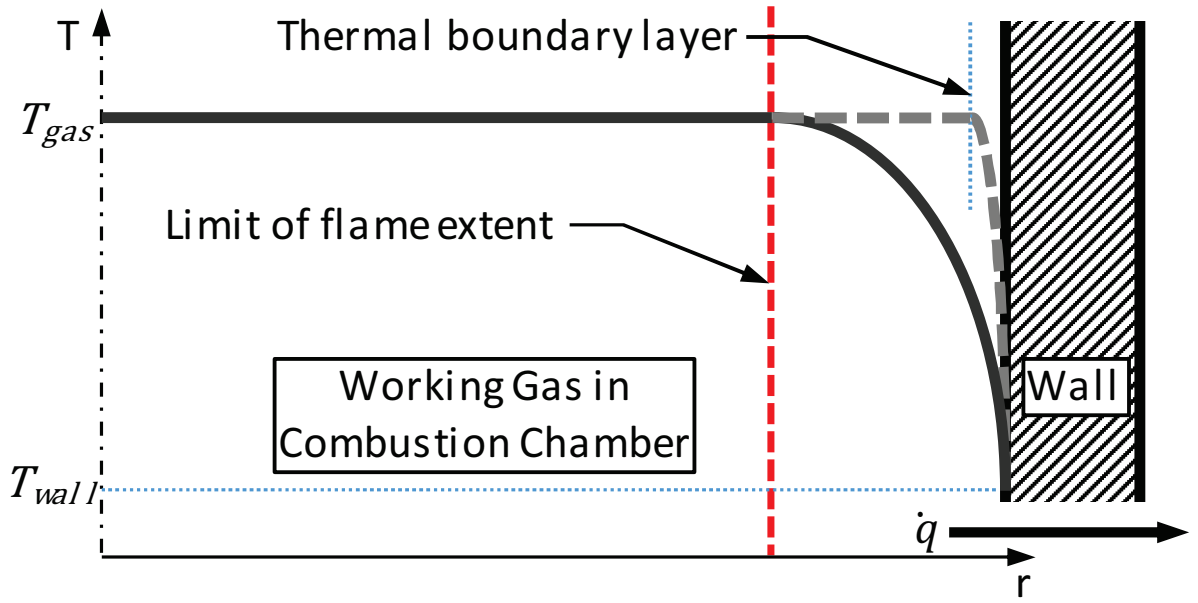

Figure 4.1: Schematic showing in-cylinder temperature profiles. The long-dash curve indicates the temperature profile in conventional combustion; the solid curve with limited flame extent.

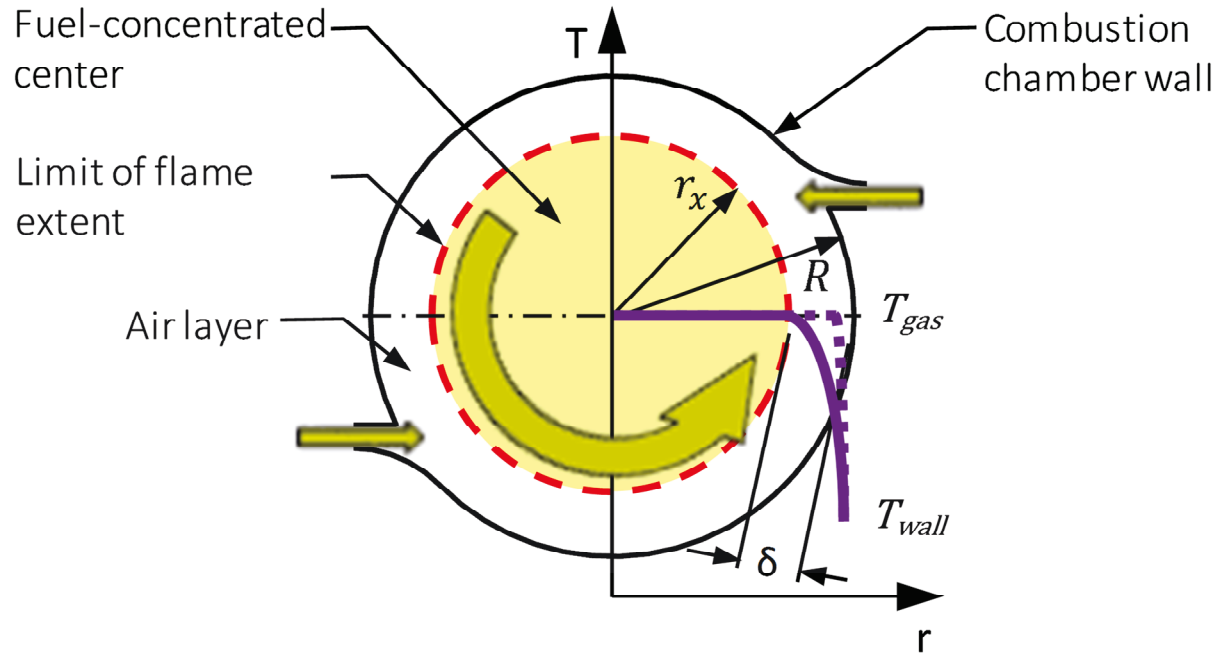

Figure 4.2: Schematic showing the flame-extent stratification process. Incoming air entering into the combustion chamber through the two side channels impart a rotational flow as indicated. Temperature profiles are sketched over with the dashed curve indicating conventional combustion; the solid curve with limited flame extent.

The prevailing burned gas temperature can be approximated as substantially constant throughout the combustion chamber but with a steep gradient in the thermal boundary layer adjacent to the wall until it matches with that of the gas-side of the wall surface, as shown in Figure 4.1. If the extent of the flame can be limited to some distance from the wall (red dashed line) – greater than the thermal boundary layer and inherent flame quenching distance but without leaving any unnecessary unburned fuel to affect the combustion efficiency deleteriously – the temperature profile would take the shape as sketched qualitatively with the solid curve with a resultant reduced heat flux to the wall.

4.4 Vortex-Stratified Combustion

Figure 4.2 shows a 2-D schematic of the cylindrical combustion chamber of radius R in used this work, although in general it could be of arbitrary geometry. Here, it is realized as separate from the main chamber containing the piston and cylinder and connected with channels, of which there have been many different design embodiments over the years, variously called divided-chamber, auxiliary-chamber, turbulent-chamber, pre-chamber, swirl-chamber, etc. In the proposed process, a rotational flow would be imparted from incoming jets of air from the main cylinder entering into the combustion chamber through two side channels offset vertically from the center. The directly injected fuel would be concentrated within combustible limits – which also limits the extent of the flame – to a radius r_x and the difference δ makes up the width of the air layer. The flow is said to be highly ordered because the channels and geometric symmetry impart momentum in 2 dimensions, while the component along the centerline axis is negligibly small. The resulting motion is one of bulk rotation and minimal cross flow.

Toulson et al (2010) gives an extensive review of pre-chamber initiated jet-ignition combustion systems derived from SI engines [52]. While the present work can be considered a form of turbulent jet or "torch" ignition system, important distinctions also become apparent:

1. The review focuses upon small pre-chamber systems whose volume comprises <3% of the total clearance volume. Here, is it in the order of 50% and furthermore, it is preferable that this proportion be maximized. In fact, in the ideal, limiting case, there is no divided chamber and there is no criteria for one at all; the principle described in this work can completely dispense with the separate volume and ostensibly be realized as an open

combustion chamber of arbitrary shape formed by the geometry of the cylinder, head and piston crown that avoids additional surface area, as well as the throttling and thermal losses associated with the narrow connecting passages, thereby further improving the thermal efficiency in the same manner seen in direct-injected Diesel engines over the indirect-injected ones;

2. Torch-ignition systems are premised upon a stoichiometric to slightly rich fuel-air mixture inside the pre-chamber located within or in close vicinity to the spark plug electrode gap in order to establish a robust flame kernel, which in turn issues into and burns up a much leaner mixture in the main cylinder volume at faster rates than can be achieved with uniformly lean mixtures; the overall or global mixture trapped and burned in each cycle remains lean or stoichiometric. Here, all the fuel is injected into the divided chamber and the main cylinder is desirably composed of only pure air, like an indirect-injected Diesel engine. Therefore, the heat release takes place and completes substantially within this chamber, so that only already burned gas issues through the connecting channels, which transfers heat to the main cylinder via mass transfer, mixing, conduction and convection rather than by a secondary combustion process;
3. Pre-chamber concepts have one or more connecting orifices designed to produce a highly turbulent flow but no ordered motion within the chamber [25].

At least since the mid-1970s, there have been work on a different classification of divided-chamber SI engines resembling the Ricardo Comet swirl chambers commonly seen in indirect-injection Diesel engines [53, 54, 55]. Like the Diesel counterpart, charge air enters from the cylinder into the swirl chamber tangentially, imparting a rotational flow. Unlike the Diesel process, however, the main cylinder charge still contains a lean fuel-air mixture rather than air alone. Additional fuel is introduced directly into the swirl chamber by means of an injector or valve. Peterson and Alkidas (1983) [56] show that the velocity near TDC in a divided Ricardo Comet swirl chamber using a rapid compression machine is in the order of 15-20 ±5 m/s at the center and outer extents of the chamber, respectively. Since the velocity does not scale with the radius, the air motion cannot be characterized as a solid-body rotation. In contrast, the charge motion in this work will be shown to behave closely to solid-body rotation through a wide range

of radii at up to 5-10 times higher tangential velocities and by consequence much higher angular accelerations.

Arcoumanis et al. showed the advantages of extending the lean combustion limit and enhanced burn rate offered by local charge stratification near the spark plug within an overall ultra-lean rotating mixture. The constant volume chamber had a tangential port for admission of a lean charge and the rotating bulk flow had mean velocity of up to 8 m/s [57].

Divided chamber and lean-burn SI engines have fallen out of favour for automotive applications because stoichiometric combustion with the three-way catalysts has been found to be the most cost-effective solution to meet increasingly stringent emissions regulations. However, the divided chamber, lean-burn design remains in use in industrial gas engines because of the unmatched fuel efficiency it provides.

Although superficial similarities might be noted between the surveyed and the present works, the authors know of no literature or working concept to date that specifically exploit the combined mechanisms of the gravitational effects of a rapidly rotating vortex flow on different-density gases and the Coandă effect to achieve the proposed simultaneous charge confinement and stratification in premixed-charge engines.

4.5 Theoretical Framework

4.5.1 Flow Dynamics

Diffusion J of any species combination is explained by Fick's first law as given in Equation 4.2:

$$J = -D\nabla c \tag{4.2}$$

The diffusive coefficient is denoted D and the negative sign indicates that the flux follows along a decreasing spatial concentration gradient ∇c. If one considers two initially separated chambers each containing pure, quiescent gas of one type or another, when the partition is removed, diffusion of the two streams will take place at the prevailing diffusive

coefficient – for hydrogen-air, this is given as 0.61E-4 m²/s at 300 K and 1 atm [8] – until the concentrations of both gases reach equilibrium spanning the combined volume, thus $\nabla c \rightarrow 0$.

Turbulence and charge motion greatly enhance diffusion, which allows homogenization of the introduced fuel-air mixture over the space of the combustion chamber in the very short timescales encountered in engines. One approach to calculate the turbulent diffusive coefficient D_T is given by Socolofsky and Jirka (2002) [58] as the product of the integral velocity and length scale, the "integral" index referring to the largest-scale structure of the turbulent flow field:

$$D_T = u_I l_I \tag{4.3}$$

This gives values for D_T in the order of 100 times higher than the laminar case when evaluated at an engine speed of 1200 RPM using length scale values from Petersen and Ghandhi (2011) [59] and flow velocities from Peterson and Alkidas [56]; the estimate stems from observations that length scale values change during the engine cycle [60]. Heywood (1988) states that Taylor micro length scales l_M are of the order of 1 mm at the end of compression and vary little with engine speed [25], and gives the relationship between the integral and Taylor micro length scales in Equation 4.4, where A is a constant of order 1:

$$\frac{l_M}{l_I} = \left(\frac{15}{A}\right)^{\frac{1}{2}} {Re_T}^{-\frac{1}{2}} \tag{4.4}$$

$$Re_T = \frac{u' l_I}{\nu} \tag{4.5}$$

where u' is root mean square value of the turbulent fluctuating velocity component and ν is the kinematic viscosity.

Heywood also states that turbulence levels scale linearly with engine speed (specifically mean piston speed). Increased turbulent flame speeds and burning rates therefore follow, such that the combustion duration in SI engines have been observed not to increase dramatically in crank angle degrees at higher engine speeds, but take place proportionally quicker in the time domain.

Three predominant forces act upon the motion of a fluid: buoyancy acts in the direction of Earth's gravity; molecular diffusion in all directions; and centripetal acceleration force radially from the axis of rotation. Where these forces are in balance, per Newton's first law of motion, there is nothing to compel a change in the state of motion of a particle or body. Importantly, diffusion can be hindered in the radial direction of a polar coordinate system if centripetal forces dominate. Also, diffusion can be slowed or reversed in a fixed frame if the velocity of one entraining species exceeds that at which diffusion proceeds; in effect, the rate at which species 1 (here assumed to be hydrogen filling the volume initially for illustration) diffuses into the entraining species 2 (e.g. air) is exceeded by the replenishment of air behind the interface of the two species.

Golombok and collaborators investigated separating methane and carbon monoxide from natural gas well streams using a centrifugal gas separation scheme similar to the process of enriching uranium [60, 61, 62]. An hypothesis considered whether this effect could be exploited in the context of an ICE, with hydrogen being injected into the cylindrical combustion chamber and by the action of tangential jets of inlet air imparting a rotational flow of sufficient angular velocity as to stratify the lighter hydrogen in a confinement field with a radial profile favoring the center. However, it is found that the timescale for separation to be 90% complete relative to the equilibrium value to be in the order of 10^2 seconds at engine-relevant pressures of >10 bar. This order of magnitude is far greater than the mixture preparation time within each cycle of an engine (~10^{-3} s). Furthermore, the result is based on the assumption of laminar flows rather than turbulent; since this does not give a directionally conservative assumption with respect to the separation time, the conclusion must be made that centrifugal gas separation on an already premixed mixture does not play a significantly active role.

Lapsa and Dahm (2009) investigated hyperacceleration effects on turbulent combustion in premixed step-stabilized flames [63]. In that work, a premixed mixture of propane and air is introduced into a semicircular channel at varying flow velocities, so that the centripetal acceleration is related by Equation 4.6 and exceeds the range of ±10000 g.

$$a_c \equiv \frac{v^2}{r} \tag{4.6}$$

They report that high centripetal accelerations induce large body forces on the high-density cold reactants and hot, low-density products. The direction of the backward-facing step – radially outward or inward in the channel – have different effects, either to force high density reactants into the recirculation zone and lower density products radially inwards into the reactant stream in the first case where $|a_c| \rightarrow +\infty$, or vice versa. This first case gives rise to a virtuous centrifugal pumping mechanism – a region of vigorous mixing and flame convection across the channel at dramatically enhanced rates. Conversely, for $|a_c| < 0$ using a radially inward step, as the acceleration level is increased the resulting body forces become sufficiently large that flame propagation is suppressed by the forced segregation of the reactants and products. The result is that the flame becomes nearly flat as large-scale distortions of the interface between high-density reactants and low-density products become essentially impossible; the flame is forced increasingly close to the radially inward wall as the body forces impede it from propagating across the channel. Although this latter case is considered inferior in terms of combustion efficiency for the U-shaped channel in the work of Lapsa and Dahm, here it is the desired mechanism to be exploited for heat loss reduction.

4.5.2 Coandă effect

Dumitrache et al (2012) give a detailed analytical solution that approximates a two-dimensional Coandă flow for both laminar and turbulent regimes in curvilinear coordinates [64]. The phenomenon that is exploited is the tendency for a flow to attach to and follow over a convex surface: the incoming flow from the main cylinder, taken to be pure air, thus remains substantially attached to the peripheral wall of the combustion chamber. A critical point is reached where the flow detaches or lifts-off from the convex surface, which is related to the free-stream velocity, viscosity of the fluid and the radius of curvature. Here, the Coandă effect introduces an additional degree-of-freedom for the optimization of wall heat transfer. Convection is greatly affected by the turbulence level and therefore velocity fluctuations in the thermal boundary layer. Absent any stratification, with burning of the fuel-air mixture until the flame is quenched by the wall, convection is further enhanced by high flow velocities. In an optimized design, the Coandă effect could be exploited using fillet radii in the transition from the channels to the combustion chamber to set up an initial attachment of the pure air flow to the surrounding chamber walls to promote charge stratification and favor rotation in the desired

direction. As the compression stroke proceeds and velocity increases, the flow would detach from the surface and the incoming fluid momentum is imparted to the inner radii of the rotating flow, forming another stratification, this time of tangential velocity with respect to the radius. Thus, the fuel-concentrated core would have a high velocity for rapid mixing and combustion but the flow of pure air at the periphery would rotate at a relatively lower angular speed to inhibit convection. In the ideal, limiting case, it would be desirable for the flow in the boundary layer to be stationary or quiescent, since heat transfer will only be primarily by conduction, that is, exclusive of convection.

4.6 Design

The basic geometry of the conceived combustion chamber is a cylinder with inlet channels offset from the centerline to impart a rotating flow. With the convention of a counterclockwise vortex from the frame of observation, one side of the interface between each channel and the chamber is radiused while the other left sharp to promote attachment of the flow to the peripheral wall along the direction of rotation due to the Coandă effect. This is illustrated in Figure 4.3 (left). For comparative purposes, a reference combustion chamber design is provided, as shown in Figure 4.3 (right), that represents current engine practice with high turbulence but no particularly ordered motion as defined in Section 4.4 – noting that high-tumble designs are presently commonplace for SI engines – and homogeneous charge mixture as an objective.

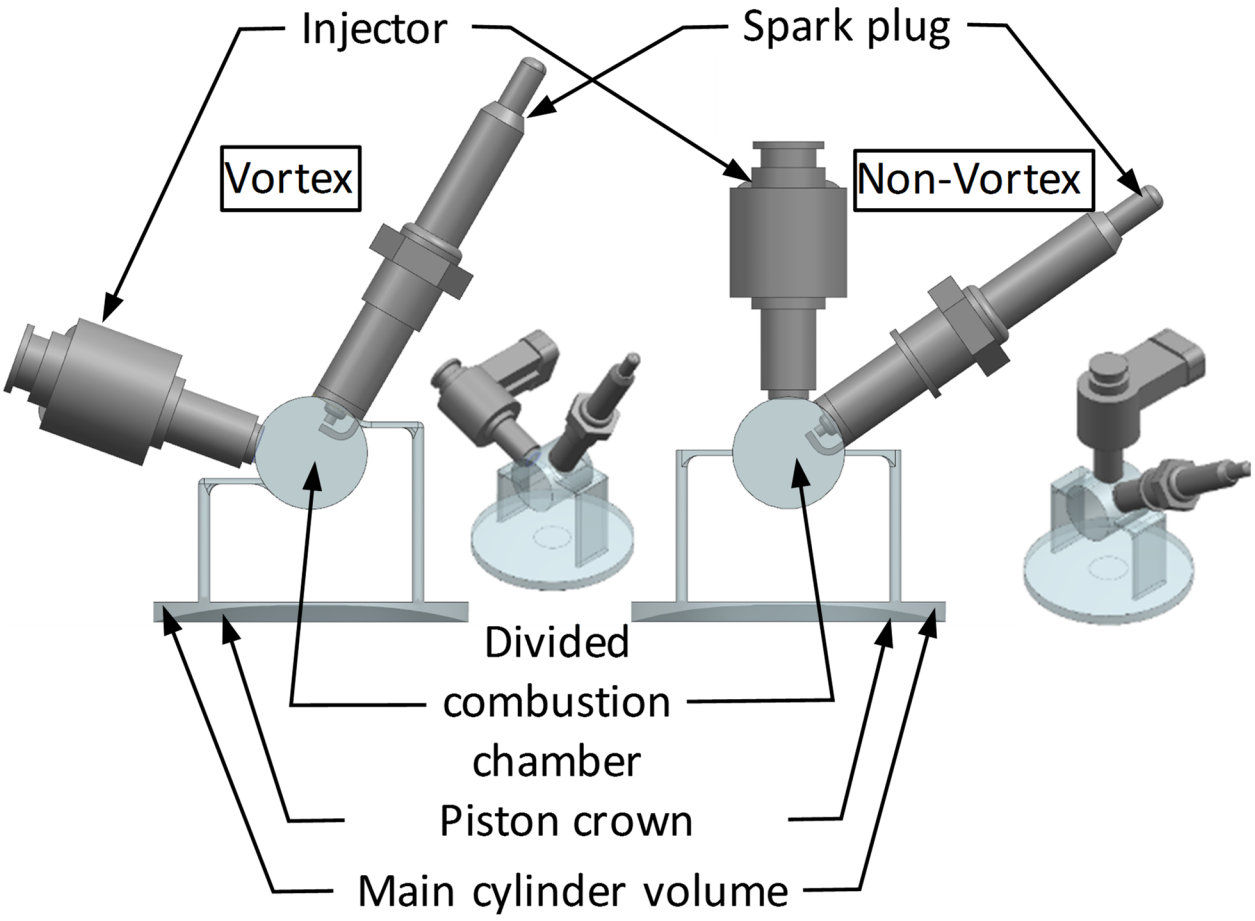

Figure 4.3: Renderings of vortex (left-half) and non-vortex (right-half) combustion chambers with injector, sparkplug and main cylinder volume shown with the piston crown at TDC.

Both vortex and non-vortex designs are very similar, including the same radius (10 mm) and length (20 mm) of the cylindrical portion of the combustion chamber and nearly identical total clearance volumes; the only significant differences being the positioning of the side air inlet channels and, due to packaging constraints, location of the fuel injectors and spark plugs. The choice of a cylindrically shaped combustion chamber and straight, diametrically opposed channels are compromises between the need to realize optical access; achieve thorough mixing and high turbulence levels of the prepared charge before ignition; and also to induce flow into the combustion chamber with a minimum of undesired charge motion in other directions –cross-swirl and cross-tumble – apart from the plane of observation. The resulting long, narrow channels and right angles connecting the divided combustion chamber and the main cylinder are

also compromises to be able to realize optical access while achieving a desirably high compression ratio. The high flow velocities through the narrow channels and 90° turns would result in high thermal and pressure losses. However, this was accepted because the objective was not for a geometry optimized for efficiency or performance per se, but rather to be able to study the flow phenomena in the visible cylindrical cross section of the combustion chamber. The design yields calculated nominal geometric and effective (trapped) compression ratios of 10.5 ±0.25 and 7.3 ±0.17, respectively, and k-factor – defined as the ratio of the volume of the cylindrical chamber and the total enclosed fluid clearance volume at piston TDC – of 0.5.

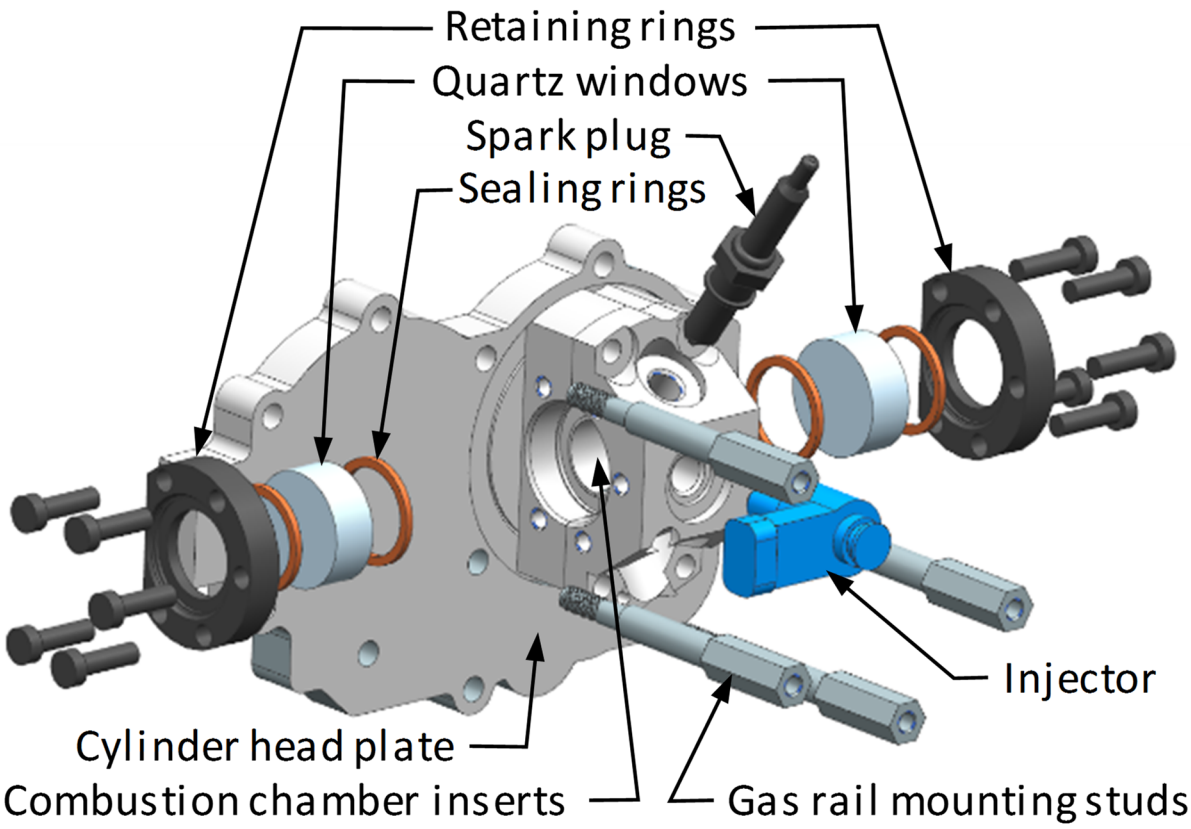

Figure 4.4: Exploded view of optically accessible cylinder head (non-vortex combustion chamber shown).

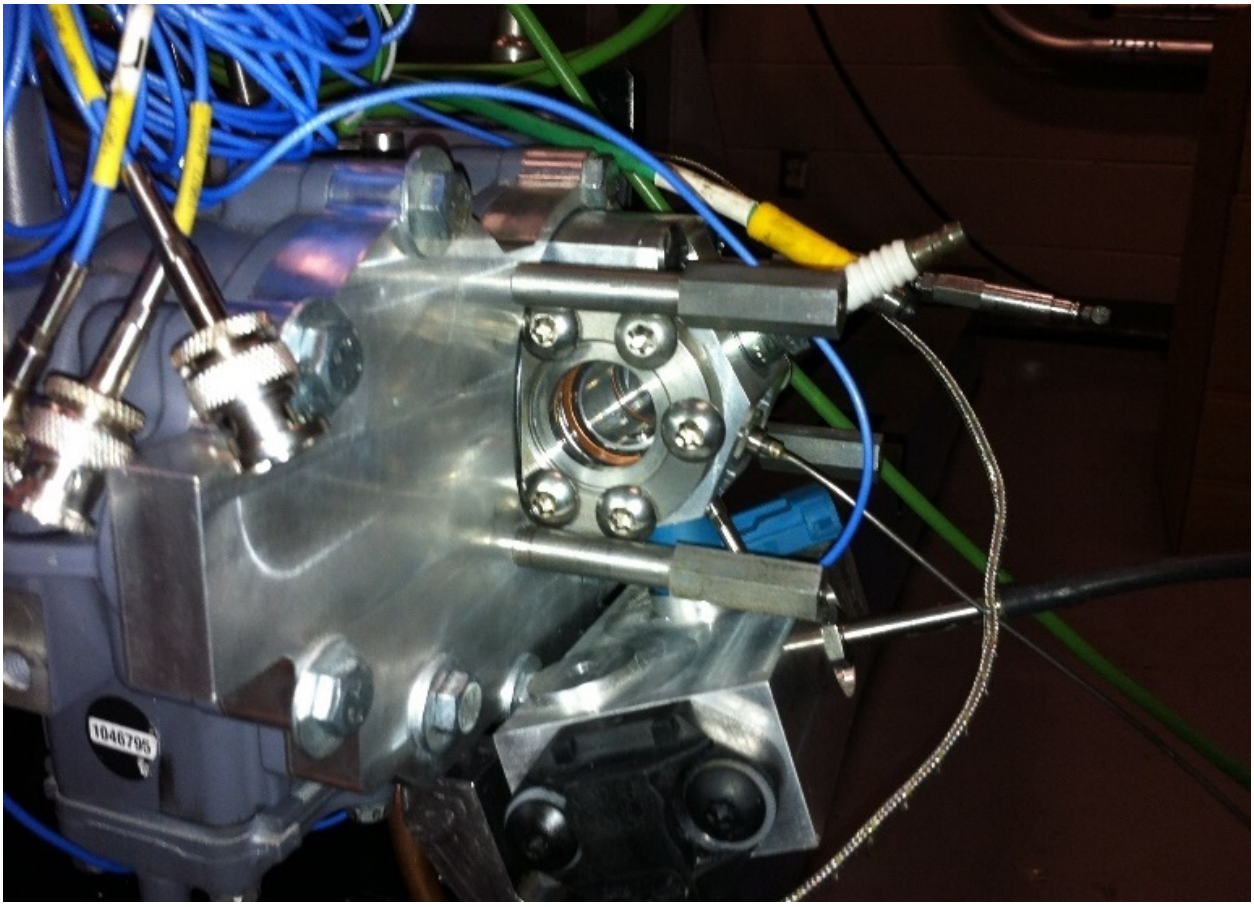

Figure 4.5: Optically accessible cylinder head assembled to engine (vortex combustion chamber with fuel rail and additional sensors shown).

Figures 4.4 and 4.5 respectively show the exploded CAD rendering and assembled cylinder head on the engine test cell. The experimental visualization of both non-vortex and vortex combustion processes are described in the following.

4.7 Experimental Investigations

The base engine for the test-cell work is a series-production 2009 model year two-stroke gasoline marine outboard with 9.9 HP rating. The basic specifications of the original engine are listed in Table 4.1. It was used in earlier investigations by the authors in [65] and has been largely carried over into this work. There, the major changes included modification to operate on hydrogen directly injected into the cylinder; changing the premixed lubrication to crankcase oil injection and the magneto ignition to a computer-controlled system. The gasoline carburetor is retained but not used. One of the two cylinders is inactive and sealed off; the remaining

working cylinder is outfitted with optical access by means of 2-piece combustion chamber inserts for each of either the vortex or non-vortex designs bolted together to a common cylinder head plate and assembled to the engine crankcase as shown in the previous figures.

Table 4.1 : Base engine specifications

No. of cylinders and layout	2 inline, 180° crankshaft
Bore x stroke (displacement)	56 x 50 mm (246 cm^3)
Connecting rod length	90 mm
Compression ratio	6.8:1 (trapped)
Scavenging type	Crankcase
Porting arrangement	Loop, Schnuerle
Lubrication type	Fuel-oil premix, 100:1 v/v
Induction	Carburetor, reed valves
Port height (transfer/exhaust)*	41/33 mm

* Measured from piston TDC position

The engine controller is modeled in Matlab®-Simulink® and actuated using Opal-RT for the hardware-in-the-loop (HiL). The system controls ignition- and injection timing events, as well as the lube oil injection rate, adjustable via a PC-based graphical user interface control panel.

Data acquisition is accomplished with an HBM eDAQ Lite system configured with 3 digital IO ports (up to 12 channels) and 16 analog input channels over a stack of 5 cards, to which diverse sensors like thermocouples and transducers are connected. Also connected to the data acquisition unit is an Alicat M-250SLPM-D laminar-type flowmeter for the hydrogen supply [66] and Superflow SF-3000 flowmeter for the engine intake air.

An AVL 4CA1 crank angle encoder and Digilent® NEXYS 4™ Artix-7™ FPGA board together act as system timekeeper to synchronize acquisition samples with crank angle events. The start and end of engine firing events, data acquisition, as well as trigger for the camera

frames, are also controlled by the combination of the engine controller software, HiL, crank angle encoder and FPGA.

4.7.1 Schlieren Imaging

In this work, the schlieren method, which displays the density gradient of a flow field as varying luminosity, is employed for flow and combustion visualization. The majority of works surveyed have been performed on engines with per cylinder displacements of 500 cm^3 and greater and, typically at engine speeds not exceeding 1500 RPM [67, 68, 69, 70, 71], with one investigation performed at 2400 RPM [72]. As previously stated, turbulence levels scale with RPM – more precisely mean piston speed. However, at the time of Heywood, direct evidence had been limited to low- to mid-engine speeds; whether the structure becomes significantly different at high speed was not known [25] and direct observation of combustion at high engine speeds have been eluded until now.

4.7.2 High-Speed Camera

The camera is a Photron Fastcam SA-X2 digital high-speed camera with a CMOS image sensor [73]. The limiting specifications are shown in Table 4.2. The lens used is a Nikon AF-S VR Micro-Nikkor 105mm f/2.8G IF-ED macro-zoom.

Table 4.2 : Camera specifications

Max. image resolution	1024 x 1024
Max. frame rate	1 000 000 FPS
Min. shutter time	1 / 3 410 526 sec (293 ns)
Recording bit depth	12-bit (4096 levels) grayscale

Observation at engine speeds of up to 5000 RPM at intervals of 0.5° CA requires a frame rate of 60000 FPS. The employed image resolution is 384x264. The fastest possible shutter time of 293 ns is chosen in order to capture the highly dynamic flow phenomena without the blurring common from conventional photography when taking fast-moving subjects. The very short shutter time therefore requires a very high luminous flux entering into the image sensor. This is

even more important given that some fraction of the light from the observed subject is cut-off from the schlieren knife-edge. The following describes the light source.

4.7.3 Light Source

The light source employs a Luminus Devices PT-121-G-C11-MPF high-power green colored (wavelength centered at 525 nm) LED [74]. The emitting area is 4 x 3 mm and typical peak luminous flux is 4000 lumens with a driving voltage and current of 4.9 V (5.9 V max.) and 30 A (36 A max.), respectively, at 50% square wave duty cycle. The green light was found by Kaiser, Salazar and Hoops (2013) to reduce chromatic aberrations in the captured images [75]. The LED also has the advantage of generating concentrated, directed light with a repeatable narrow spectral width compared to other forms like arc or gas discharge lighting. These properties also have benefits for reducing chromatic aberrations. With forced air cooling of the chip, the LED is able to survive operation with sustained high driving direct currents exceeding 30 amperes, rather than a pulsed square-wave power supply synchronized with camera shutter events, which would have greatly increased complications of the driver circuit design. The employed power supply is a Sorensen XPF 60-20-D set in the tests nominally to 5 ±0.1 VDC and 27 ±3 A.

Figure 4.6 shows the installation of the single axis optical rail in the test cell. The light source is on the top of the image and the combustion chamber under study is located in the zone of parallel (collimated) light beams between two lenses. The knife-edge is placed at the focal point ahead of the camera. The length of the optical rail is 2 meters. The engine is connected to a Unico AC induction motor, which spins and holds the engine to the test operating speed, then firing events and acquisitions are toggled through the HiL controller from the test bench.

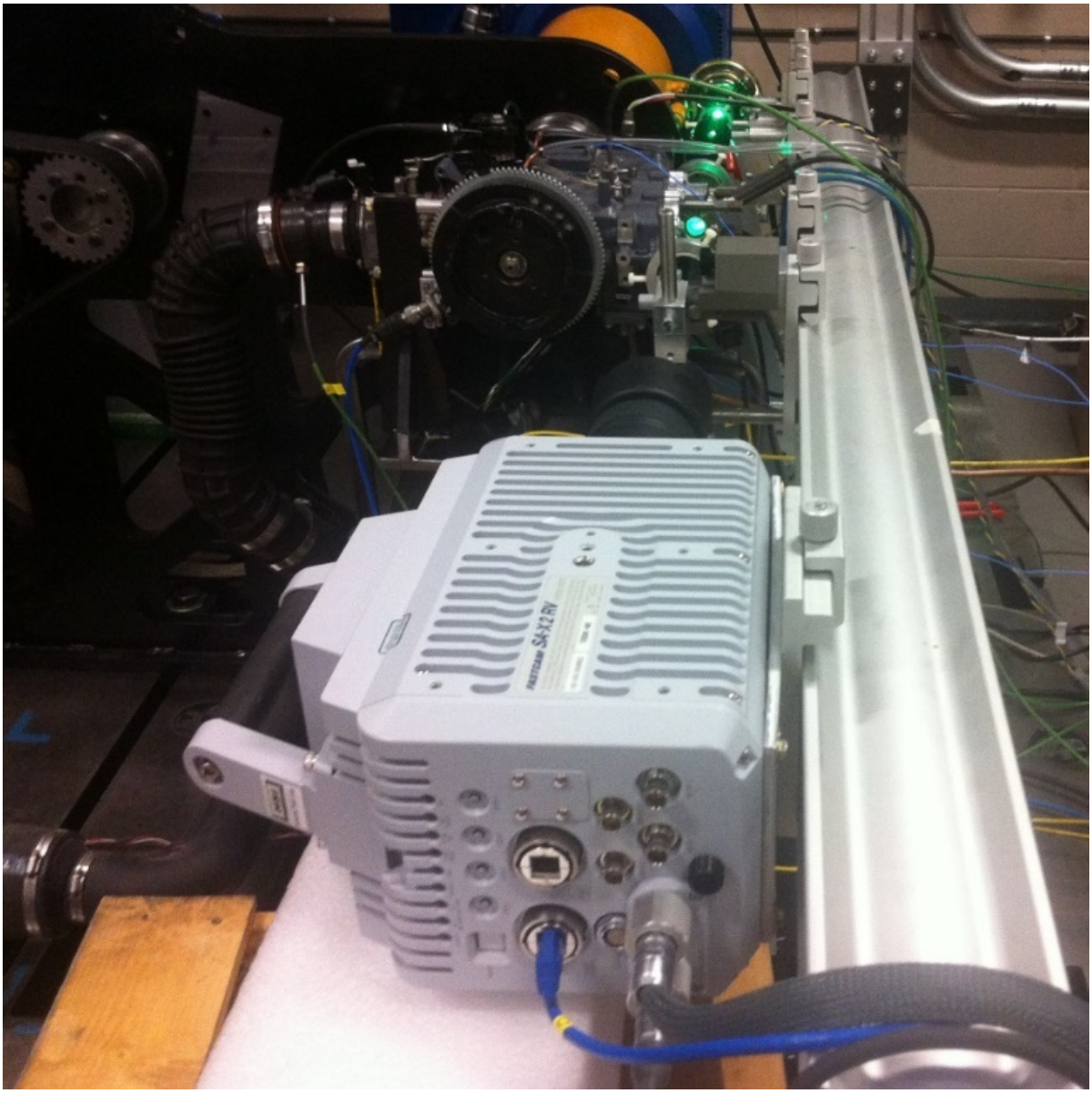

Figure 4.6: Photograph showing the optical rail and engine set-up in the test cell.

4.7.4 Optical Observations

The unprocessed schlieren images for the non-vortex combustion chamber are shown in Figures 4.7 and 4.8. Injection of hydrogen can be seen at the top of each frame in the first two rows. The timed start of injection takes place at -90° CA for an energized duration of 10° CA at an average rail pressure of 10 bar absolute. There is visual evidence of the hydrogen jet entraining the combustion chamber outside of this duration as well. The reason is imperfect

sealing of the poppet valve with the seat permitting hydrogen under pressure, given its small molecular size, to leak through. As cylinder pressure rises during the compression stroke, the adverse pressure gradient eventually decreases, disappears and reverses. Simultaneously, the increasing force of the cylinder pressure acting upon the exposed bottom surface area of the injector valve improves the sealing effectiveness until no more leakage becomes apparent.

Optical investigations of the mixture preparation and combustion yield the following observations germane for consideration and qualitative validation of the subsequent CFD modeling and analysis:

1. The incoming flow from the main cylinder during the compression stroke via the diametrically opposed air inlet channels deflects up or down in a consistent manner. The right-hand jet deflects toward the sparkplug ground electrode and the other downward. This may be caused by perturbations either by the asymmetry of the chamber geometry (e.g. presence of the spark plug and sensors) or pre-existing anisotropy in the flow. This behavior is consistent in all observed cycles and will also be shown to exist in the CFD models even though there is no geometric asymmetry to promote this.
2. Flame propagation takes place with similar structure and characteristics as has been widely observed in the literature, with the exception here of the very fine wrinkling and rapid rate; the flame is seen to engulf most of the visible cross-section only 5° CA after ignition start with local flame extinction apparent behind the front at +5.5° CA. This is indicative of the high turbulence intensity and confirms its scaling with engine speed, even at the high RPMs not observed until now.
3. The residual ignition energy causes a visible spark over some 10° CA, corresponding to over 300 μs. This spark duration is carried over in subsequent numerical models.

Figures 4.9 and 4.10 show the unprocessed schlieren images for the vortex combustion chamber. Fuel injection is highly obscured in part due to the 3-dimensional spray plume being projected onto 2-dimensional images focused on the sparkplug electrode with a shallow depth of field by the lens employed. The images are also obscured by artefacts that are not caused by the flow but rather by contamination on the glass window surfaces; these can be due to dirt, scratches, wiping streaks, condensed lube oil, carbon particles or other foreign matter. Beginning from about -64.5° CA a dark spot at about the 8 o'clock position can be seen

corresponding with the entry of air from the left side channel. The incoming air from the right side channel is obscured by the sparkplug. By the end of the compression stroke in the last frames of Figure 4.9, a bulge at the center of a diameter reaching to the tip of the ground electrode can be clearly distinguished. This indicates a radial density gradient at the transition between light and dark shades and can be caused by local gradients of pressure, temperature or gas constant per the ideal gas law. Pressure and temperature gradients are relatively small during the compression stroke, so the main cause of these gradients are due to the gas constant and, by consequence, the species fractions.

Upon start of ignition at the top left frame of Figure 4.10, a kernel can be seen forming in the spark gap. The density gradient cloud, corresponding to the temperature rise of the burning gas of the forming flame front, grows rapidly but unlike the non-vortex case that expands with a roughly monotonically increasing radius from the sparkplug, propagates initially along the flow rotation and can be seen to curl inwards toward the center in a similar manner as observed by Lapsa and Dahm [63], preferentially consuming the charge therein and delaying contact of hot burned gas with the peripheral wall.

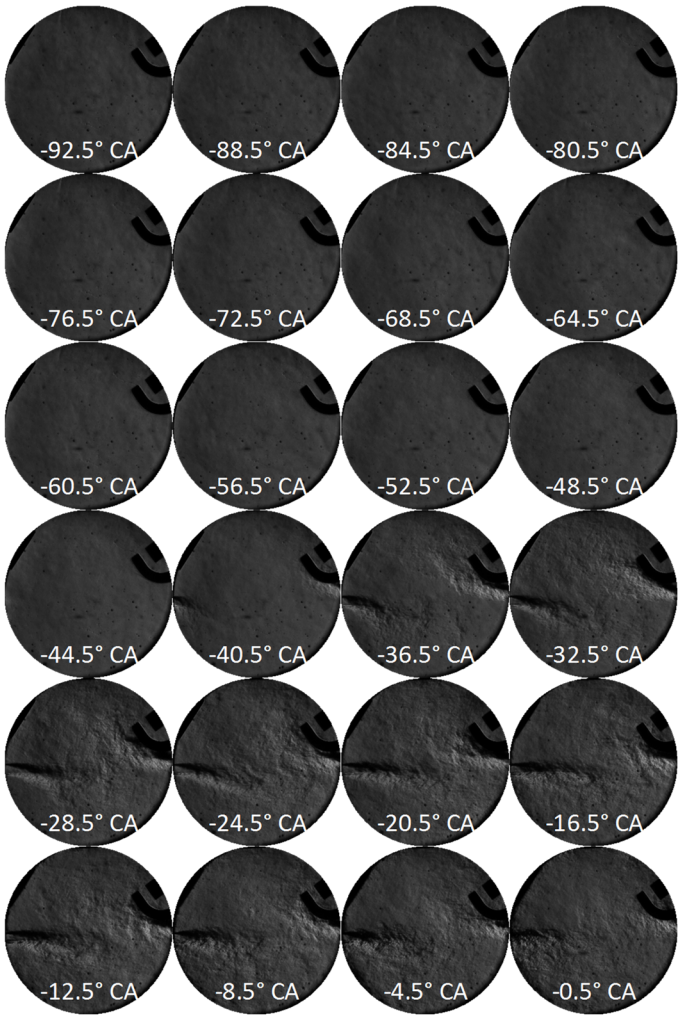

Figure 4.7: Non-vortex schlieren images taken at 5000 RPM from -92.5° CA to -0.5° CA before ignition start; each frame represents 4° CA interval. Timed start of injection takes place at -90° CA for an energized duration of 10° CA.

Figure 4.8: Non-vortex schlieren images taken at 5000 RPM from ignition start (0° CA) to +19.5° CA; each frame represents 0.5° CA interval.

Figure 4.9: Vortex schlieren images taken at 4500 RPM from -92.5° CA to -0.5° before ignition start; each frame represents 4° CA interval. Timed start of injection takes place at -90° CA for an energized duration of 10° CA.

Figure 4.10: Vortex schlieren images taken at 4500 RPM from ignition start (0° CA) to +19.5° CA; each frame represents 0.5° CA interval.

4.7.5 Cylinder Pressure and Heat Release Analysis

Cylinder pressure data are taken using AVL GH12-D transducers and AVL Indismart acquisition system. Thermodynamic statistics for 100-cycle ensemble averages are summarized in Table 4.3 as are corresponding indicator diagrams in Figure 4.11 and 4.12.

Table 4.3 : Summary of thermodynamic statistics at 4500 RPM, 100 cycles.

	Vortex	**Non-Vortex**
IMEP (gross)	Mean: 3.6 bar	Mean: 3.04 bar
	Std. deviation: 0.13 bar	Std. deviation: 0.188 bar
MFB10%	Mean: 2.72° CA	Mean: 2.55° CA
	Std. deviation: 0.478° CA	Std. deviation: 0.912° CA
MFB50%	Mean: 5.55° CA	Mean: 6.01° CA
	Std. deviation: 0.468° CA	Std. deviation: 1.12° CA
MFB90%	Mean: 13.77° CA	Mean: 11.33° CA
	Std. deviation: 5.408 bar	Std. deviation: 1.215 bar
Comb Duration 10-90%	Mean: 11.05° CA	Mean: 8.78° CA
$\mathbf{p_{max}}$	Mean: 35.45 bar	Mean: 35.02 bar
	Std. deviation: 1.333 bar	Std. deviation: 2.019 bar

Both vortex and non-vortex cases show stepped pressure traces during combustion. This is directly visible in the schlieren imaging by pulsations at the interface of the combustion chamber and side channels after the main observable combustion event. This pressure pulsation is because the divided chamber and main cylinder volume connected by long channels form a Helmholtz resonator system. The peak pressures are comparable in light of the small difference in compression ratio. On average, the vortex chamber has a slightly faster 10-50% MFB duration

and reaches p_{max} at an earlier crank angle, but the non-vortex case completes the second half of the heat release significantly quicker. This is due to the very high turbulence of the impinging side air jets that the vortex design does not have.

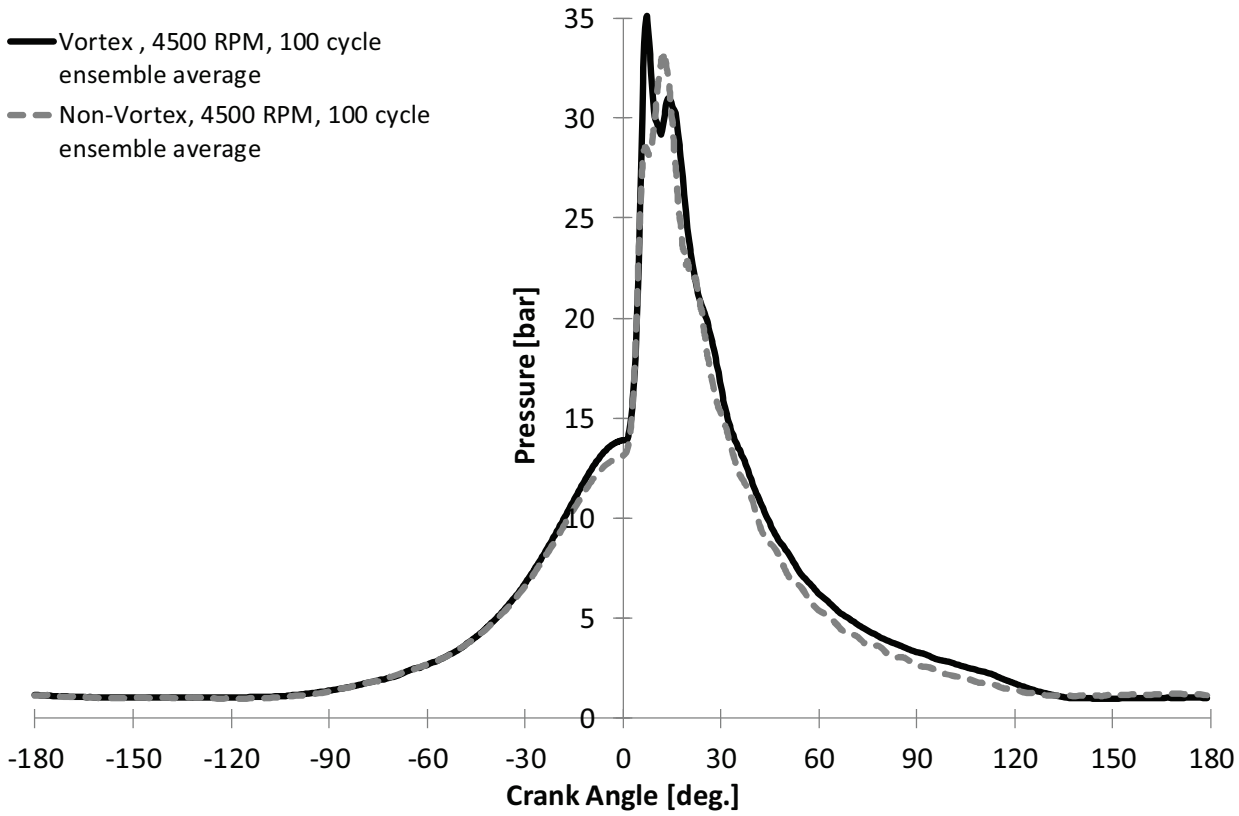

Figure 4.11: Comparison of cylinder pressure indicator diagrams, vortex vs. non-vortex, ensemble averages of 100 cycles at 4500 RPM.

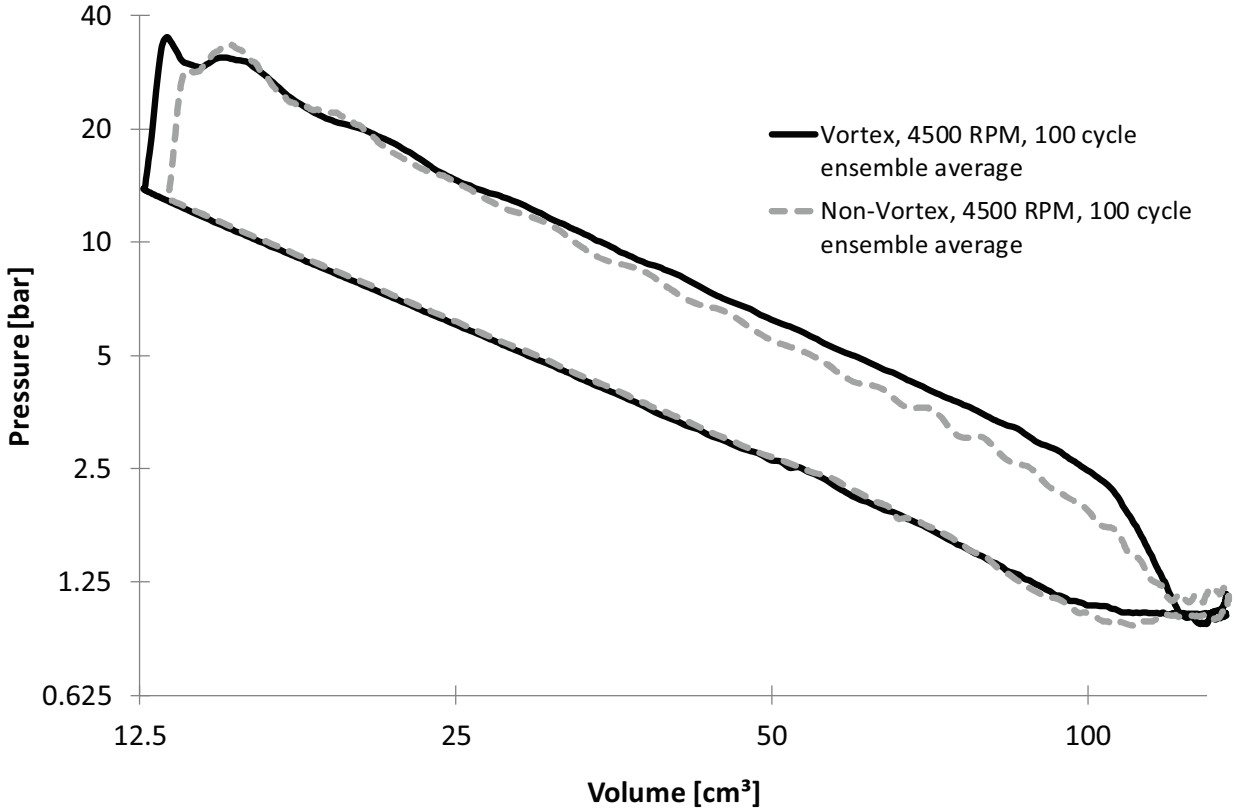

Figure 4.12: Comparison of log P-log V diagrams, vortex vs. non-vortex, ensemble averages of 100 cycles at 4500 RPM.

Looking at Figures 4.11 and 4.12, the vortex chamber shows a higher peak pressure compared to the non-vortex counterpart. The log P-log V diagrams in Figure 4.12 clearly show different slopes of the pressure traces during expansion, indicating differences in the expansion polytropic coefficient n. During compression, heat and mass losses make n lower than the isentropic exponent coefficient, analogously the specific heat ratio $\gamma = C_p/C_v$. During expansion, heat and mass losses make n higher than γ by a similar amount, but γ is lower during expansion due to the higher temperature and changed working fluid composition from a mixture of fuel and air to burned products. Particularly during expansion, however, γ is not known a priori, because the precise gas composition is unknown and moreover, γ varies at elevated temperature (and pressure, to a lesser degree). Also, neither n nor γ remain constant throughout the compression and expansion strokes.

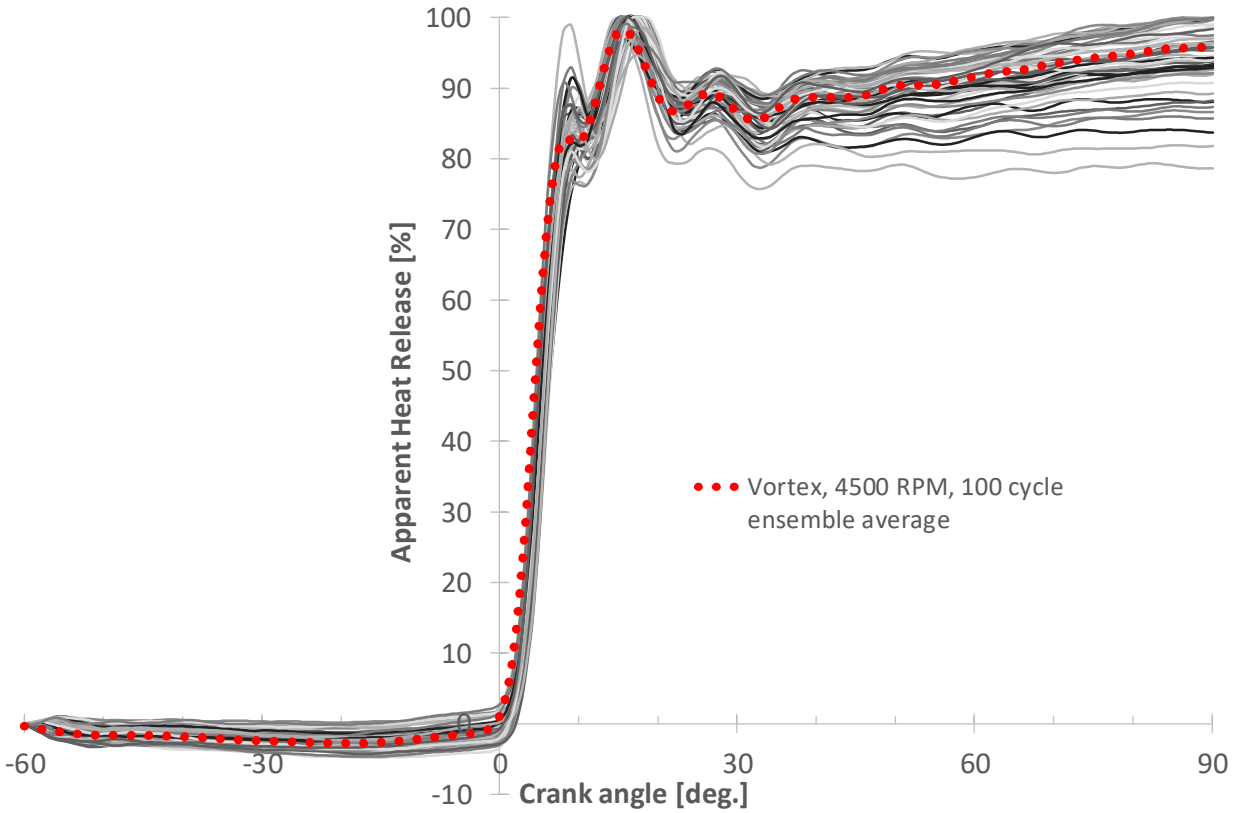

Figure 4.13: Cumulative apparent heat release rate plots of 50 cycles and 100 cycle ensemble average (dotted curve), vortex, 4500 RPM.

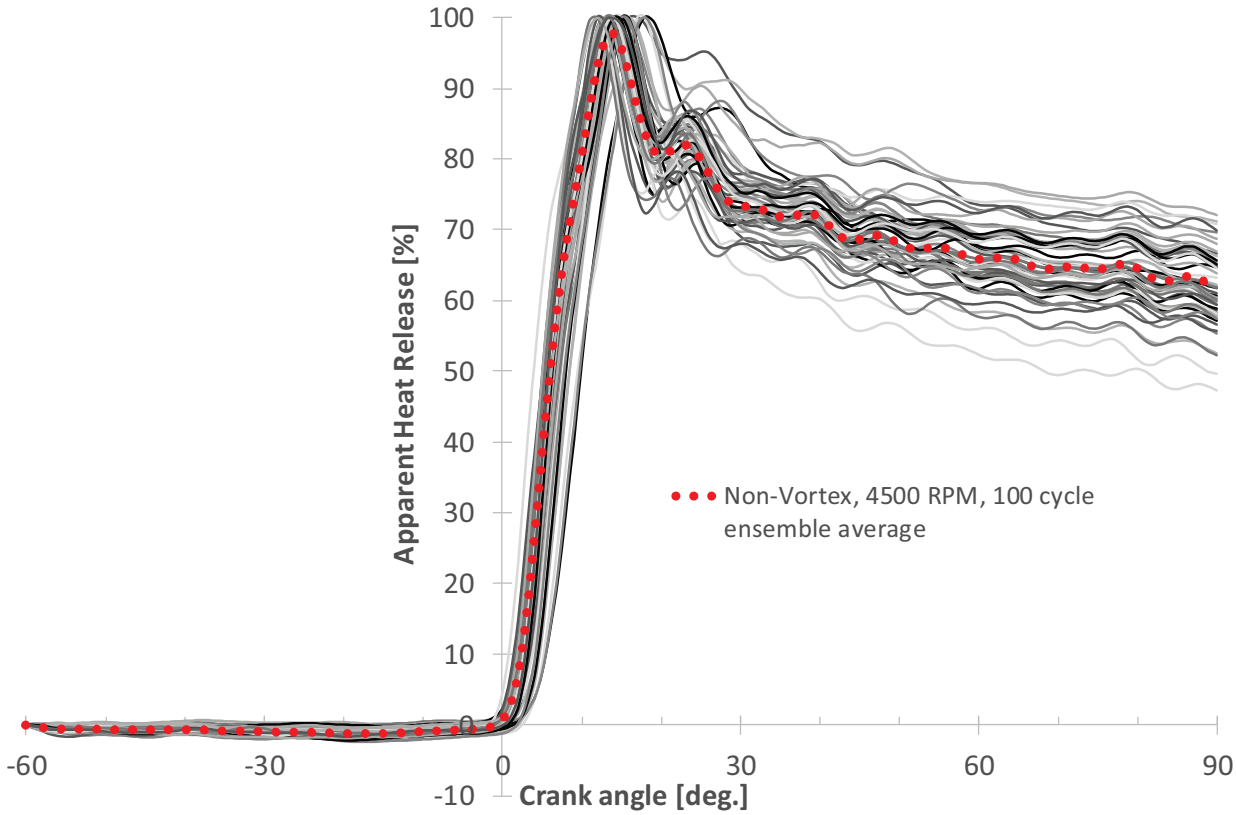

Figure 4.14: Cumulative apparent heat release rate plots of 50 cycles and 100 cycle ensemble average (dotted curve), non-vortex, 4500 RPM.

Nevertheless, calculating the expansion polytropic coefficients on the ensemble averaged cylinder pressure indication data give the mean values for the vortex and non-vortex cases as 1.305 and 1.401, respectively. A constant value of $n = 1.35$ is used for the determination of the apparent heat release curves for both cases plotted in Figures 4.13 and 4.14. These curves are said to be apparent because, in reality, heat release from combustion is irreversible; that is to say, the plots cannot decrease. That they do – particularly as can be seen in Figure 4.14 – is an artefact due to the chosen polytropic coefficient and is not indicative of actual progress of heat release. The magnitude of n, or more importantly its relationship to γ, gives a comparative indication of the heat transfer. During expansion, n cannot be less than γ, which would imply heat transfer from the relatively cold walls to the hot gas, in violation of the Second Law of Thermodynamics.

As Figures 4.13 and 4.14 illustrate, the vortex and non-vortex combustion chambers indicate different heat release behaviors after the reaching their respective peaks. Whereas the vortex design shows heat release gradually continuing late in the expansion stroke, the non-vortex counterpart appears to be losing heat by the declining apparent heat release curves. A rising curve after the peak in the vortex case is due to the chosen expansion polytropic coefficient being higher than is actually the case, that is, overestimating the losses. Conversely, a falling curve is due to n being too low. With a correct polytropic coefficient, the curves would hold constant horizontally. The observed behavior in the heat release curves is consistent with the relationship of the imposed polytropic coefficient with counterparts calculated from the pressure indication data. That the plots fall after the peak in the non-vortex case while rising with the vortex chamber indicate a higher degree of heat wall heat transfer losses in the former due to the deviation of n from γ.

Engines with divided combustion chambers tend to have greater thermal losses than non-divided counterparts on account of the higher surface area-to-volume ratio and high flow velocities through the connecting passages. However, as both concepts compared here are divided chambers with very similar geometries, the magnitude of the difference in polytropic coefficients evaluated at the same engine speed and injection timings between the two combustion chamber designs cannot be attributed solely to differences in heat transfer losses alone. The significantly lower value of n for the vortex case could be explained by the presence of residual unburned hydrogen confined in the center of the combustion chamber. This occurs if the equivalence ratio in this core is richer than stoichiometric. Heat release first peaks and further reaction stops when oxygen is depleted in this core. As the expansion stroke takes place, the mixture comprising burned gas products and unburned fuel in the divided chamber get transported through the side channels into the main combustion chamber, where there is oxygen present to react with the still hot residual hydrogen. On the other hand, the non-vortex design has a homogeneous, overall lean mixture; thus, heat release peaks and ceases once all the fuel is burned.

4.8 Summary

A novel vortex-stratified combustion process has been visualized experimentally in a fired, optically accessible, 2-stroke H2-DI engine with the objective of reducing convective heat transfer losses to the surrounding walls during combustion. This reduction can be realized by confining the fuel-air mixture and thus limiting the extent of the flame to some distance away from the walls and the theoretical background has been explained: This is achieved by air entering into a divided combustion chamber tangentially and preferentially along the circumference due to the Coandă effect. This sets up a vigorous, highly ordered rotational field upon the charge, but mixing with the directly injected fuel is outpaced by the replenishment of air at the periphery, which causes the fuel to be concentrated at the center. Combustion takes place with a flame propagation that initially follows the rotation of the bulk flow but also curls radially inward toward the center as a result of centripetal body forces acting upon the different density burning and unburned gases.

Schlieren images have been recorded at up to 5000 RPM to compare visually the mixture formation and flame propagation characteristics of two combustion chamber designs – one that actualizes a homogeneous mixture without specific charge motion directionality, and another that demonstrates the vortex approach introduced in this work. These visualizations show qualitatively that the vortex process is effective in preventing or delaying the flame from reaching the combustion chamber walls; this is supported by quantitative observations of 0-D cylinder pressure and apparent heat release measurements that indicate higher thermal losses in the non-vortex case. The schlieren observations shall be compared against CFD analyses in the next chapter.

CHAPTER 5 NUMERICAL ANALYSES

Foreword

Authors and affiliation:

David Oh: Doctoral candidate, Université de Sherbrooke, Faculty of Engineering, Department of Mechanical Engineering.

Martin Brouillette: Professor, Université de Sherbrooke, Faculty of Engineering, Department of Mechanical Engineering.

Jean-Sébastien Plante: Professor, Université de Sherbrooke, Faculty of Engineering, Department of Mechanical Engineering.

Date of submission: April 14, 2016

Journal: SAE International Journal of Engines

Reference:

Oh D., Brouillette, M., Plante J., "Reduced Convective Combustion Chamber Wall Heat Transfer Losses of Hydrogen-Fueled Engines by Vortex-Stratified Combustion – Part 2: Numerical Analyses," SAE Int. J. Engines 16JENG0021, 2016.

Titre français : Réduction des pertes de chaleur par convection aux parois de la chambre de combustion des moteurs à hydrogène grâce à la combustion stratifiée par vortex – Partie 2 : Analyses numériques.

Contribution to the document:

This article builds upon the concept of exploiting a vortex-stratified approach to reduce wall heat transfer losses of hydrogen-fueled engines. The previous paper/chapter presented visual evidence of the formation of a radial density gradient using the schlieren approach and also showed the propagating heat release curling toward the centre and being inhibited or delayed from reaching the combustion chamber walls. This article goes into more details to explain and describe this phenomenon using CFD analysis.

Résumé français :

Cet article a pour objectif de mieux comprendre les principes fondamentaux des pertes de chaleur aux parois par convection, afin d'en limiter les effets dans un moteur à injection directe d'hydrogène utilisant une chambre de combustion à vortex stratifié. Une étude comparative CFD 2-D en régime transitoire a 4500 1/min est réalisée entre une chambre à combustion représentant de référence et celle mettant en jeu la configuration stratifiée par vortex. Une réduction d'environ 50% du flux de chaleur convectif de pointe lors de l'utilisation de vortex stratifié est observé. La simulation montre que cette réduction du flux de chaleur avec l'utilisation du vortex est due à une combinaison de deux phénomènes : (1) Le premier est que le temps du mélange diffusif est plus long que le temps de remplissage d'air pur étant donné que l'air remplit le long de la circonférence de la paroi de la chambre de combustion grâce à l'effet Coandă. Il en résulte une stratification de la charge radiale distincte pendant la préparation du mélange lors de la course de compression ; le combustible se retrouve donc concentré au centre alors que l'air essentiellement pur est à la périphérie. (2) Le second phénomène observé est la ségrégation forcée durant le processus de combustion, provoquée par les forces de volume dues à l'accélération gravitationnelle du mélange des gaz avec des densités différentes en rotation rapide. Il n'y a alors pas de combustion en périphérie et la propagation de la flamme se fait vers le centre de la chambre de combustion. La preuve de cela est apportée par l'observation des résultats d'analyse numérique montrant que l'hydrogène, sous l'effet de sa haute température et de sa faible densité, est forcé de rester près du centre de la chambre de combustion, alors que l'oxygène, plus lourd et plus froid, est maintenu en périphérie et ne peut pas aller réagir avec l'hydrogène. En outre, le profil de température commence à courber à une distance de la paroi beaucoup plus grande que l'épaisseur de la couche limite thermique.

Note : À la suite des corrections demandées par les membres du jury, le contenu de cet article peut différer de celui qui sera accepté.

Following the corrections requested by members of the jury, the content of this article may differ from the one that will be accepted.

5.1 Abstract

The fundamentals of convective wall heat transfer losses are elucidated in the context of the desired objective toward its reduction in a direct-injected, hydrogen-fueled internal combustion engine. A comparative, transient 2-D CFD analysis evaluated at 4500 RPM between a combustion chamber design representing current practice and the here-introduced "vortex-stratified combustion" process finds an approximately 50% reduction in the peak convective flux with the latter. The simulation results show that reduced heat flux of the vortex approach is driven by the combination of two effects. The first is finite-time diffusive mixing getting outpaced by the replenishment of pure air being introduced preferentially along the circumference of the combustion chamber due to the Coandă effect; this results in a distinct radial charge stratification during mixture preparation in the compression stroke with a fuel-concentrated center and essentially pure air at the periphery. The second effect is the forced-segregation of different density reactants during the course of the combustion process caused by large body forces that result from the gravitational acceleration of the rapidly rotating charge, thereby constraining the combustible mixture and the flame to some distance from the walls. Evidence for this is observed by hot, low-density hydrogen being forced to remain near the center and cooler, heavier oxygen being inhibited from migrating from the outer periphery to react with the aforementioned hydrogen, and the distinct curvature of the radial gas temperature profile at a substantially greater distance from the wall than the thermal boundary layer thickness.

5.2 Introduction

In the previous chapter, the authors conduct an extensive literature review on hydrogen-fueled ICEs that identify wall-heat transfer as the predominant factor of reduced efficiency in hydrogen-fueled engines and a key to its improvement. It introduces a combustion chamber design using a "vortex-stratified combustion" approach, aiming to isolate the hot burned gas products from the cold combustion chamber walls using an insulating air layer. Experimental evidence from a schlieren optically accessible engine demonstrates the effectiveness of the concept in setting up the vigorous rotational flow field that forms a radial density gradient of the gas mixture before ignition. This gradient is found to be caused by species stratification that results in a fuel-concentrated core at the center of the combustion chamber and a layer of

essentially pure air at the periphery. During combustion, there is visual evidence of the flame propagation being directed radially inward by the effect of centripetal body forces, delaying or inhibiting the contact of hot burned gases with the peripheral combustion chamber walls. This part now provides the numerical analyses of the flow mechanics involved to correlate and explain the experimental observations of the last chapter, and most importantly, quantifies the potential reduction in peak convective wall heat flux in the order of 50% compared to a combustion chamber design that represents current engine practice with high turbulence but no particularly ordered motion and homogeneous charge mixture as an objective, given identical injection timings, boundary conditions and all other parameters in the numerical model.

5.3 Background

Demuynck et al (2009) [76] measured peak heat flux of a CFR SI engine under stoichiometric hydrogen operation to be three times higher than stoichiometric methane at the same power output (the hydrogen case was operated at WOT, but throttled on methane). Total heat loss on an absolute basis is 40% higher for hydrogen. Due to heat release taking place over fewer crank angle degrees on account of the high flame speed, the cooling loss ratio – defined as the total cycle heat loss divided by the released energy during combustion – is about 29% higher. Where the methane case is tested also at stoichiometric and WOT conditions, the hydrogen cooling loss ratio is 52% higher. At $\lambda = 1.5$ ($\phi = 0.67$), the peak heat flux and cooling loss ratio on hydrogen is comparable to that of stoichiometric methane, but power output is only about 75% that of methane.

Watts and Heywood (1980) calculated that in order to increase the brake thermal efficiency by about 10%, heat transfer must be reduced in the order of 50% from the baseline value in low-speed, full-load conditions of two different automotive SI engines investigated [77]. Kamo, Bryzik and Glance (1987) reported on earlier work on a low-heat rejection prototype based on a Cummins turbodiesel engine where ceramic coatings were employed on all combustion-exposed surfaces and the water cooling system was eliminated. Specific heat rejection was reduced by 38% from the baseline engine and dynamometer data indicated a fuel economy gain of 5-10% over the same speed range at full load. Vehicle data indicated a fuel economy benefit in excess of 20% when a domestic road cycle of transient load and speed points

was followed [78]. Oppenheim et al (1996) computed a 24.9% decrease in indicated specific fuel consumption by halving the wall heat transfer [79]. Therefore, it is clear that reducing wall heat transfer losses have significant implications on improving the fuel efficiency of hydrogen-fueled engines, as well as engines operating on any fuel.

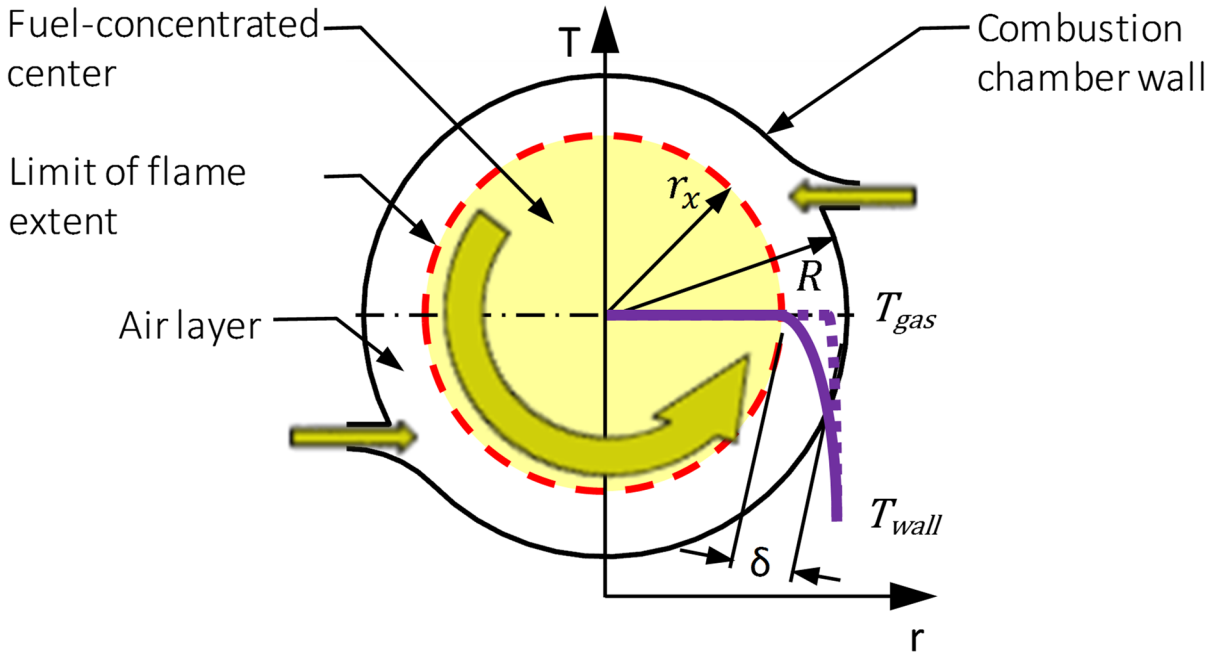

Figure 5.1: Schematic showing the flame-extent stratification process. Incoming air entering into the combustion chamber through the two side channels impart a rotational flow as indicated. Temperature profiles are sketched over with the dashed curve indicating conventional combustion; the solid curve with limited flame extent.

Figure 5.1 presents schematically the vortex-stratified combustion chamber studied in this paper – shown as having a round cross-section of radius R – and how it reduces heat transfer losses. In the combustion chamber of a conventional, homogeneous-charge SI engine the burned gas temperature T_{gas} will take on a nearly constant profile with respect to the radius, with a drastic reduction at the thermal boundary layer close to the wall until matching that of the gas-side wall surface T_{wall}, as sketched qualitatively with the dashed curve. If the combustible charge could be confined to a radius r_x leaving a distance δ from the wall, the temperature profile would take on a more gradually declining shape as illustrated by the solid curve, beginning at the limiting extent of the flame due to the presence of a fuel-air mixture within

flammability limits illustrated by the shaded core. Should δ be greater than the boundary layer thickness and inherent flame quenching distance, a reduction in convective heat flux results. The mechanisms of this phenomenon are explained in the following.

5.3.1 Convective Heat Transfer Fundamentals

All three heat transfer modes of conduction, convection, and radiation are simultaneously active in the working gas. However, Borman and Nishiwaki (1987) state that for SI engines, heat transfer due to gas radiation is small (<10 %) compared to convection [80] and is thus not considered here. The heat transfer rate or flux $\dot{Q}_{wall}$, which includes the effects of gas conduction and convection, is described by Equation 5.1, with A being the surface area:

$$\dot{Q}_{wall} = h \cdot A \cdot \left(T_{gas} - T_{wall}\right) \tag{5.1}$$

The empirically derived heat transfer coefficient h is related to the Nusselt number, which is a function of the Reynolds and Prandtl numbers, where m and n are constants:

$$Nu = \frac{h \cdot l}{k} \propto Re^m \cdot Pr^n \tag{5.2}$$

$$Re = \frac{\rho \cdot v \cdot l}{\mu} = \frac{v \cdot l}{\nu} \tag{5.3}$$

$$Pr = \frac{\rho \cdot \nu \cdot C_p}{k} = \frac{\mu \cdot C_p}{k} \tag{5.4}$$

Heywood [25] cites works that propose the use of the flat-plate forced-convection heat transfer correlation formula:

$$\frac{h \cdot l}{k} = 0.036 \cdot \left(\frac{\rho \cdot v \cdot l}{\mu}\right)^{0.8} \cdot \left(\frac{\mu \cdot C_p}{k}\right)^{0.333} \tag{5.5}$$

Collection and arrangement of the terms give an expression for the surface area-specific heat flux as:

$$\dot{q}_{wall} = \frac{\dot{Q}_{wall}}{A} \propto \frac{\rho^{0.8} \cdot v^{0.8} \cdot k^{0.667} \cdot {C_p}^{0.333}}{\nu^{0.4\ 67} l^{0.2}} \cdot \left(T_{gas} - T_{wall}\right) \tag{5.6}$$

Or, in terms of dynamic instead of kinematic viscosity:

$$\dot{q}_{wall} \propto \frac{\rho^{0.333} \cdot v^{0.8} \cdot k^{0.667} \cdot {C_p}^{0.333}}{\mu^{0.4\ 67} l^{0.2}} \cdot \left(T_{gas} - T_{wall}\right) \tag{5.7}$$

By inspection of the magnitudes of the exponents, it is clear that the largest contributing parameters to wall heat transfer are the temperature gradient, as well as the flow velocity and density within the Reynolds number term, so any systematic approach to its reduction should fundamentally be focused in these areas. To address the temperature on the wall side, extensive research has been done in so-called "adiabatic" engines [78, 81], and current investigations into "low-temperature combustion" (LTC) schemes like HCCI [82], PPC [83] and RCCI [84] are in vogue, partially due to the efficiency gains afforded by reduced wall heat losses from lower burned gas temperatures using highly dilute mixtures typical of these processes. However, it is overly simplistic to conclude that one should only indiscriminately reduce the temperature difference or turbulence, as these would give rise to other compromises and complex interactions in practical engine realization and operation, as seen in the presented development challenges of adiabatic and HCCI engines.

5.3.2 Charge Density Effect On Turbulence And Heat Transfer

LeFeuvre et al (1969) showed that increasing the density ratio results in increasing heat flux in a Diesel engine at fixed operating speed, nominal equivalence ratio and injection advance [85]. Alkidas and Myers (1982) showed in a gasoline SI engine that an increase in volumetric efficiency corresponding to an increase of peak gas pressure in from 2363 to 3581 kPa results in peak heat flux increasing 19% to 30% depending on the location of the polled sensor reading in the cylinder head [86]. Demuynck et al (2009) showed that under motored conditions, the measured heat flux in their setup during WOT is about twice that for closed throttle. However, they report that the flux is higher at 75% throttle opening than even the WOT case; the lower cylinder density is more than offset by increased overall turbulence as a result of the butterfly throttle angle upstream from the intake ports [76].

At a given part-load operating point, a hydrogen-fueled engine, by virtue of lean operation, will require less intake air throttling. This will trap a higher mass of fuel-air charge in the cylinder compared to a stoichiometric gasoline case, independent of whether mixture formation is accomplished externally to the cylinders or by direct injection. This will result in higher charge density at the start of ignition. Consequently, turbulence levels and heat transfer coefficients will also be higher by their dependence on the Reynolds number (see Equation 5.3)

and the density term in Equations 5.6 or 5.7. However, despite the inevitable effect that higher charge density has on increasing heat transfer, it is not the focus of this study.

5.3.3 Heat Transfer Effects From Fuel Properties

Hydrogen possesses a faster laminar flame speed than gasoline, between factors of 5-6.5 at stoichiometric fuel-air ratios [8,19]; however, in practice, hydrogen-fueled engines are not typically operated globally and homogeneously stoichiometric due to NOx emissions and high sensitivity to abnormal combustion. At hydrogen-air equivalence ratios of $0.3 < \phi < 0.5$, the laminar flame speed is of comparable magnitude to stoichiometric gasoline-air mixtures. Where the hydrogen equivalence ratio is 0.6, the laminar flame speed is about twice that of stoichiometric gasoline.

Adiabatic flame temperatures are also of comparable magnitude for both stoichiometric hydrogen-air and gasoline (analogously isooctane)-air mixtures; Verhelst and Wallner (2009) [8] report a value of 2390 K for stoichiometric hydrogen-air and 2276 K for stoichiometric isooctane-air (all values at 300 K and 1 atm initially). The hydrogen-air values are very similar to those from Drell and Belles (1958) [87] and Das (1996) [88]. However, White et al reports the adiabatic flame temperature for a stoichiometric gasoline-air mixture to be higher than hydrogen-air at 2580 K [19]. These differences turn out to be trivial for the present purposes because, again, only overall lean hydrogen combustion is so far found to be of relevance in practical engines. The equilibrium adiabatic flame temperature at $\phi = 0.5$ for hydrogen-air is 1643 K according to Drell and Belles.

Both flame speed and temperature increase with initial temperature and pressure, especially for near-stoichiometric mixtures, although the pressure effects on flame temperature are minimal at both extremes of equivalence ratios ($0.5 > \phi > 4$) between 0.01 – 100 atm. Nevertheless, experiments have shown that wall heat transfer losses for hydrogen-fueled engines are significantly higher than the same engine operating on stoichiometric gasoline at the same operating load and speed [8,44]; an increase is evident even when the hydrogen case operates significantly lean of stoichiometric as shown by several researchers [41, 89]. These results contradict the similar (in stoichiometric) or lower flame temperatures in lean hydrogen

combustion, compared to stoichiometric gasoline, even when charge density-induced turbulence and flame speeds – with heat release rates by consequence – are taken into account. Therefore, some other mechanism or mechanisms must be responsible for the higher measured wall heat flux and focusing upon this area would be the key to reducing the rejection losses and thus contribute to improving the efficiency of internal combustion engines.

5.3.4 Flame Quenching Distance

One mechanism affecting the heat flux is the quenching distance due to its effect on the temperature gradient between the burned gas and the wall; greater heat flux follows a higher gradient. This distance is much lower for hydrogen flames than for hydrocarbon fuels like methane, propane and isooctane. Table 5.1 summarizes the relevant properties of these fuels:

Table 5.1 : Quenching distance between parallel plates for various fuels and equivalence ratios in air at 1 atm, 298 K.

Fuel and equivalence ratio	Quenching distance, cm
Hydrogen $\phi = 1$	0.063 [87]
Hydrogen $\phi = 0.5$	0.08 [87]
Methane $\phi = 1$	0.21 [90],0.23 [91]
Propane $\phi = 1$	0.205 [91], 0.203 [92]
Isooctane $\phi = 1$	0.22 [93]†

†At 100°C

The quenching distance is not constant but rather a function of both pressure and mixture composition, decreasing with increasing pressure and also with increasing equivalence ratio up to the stoichiometric value, whereupon quenching distances increase with even richer mixtures. Drell and Belles state that it may be assumed that the quenching distance decreases as the temperature of the mixture (and of the surface) is raised [87]. The same pressure and air-fuel ratio dependence are also observed in a wide variety of hydrocarbon fuels [90, 91, 92, 93].

Once all the likely factors to influence the higher observed wall heat transfer in hydrogen-fueled engines compared to gasoline ones are taken into account – flame temperature;

heat release rate; trapped charge density; and in-cylinder turbulence levels – it becomes apparent that the key to the wall heat rejection losses in hydrogen-fueled engines lies in the flame quenching distance and this should be the focus of measures toward the reduction of these losses.

5.3.5 Vortex-Stratified Combustion

In light of this, a sensible approach is to confine the extent of the fuel-air charge and thus the flame to some distance away from the walls, as previous works already cited have attempted by means of fuel injection strategy [47] and the use of air blast injections [49]. The authors introduce and elucidate in the Chapter 4 a novel 2-part mechanism of achieving this. First, by setting up a rotating vortex flow in the combustion chamber and exploiting the Coandă effect, diffusive mixing with fuel is outpaced by the replenishment of pure air being introduced preferentially along the circumference, resulting in a distinct radial charge stratification during mixture preparation in the compression stroke with a fuel-concentrated center and essentially pure air at the periphery. The second effect is the forced-segregation of different density species during the course of the combustion process caused by large body forces that result from the centripetal force acceleration of the rapidly rotating charge, thereby causing the propagating flame front to curl radially inwards and constraining it at some distance away from the outer walls, as have been observed by Lapsa and Dahm (2009) in experiments using premixed propane in a U-shaped channel [63].

In order to perform a first-order, analytical estimate of the potential for wall heat transfer reduction by means of flame-extent confinement, Fourier's Law used to formulate gas-side thermal conduction could be applied for convection by substituting the conductive coefficient k for the appropriate relation with an effective convective coefficient h, and analogize a solution as a concentric superposition of thermal resistances as shown in Figure 5.2, also known as cylindrical shells.

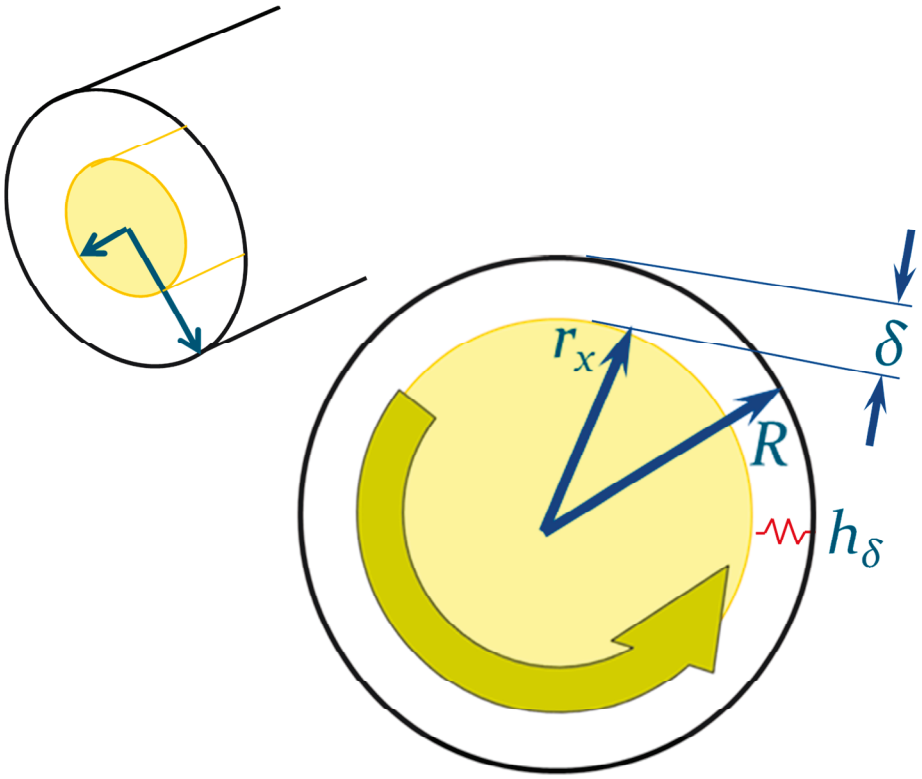

Figure 5.2: Schematic showing a first-order analytical consideration of heat transfer using the analogy of thermal resistance or cylindrical shells.

In the following relationship, derived from Equation 5.2 with R in place of the characteristic length dimension l, the subscript δ denotes the respective fluid properties in the non-combusting stratification zone and the overbars denote averaged values:

$$\overline{h_\delta} = \frac{\overline{k_\delta} \cdot \overline{Nu_\delta}}{R} \tag{5.8}$$

Solving the differential equation for Fourier's Law and substituting Equation 5.8, where r_x is the limit extent radius of the burned gas:

$$\frac{\dot{Q}}{A} = -k \frac{dT_{fluid}}{dr} \tag{5.9}$$

$$\frac{\dot{Q}}{2\pi l} \int_{r_x}^{R} \frac{1}{r} dr = -\overline{k_\delta} \int_{T_{gas}}^{T_{wall}} dT_{fluid} \tag{5.10}$$

$$\dot{Q} = \frac{2\pi l \overline{k_\delta}}{\ln\left(\frac{R}{r_x}\right)} \left(T_{gas} - T_{wall}\right) \tag{5.11}$$

$$\therefore \dot{Q} = \frac{2\pi l \overline{h_\delta} R}{\overline{Nu_\delta} \ln\left(\frac{R}{r_x}\right)} \left(T_{gas} - T_{wall}\right), r_x < R \tag{5.12}$$

For the same envelope geometry, temperature delta and fluid properties, the difference in heat fluxes between any two compared cases is limited only to the term $\ln\left(\frac{R}{r_x}\right)$. In the case of a homogeneous fuel-air mixture, we take $R - r_x = \delta$ to be the flame quenching distance. With $R = 10\,mm$ and $r_x = 8\,mm$ imposed by the vortex stratification process – a value obtained from CFD analysis presented later in this paper from schlieren imaging and CFD analysis presented later in this paper – the heat transfer rate is reduced by 71% compared to the homogeneous case. Equation 5.12 is useful for another purpose: consider that the stoichiometric flame quenching distance of methane (see Table 5.1) is similar in magnitude to the flame-extent limit of the hydrogen vortex-stratified case just calculated, and the 243% increase of the heat flux $\dot{Q}$ of the homogeneous stoichiometric hydrogen result agrees reasonably well with the factor 3 higher peak heat flux reported by Demuynck et al (2009), noting that the stoichiometric adiabatic flame temperature of methane is in the order of 200 K lower than the hydrogen counterpart.

5.4 Numerical Analysis

CFD analyses are performed in ANSYS® Fluent (V16.2). In order to minimize solution time, they are performed in 2-D rather than 3-D space, greatly reducing the number of cells. This is a reasonable approximation given the nature of the flow field. In all cases considered, the models employ the RANS approach due to its low computational expense compared to LES and DNS. In the present study, the pressure-based, coupled pressure-velocity solver is used with second-order upwind discretization of all variables. The Realizable k-ε turbulence model is used here, having been compared and employed extensively amongst other turbulence models against experimental validations in investigations of engine in-cylinder flow featuring under-expanded hydrogen direct injection [94, 95].

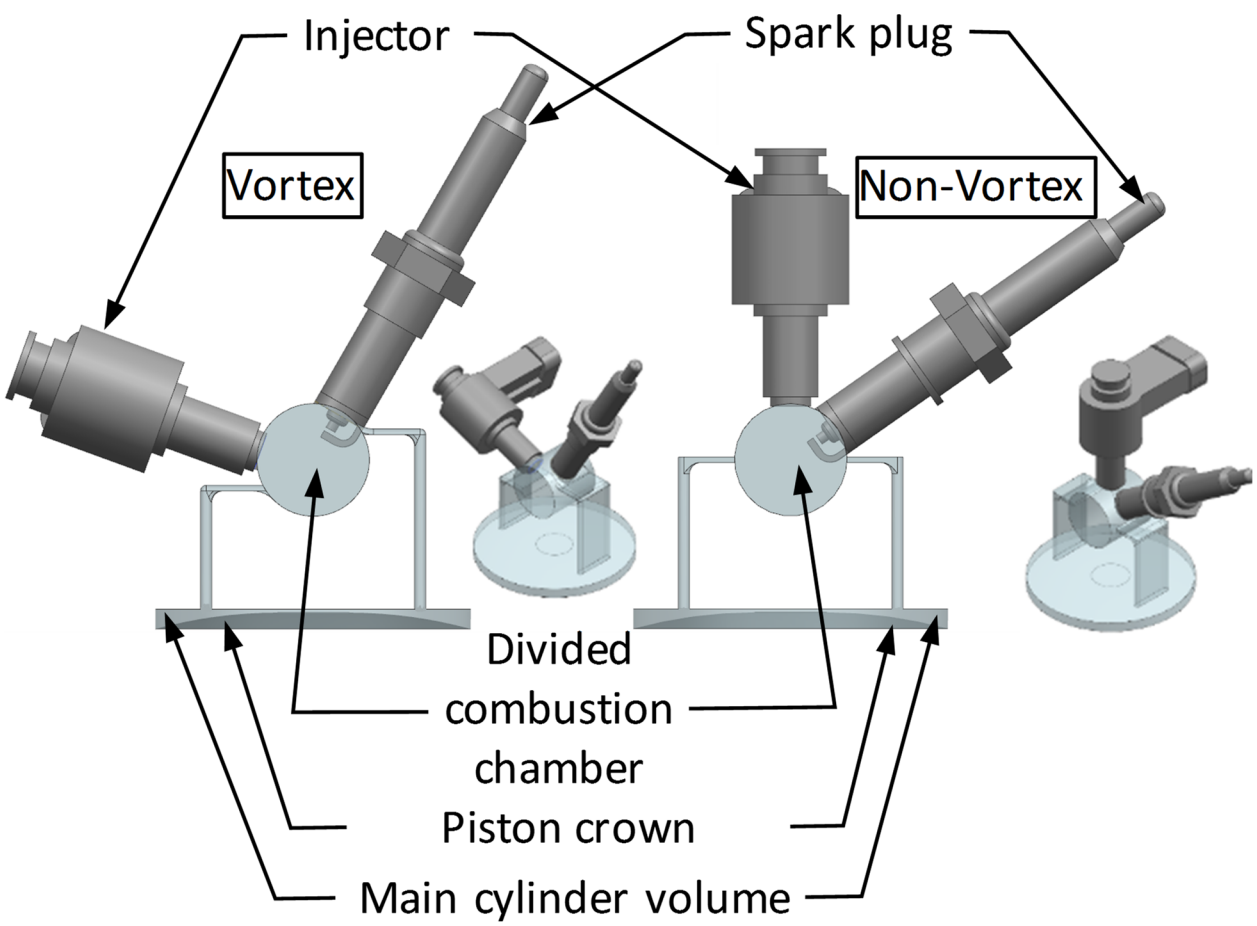

Figure 5.3: CAD renderings of vortex (left-half) and non-vortex (right-half) combustion chambers with injector, sparkplug and main cylinder volume at TDC.

Figure 5.3 shows 3-D solid models of the vortex and non-vortex the combustion chambers. Only the fluid-exposed surfaces are shown along with the respective locations of the injector and spark plug, without the surrounding engine body.

Figure 5.4 shows the computational domain and meshes of the 2-D faces, taken to be the mid-plane cross-sectional cuts of the 3-dimensional parts. The protruding spark plug electrodes are neglected. The outward-opening poppet valve-type hydrogen injectors, which in reality would form a moving annulus, are simplified in the model as being fixed.

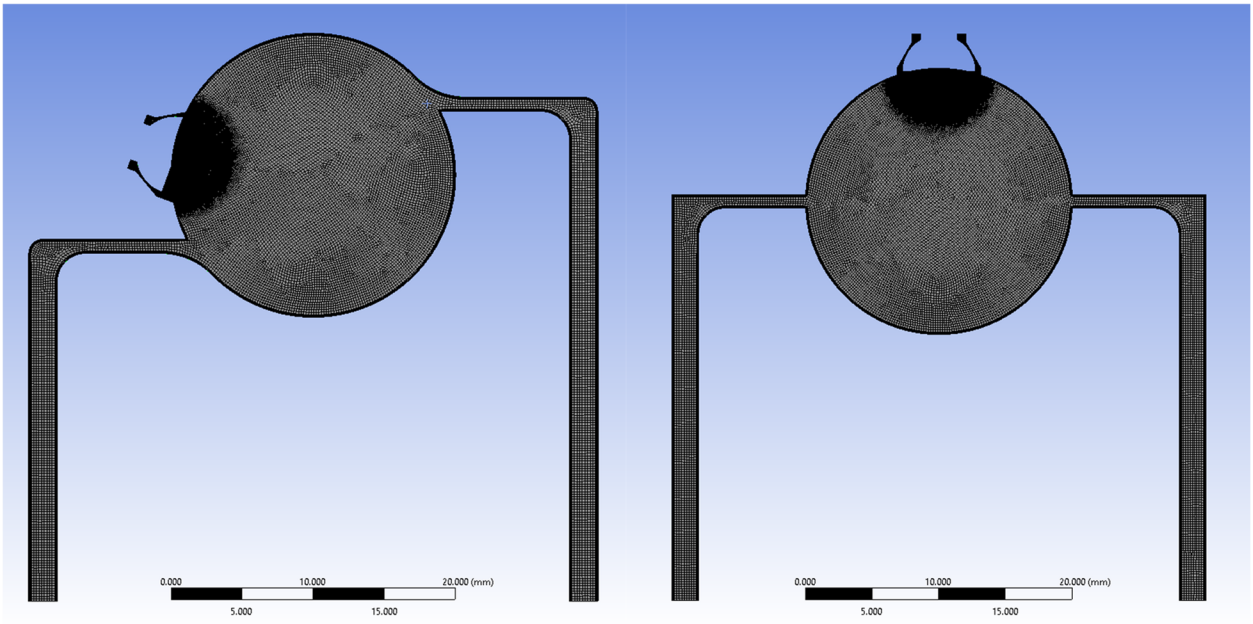

Figure 5.4: Vortex (left-half) and non-vortex (right-half) combustion chamber meshes showing local refinement in the area around the injector.

Sensitivity analyses of mesh density and timestepping were first preliminarily conducted. Particular refinement is necessary in four zones of the combustion chamber mesh:

- Near the walls;
- Internal gas injector geometry;
- In the area near the modeled spark ignition source;
- In the region of very high velocities of the under-expanded hydrogen injection jets.

The vortex combustion chamber geometry generally has been found to have more rigorous sensitivities to mesh refinement, timestepping and underrelaxation factors. For equal treatment and comparability of results the more conservative settings of either case are simultaneously applied to both the vortex- and non-vortex cases. In fact, the sole difference in the simulations distills only to the vortex- and non-vortex geometries. For non-injection and ignition/combustion events, a timestep value of 1.85185E-5 seconds corresponding to 0.5° crank angle intervals at 4500 RPM proves sufficient, but during injection and ignition/combustion, the interval must be shortened to 0.25° CA (9.25926E-6 seconds). Rather than having different time step intervals between the injection, ignition and combustion events from the rest of the

simulated cycle, it was decided to choose a single fixed timestep interval at the more conservative value, that is, 9.25926E-6 seconds. After initializing the model with the default underrelaxation factors and flow Courant number until start of injection, the latter is reduced from 200 to unity for the rest of the simulation. The underrelaxation factors need to be progressively reduced during the course of the simulations for residuals stability, reaching the convergence criteria acceptably rapidly and avoiding floating-point exceptions.

Rather than performing intricate manual mesh refinements in each of the aforementioned zones and in the area of highest velocity of the under-expanded hydrogen jet, customized for nozzle configuration as done by Scarcelli et al (2011) [96], or using an adaptive mesh refinement (AMR) technique as done by Lin (2010) [97], Sukumaran and Kong (2010) [98] and Le Moine et al (2015) [99] – moreover for the very different bulk flow regimes of each of the vortex- and non-vortex cases here – the whole combustion chamber uses the finer mesh near the ignition source and additional local refinement is reduced to 2 operations applied consistently to both geometries:

- Near wall region;
- Internal injector geometry and under-expanded jet region encapsulated within a sphere of influence of 4mm diameter centered on the injector valve.

The combined result of the above actions increases the number of timesteps by 33% and double the number of nodes over what is considered optimum solely from a sensitivity analysis without local refinement. However, this is a luxury permitted by 2-D models where the final meshes only have about 35000 elements rather than millions in 3-D models. Any slowdown in solution time due to the added node and timestep counts is far more than offset in the convergence behavior, permitting the entire solution to be completed in less than half the total number of iterations and overall faster wall clock time using the same convergence criteria. Moreover, the differently tailored mesh refinements and timestep intervals that would be required for the vortex- and non-vortex cases greatly increase pre-processing effort and make it impossible to have identical models that compare only the substantive differences due to the respective geometries. This was considered to be of paramount importance over sensitivity optimization and was therefore an area of considerable time spent. All other parameters (e.g.,

employed physics and their settings/constants; boundary/initial conditions and underrelaxation factors) are kept the same.

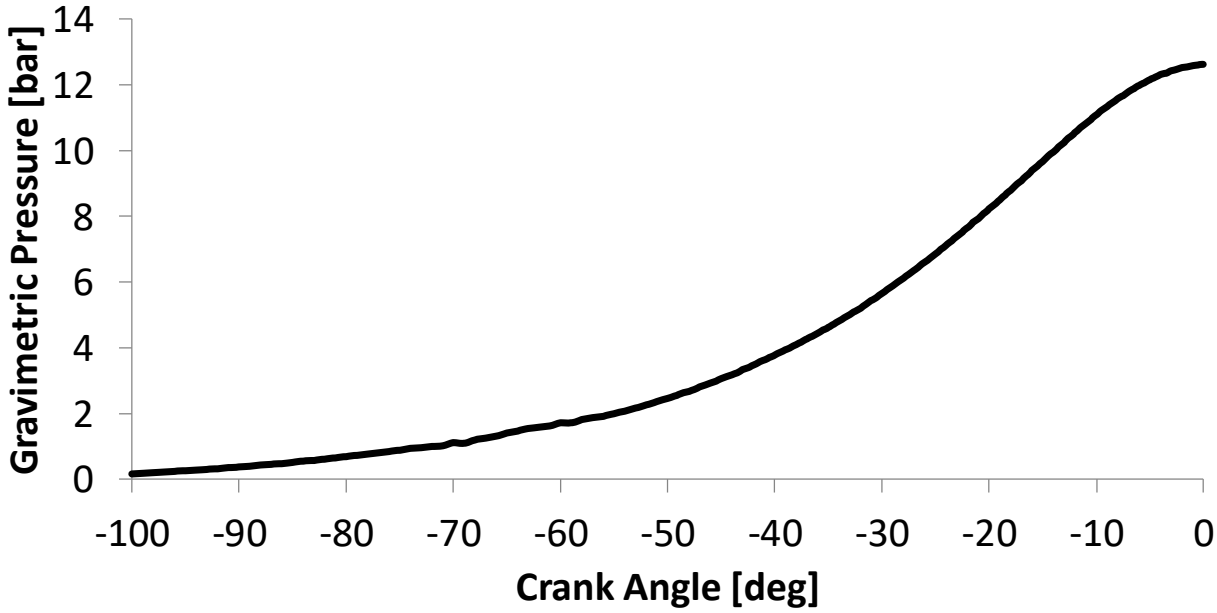

Figure 5.5: Chamber pressure profile during the compression stroke from ensemble average of experimental measurements.

The model replaces the deforming mesh of a moving piston with an ensemble-averaged cylinder pressure profile during the compression stroke from experimental measurements, as shown in Figure 5.5, applied as a boundary condition at the open end of the channels. Instead of modeling the moving injector valve lift with deforming meshes, at the end of the timestep before start of injection, the simulation stops and the wall boundary condition upstream of the injector throat is changed to a pressure inlet and the imposed pressure follows the profile shown in Figure 5.6. Start of injection occurs at -90° CA with a duration of 10° CA. The throat clearance of the injector valve from its seat is 200 microns. It is neither the realistic possibility nor the intention to match the hydrogen flow rates of the numerical models with the metal engine exactly. This is partly due to the fact that the experimental optical engine is run at low loads (IMEP ≈ 3-3.5 bar) for protection of the equipment and safety. These imply lean overall equivalence ratios and is not a good showcase of the heat flux difference of the two combustion chamber designs. Furthermore, optical observations show noticeable hydrogen leakage even when the injector valve is not energized. Therefore, there is some quantity of injected hydrogen

in the experiments that is not accounted for in the numerical models. By dispensing with the main cylinder and its moving piston in the model, any hydrogen that backflows outside of the domain under investigation is lost, rather than entering into the main cylinder volume and is reintroduced when the piston displaces the contents back into the combustion chamber; therefore, numerical results are to be evaluated on the background of identical injection timing and trapped average hydrogen mole fraction. Again, this is a justified simplification given the objective of comparing the heat transfer and thermodynamic properties of the two combustion chamber designs. At the end of injection, the boundary condition is changed again to a wall and the simulation is resumed.

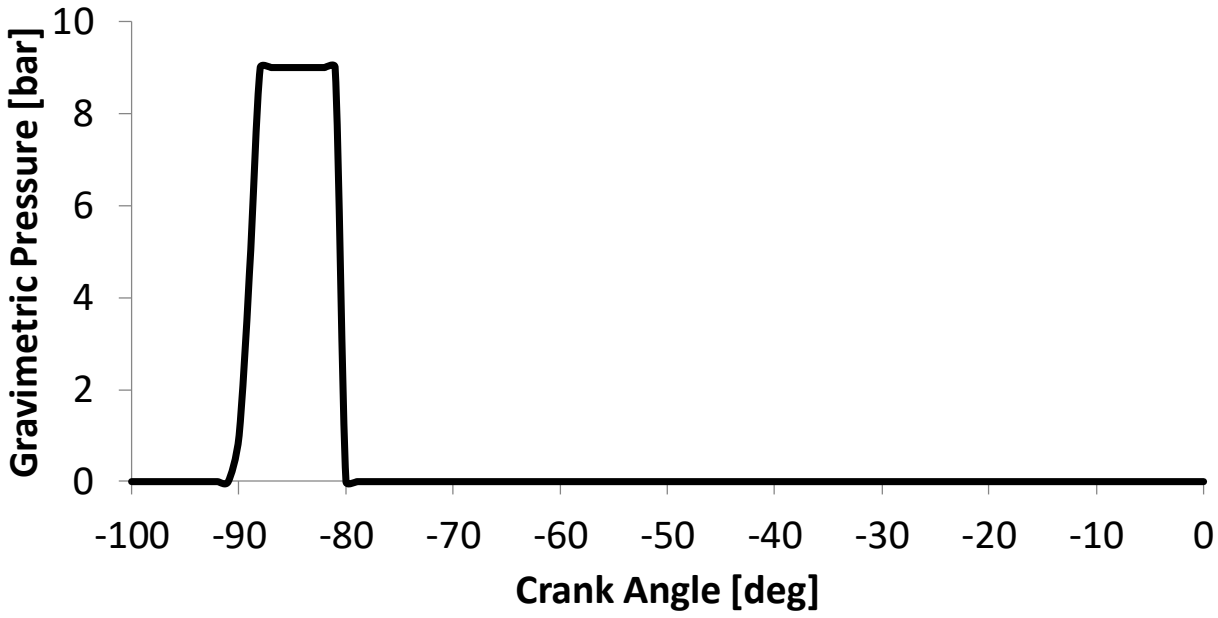

Figure 5.6: Fuel injection profile used for pressure inlet boundary condition.

At the end of the timestep before TDC, which corresponds with start of ignition, the simulation is stopped again and the pressure-inlet boundary conditions at the ends of the side channels connecting to the main cylinder volume are changed to walls and the simulation restarted. This is a big deviation from the metal engine and, in effect, combustion is thus modeled as taking place at constant volume. This has the implication of giving the worst-case wall heat flux, but recalling the prime objective of this study only to compare heat transfer losses between the vortex- and non-vortex principles under otherwise identical parameters, this simplification is justified.

The C-equation partially premixed combustion model is used [100], as is the turbulent flame speed model by Peters [101] and Enhanced Wall Treatment for the near-wall modeling [102]. Model constants are left at the default values.

Because of these simplifications and the lack of experimental data for model validation, the CFD results cannot be taken to be identical to the experimental schlieren observations in the Chapter 4. They are, however, similar and thus useful to make qualitative comparisons for validating the important phenomena seen in both, such as the deflection of the incoming air jets in the non-vortex combustion chamber; the formation of a radial density gradient by way of a visible center "bulge" in the vortex case; and bending of the burned gas zone radially inwards due to gravitational effects, observed in both the experimental schlieren images and numerically derived counterparts.

Post-processing of the CFD results permits deriving the density gradient, thereby enabling the possibility to render "pseudo-schlieren" images from the numerical analyses that can then be compared qualitatively with experimentally obtained counterparts from the optical engine investigations. Figures 5.7 and 5.9 show these images for the non-vortex chamber in the compression stroke/mixture preparation and combustion phases, respectively. These are obtained by performing a secondary gradient operation to the recorded density data. As a matter of fact, the images represent the partial derivative in the x direction, giving rise to alternating dark and light bands on either horizontal side of the gradient. The presented images are optimized for visual contrast to highlight the important phenomena and not to attempt exact correspondence to selected experimental schlieren images compared against, which are elucidated in Chapter 4.

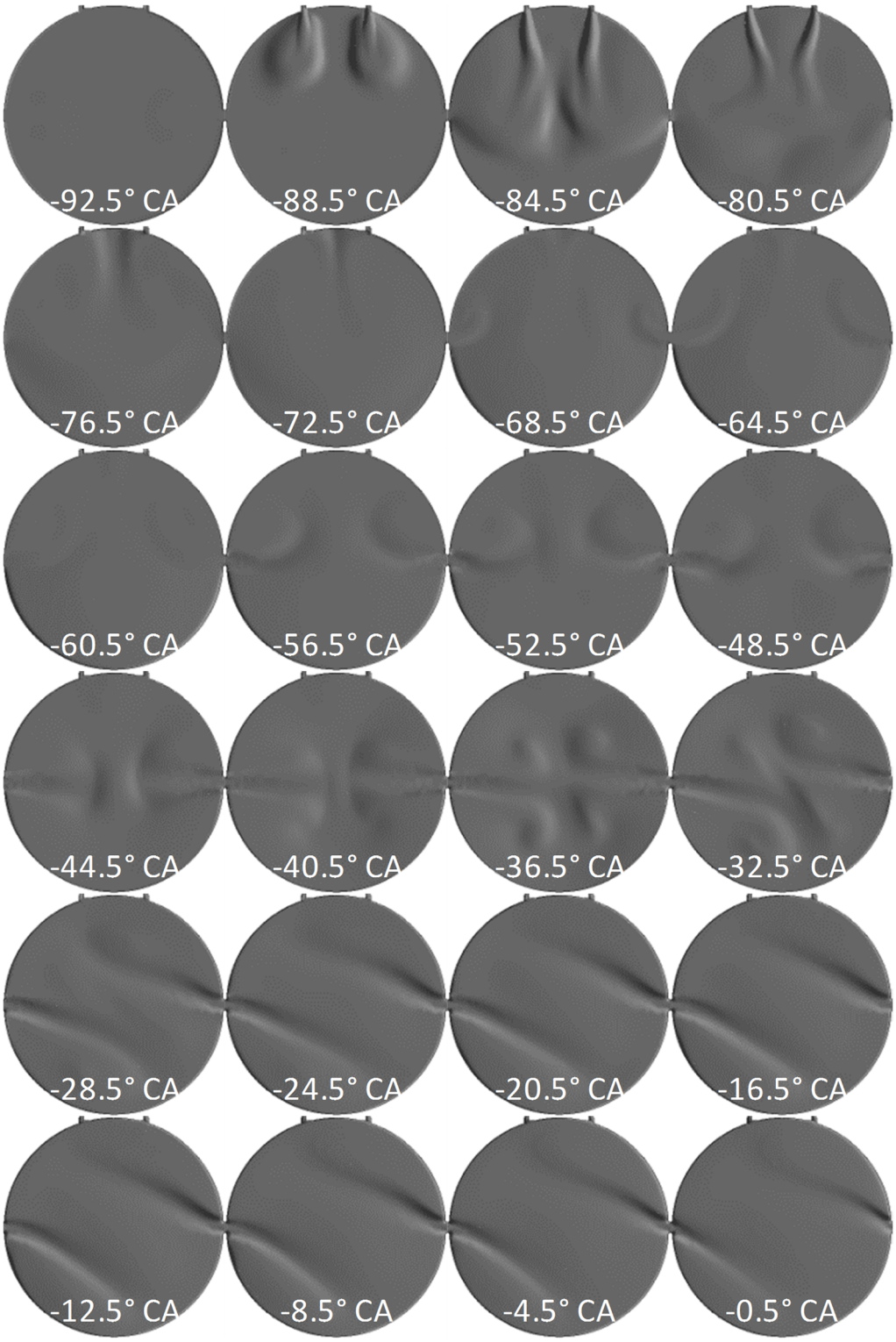

Figure 5.7: Transient density gradient (pseudo-schlieren) images of the non-vortex combustion chamber. Each image represents 4° crank angle for the interval of -92.5° to -0.5° CA.

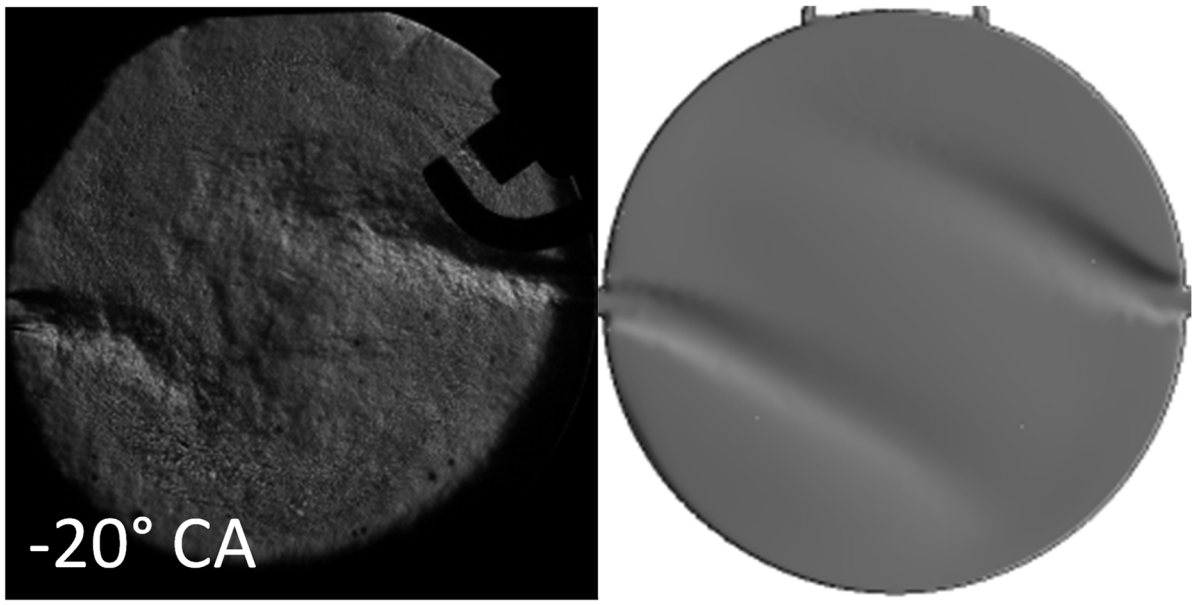

Figure 5.8: Comparison of experimental schlieren (left) and CFD pseudo-schlieren (right) images of non-vortex chamber at -20° CA.

After fuel injection, air enters into the combustion chamber from the side channels by the action of rising cylinder pressure. Two jets are seen first to impinge radially against one another (Figure 5.7, fourth row, left 2 frames) and then each jet deflects to one side either above or below the horizontal centerline. The same behavior is also seen in the experimental schlieren images, see Figure 5.8. This could be explained in the metal engine by perturbations either by the asymmetry of the chamber geometry (e.g. presence of the spark plug and sensors) or to pre-existing anisotropy in the flow; however, there is no physical spark plug or sensors in the model. This lends credibility that the CFD models properly capture the important flow phenomena observed in engine experiments.

Figure 5.9 shows the progress of density gradient beginning from start of ignition. Spark ignition is modeled as circular in 2-D; an initial radius of 1 mm is defined and can be seen on the upper right of the chamber with its center corresponding with the coordinates of the actual sparkplug gap (see Figure 5.9, first row). The front of the density gradient substantially traverses the face of combustion chamber about 10° CA after start of ignition. Density gradient signals from the side channels are visible after combustion as a result of gas oscillations due to the modeled wall boundary condition at the ends of the side channels.

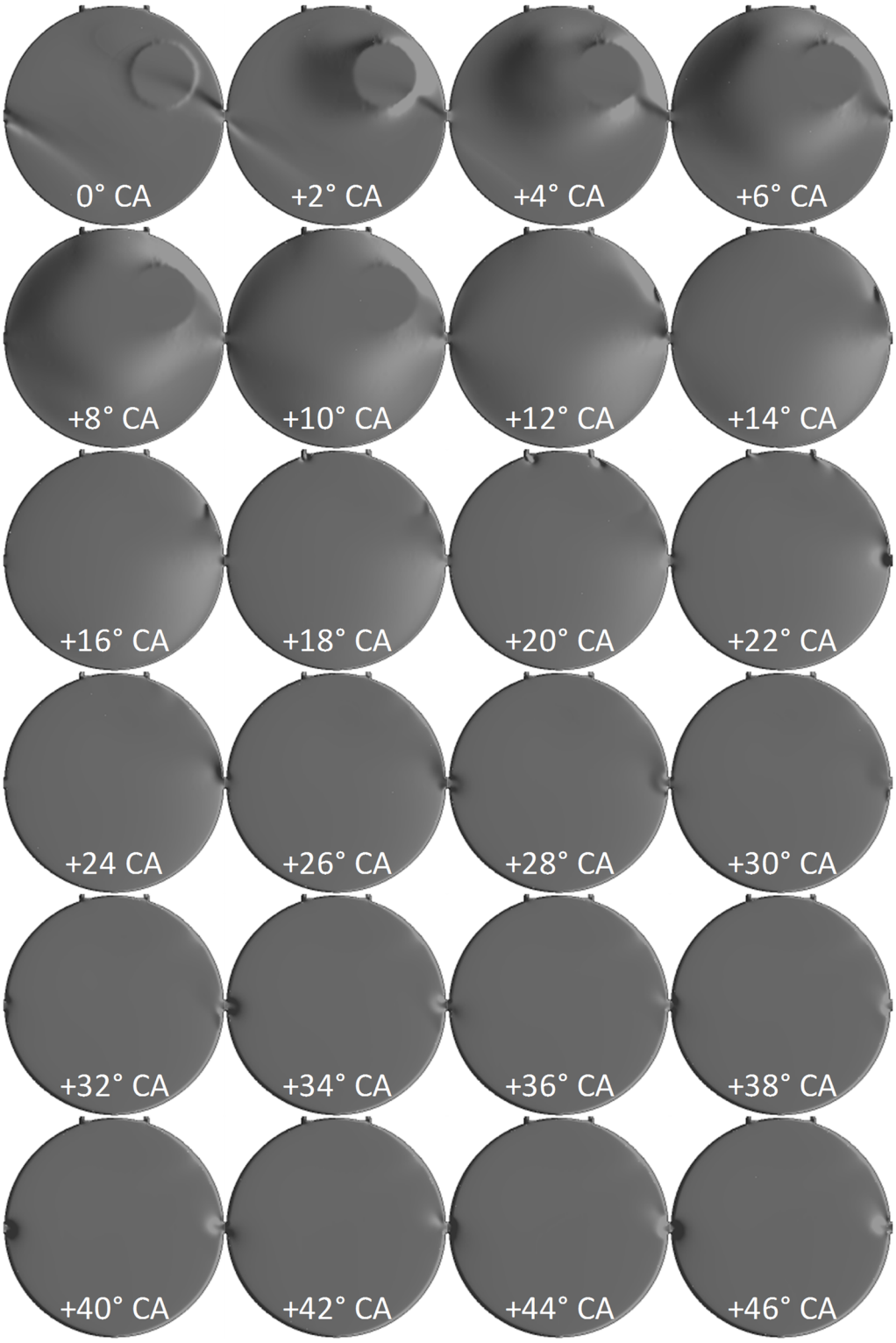

Figure 5.9: Transient density gradient (pseudo-schlieren) images of the non-vortex combustion chamber. Modeled spark is seen as the circle on the upper right of each image and is active in the first 10° CA. Each image represents 2° CA for the interval from start of ignition at 0° (TDC) to 46° CA.

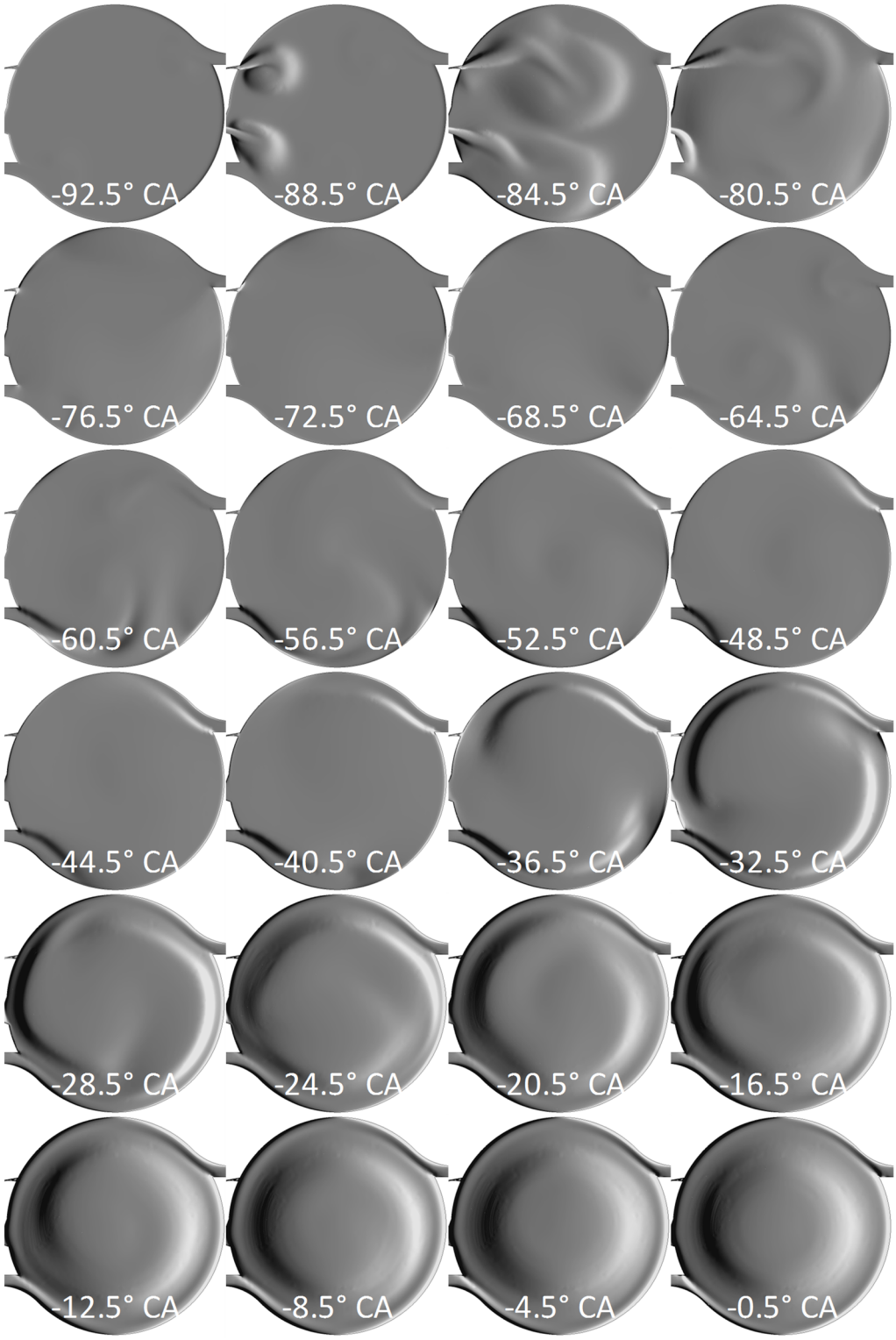

Figure 5.10: Transient density gradient (pseudo-schlieren) pseudo-schlieren images of the vortex combustion chamber. Each image represents 4° crank angle for the interval of -92.5° to -0.5° CA.

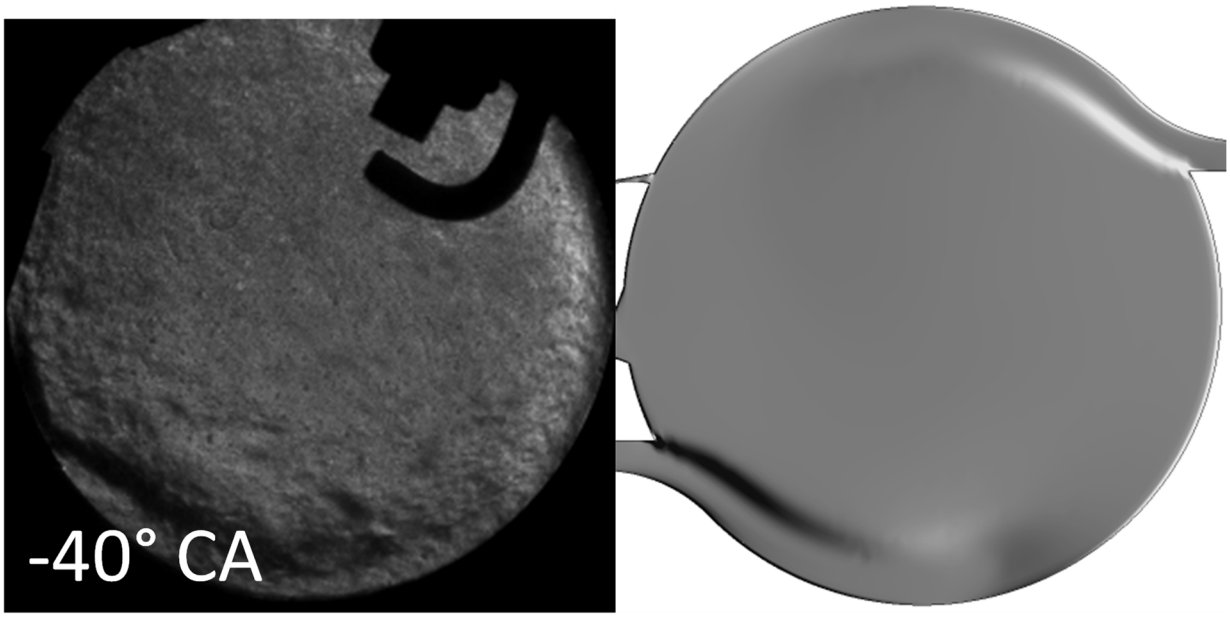

Figure 5.11: Comparison of experimental schlieren (left) and CFD pseudo-schlieren (right) images of vortex chamber at -40° CA before ignition start.

Figure 5.10 shows the pseudo-schlieren images during fuel injection and the compression stroke for the vortex combustion chamber. A density gradient can be initially detected at the interface between the side channel and combustion chamber at -64.5° CA. Mixture formation continues with the flow from the side channels continuing to follow along the periphery of the combustion chamber wall (see Fig 5.10, last four rows). Figure 5.11 shows that the pseudo-schlieren image at -40° CA, with the density gradient corresponding to the lower jet, correlates well with the experimental counterpart at the same crank angle.

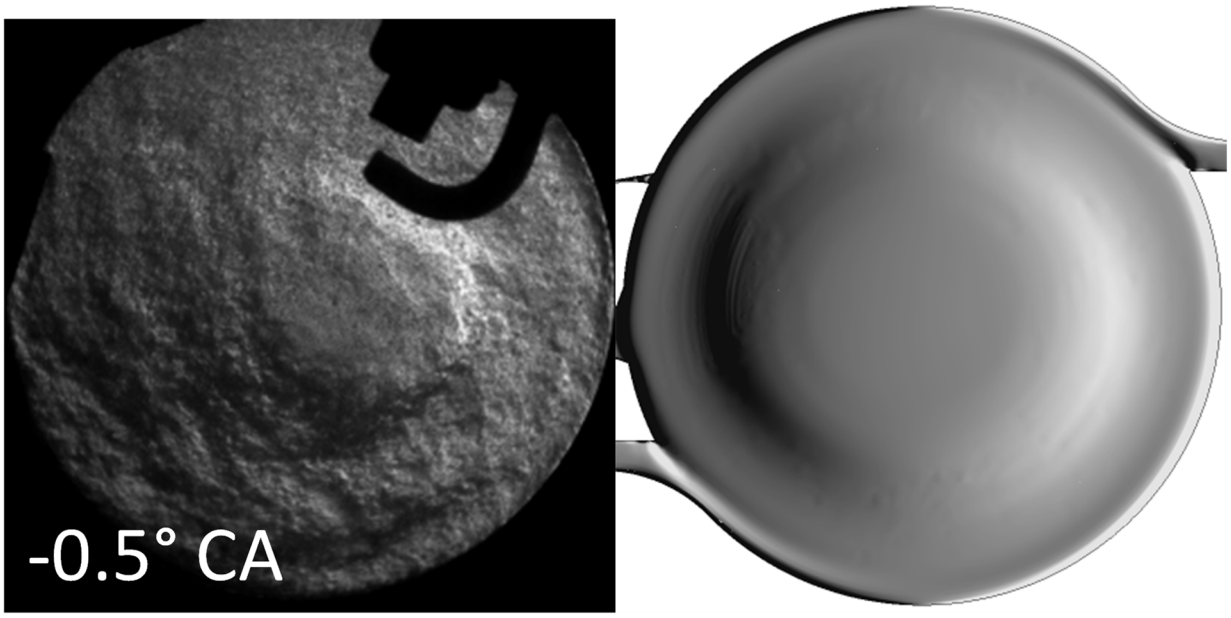

Figure 5.12: Comparison of experimental schlieren (left) and CFD pseudo-schlieren (right) images of vortex chamber at -0.5° CA before ignition start.

The compression stroke culminates with a noticeable bulge in the center that becomes progressively smaller in diameter and forms a more regular circular shape (Figure 5.10, last two rows). This is clearly seen in both in the optical engine and pseudo-schlieren images in Figure 5.12 at -0.5° CA before ignition start.

As in the non-vortex case, the modeled spark ignition has an initial radius of 1 mm centered on the coordinates of the sparkplug in the metal engine. However, the flame propagation is drastically different; here, it not only follows the direction of rotation, but curls radially inwards (Figure 5.13, top row). Large contrasts can be seen on the left and right peripheral extremities not observed in the non-vortex pseudo-schlieren images, indicating spatially wide density gradients between the hot burning gas in the center and the cooler near-wall region. The numerical model also correctly captures the phenomenon of the apparent leading edge of the flame front thinning and moving radially inward into the rotational center of the bulk flow and the inner curvature of the burned-unburned interface becoming smaller, as also seen in the experimental schlieren images (see Figure 5.14).

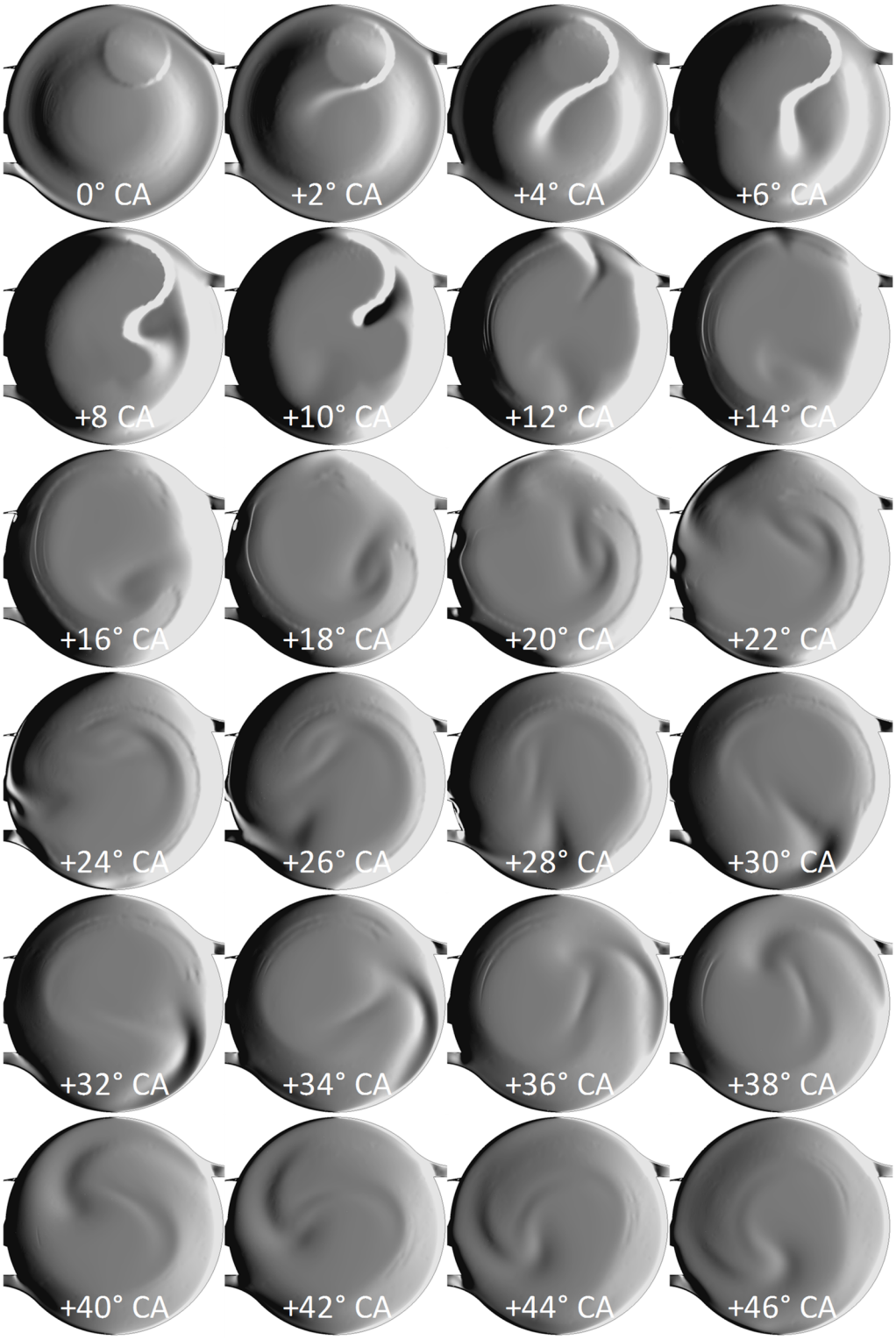

Figure 5.13: Transient density gradient (pseudo-schlieren) images of the vortex combustion chamber. Modeled spark is seen as the circle on the upper right of each image and is active in the first 10° CA. Each image represents 2° crank angle for the interval from start of ignition at 0° (TDC) to 46° CA.

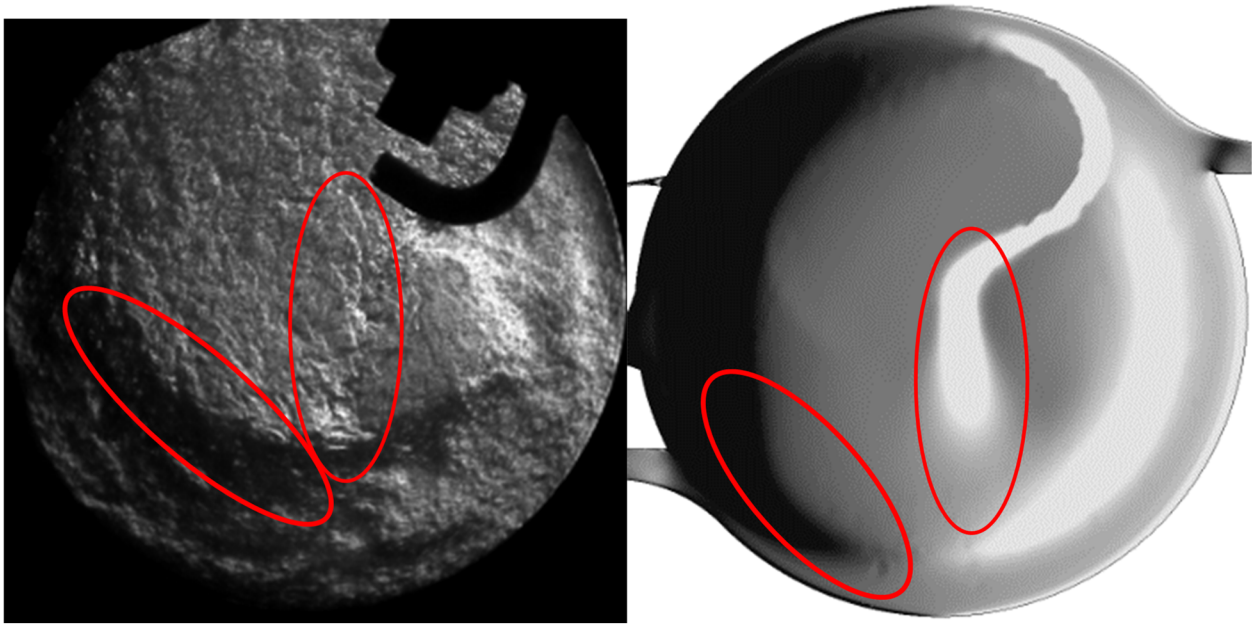

Figure 5.14: Comparison of experimental schlieren (left) and CFD pseudo-schlieren (right) images of vortex chamber showing curling of the flame front toward the center and thinning of the tail-end. Images are not synchronized in crank angle.

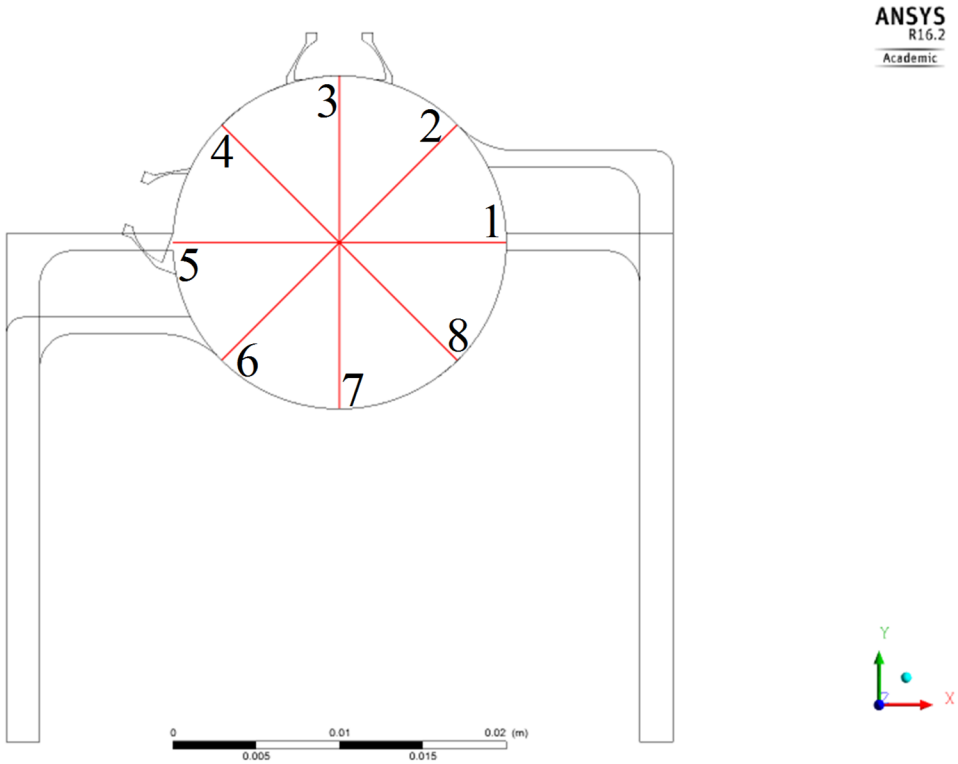

Figure 5.15: Outline wireframes of both vortex and non-vortex chambers superimposed with lines of dividing sectors for probing data values.

In order to extract quantitative data in the post-processing software, the circular faces of the two combustion chamber designs are divided into 8 equiangular radial sectors as shown in Figure 5.15. Along each sector, values of the parameters of interest to be analyzed can be plotted on the ordinate, with the abscissa denoting the radial distance from the center. The qualitative pseudo-schlieren images can thus be quantified by plotting the density gradient, as shown in Figure 5.16 (a). The set of curves corresponding with the vortex case display peaks at 6-7 mm from the center. The location of the peaks in the gradient plot would indicate an inflection point in one or more of the parameters affecting the local density, namely pressure, temperature and gas constant – analogously composition – through the ideal gas law, see Figure 5.16 (b, c, d, e). The density experiences a two-fold increase from the center to the peripheral zone, with only relatively small variance in absolute pressure and the temperature remaining nearly constant except near the wall. By consequence, the plot of gas constant – and additionally the peaks of the density gradient at ≈7 mm indicating the inflection points – correspond very well to the hydrogen mole fraction in Figure 5.16 (f) and conversely the oxygen mole fraction in Figure 5.16 (g). The CFD simulations, which show the formation of a radial stratified charge, thus decisively validate the same phenomenon observed in the optical engine schlieren images.

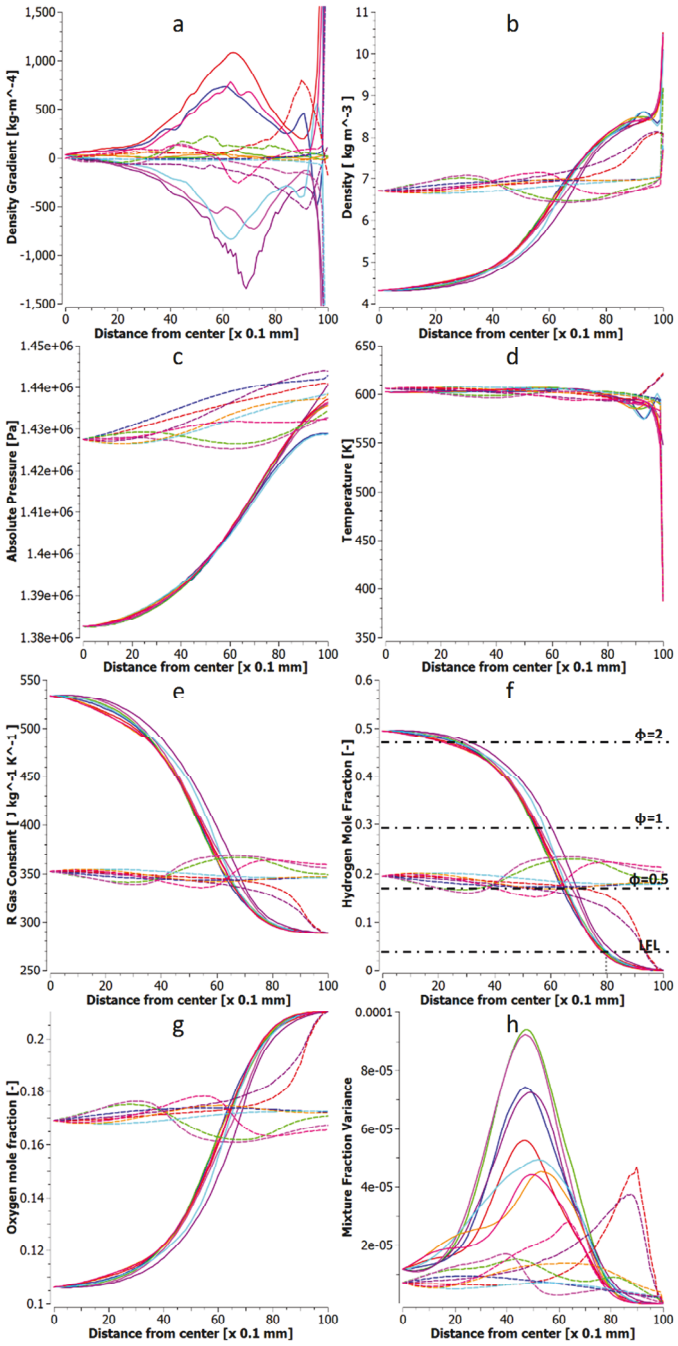

Figure 5.16: Charge properties at moment before start of ignition (-0.5° CA). Solid curves – vortex; dashed curves – non-vortex.

Figure 5.16 (f) shows that the prepared mixture of the vortex case just before ignition possesses a very distinct radial stratification of hydrogen mole fraction. Toward the center, the mixture is substantially rich of stoichiometric, with portions where $\phi > 2$. The lean flammability limit (LFL), corresponding to $x_{H_2} = 0.04$, previously defined as the flame-extent

limit radius r_x, is shown to have a value of 8 mm. The non-vortex case has a relatively consistent equivalence ratio of $\phi \approx 0.6$. Figure 5.16 (h) shows the mixture fraction variance, which is an indicator of spatial homogeneity. The vortex design shows the radial stratification and a high degree of uniformity in the azimuthal direction among its set of 8 curves. This contrasts with the desired objective of the overall homogeneous non-vortex chamber, yet they are still in the same order of magnitude.

With confidence in the correlations between the experimental schlieren observations and the numerically derived density gradient, attention can be directed to the detailed implications on the composition and flow field – properties such as species fractions, velocity and gas temperature – with the ultimate objective of quantifying and comparing the convective wall heat flux. Figure 5.17 shows plots of the transient evolution of hydrogen mole fraction, while Figure 5.18 shows the iso-contours in the respective combustion chambers at the same corresponding timesteps. For the vortex case, after injection the admission of air from the side channels causes the hydrogen-rich zone to be confined toward the center, as seen by pure air entering the combustion chamber along the peripheral wall and successively thickening by outpacing diffusion in the radial direction. Thus the region of low H_2 mole fraction appears to move toward smaller radii. Spatial uniformity also progressively improves as the set of 8 curves become closer to one another as indicated from -40° to 0° CA in Fig 5.17. At the end of combustion, there remains unburned hydrogen at the center due to the initially fuel-rich mixture there.

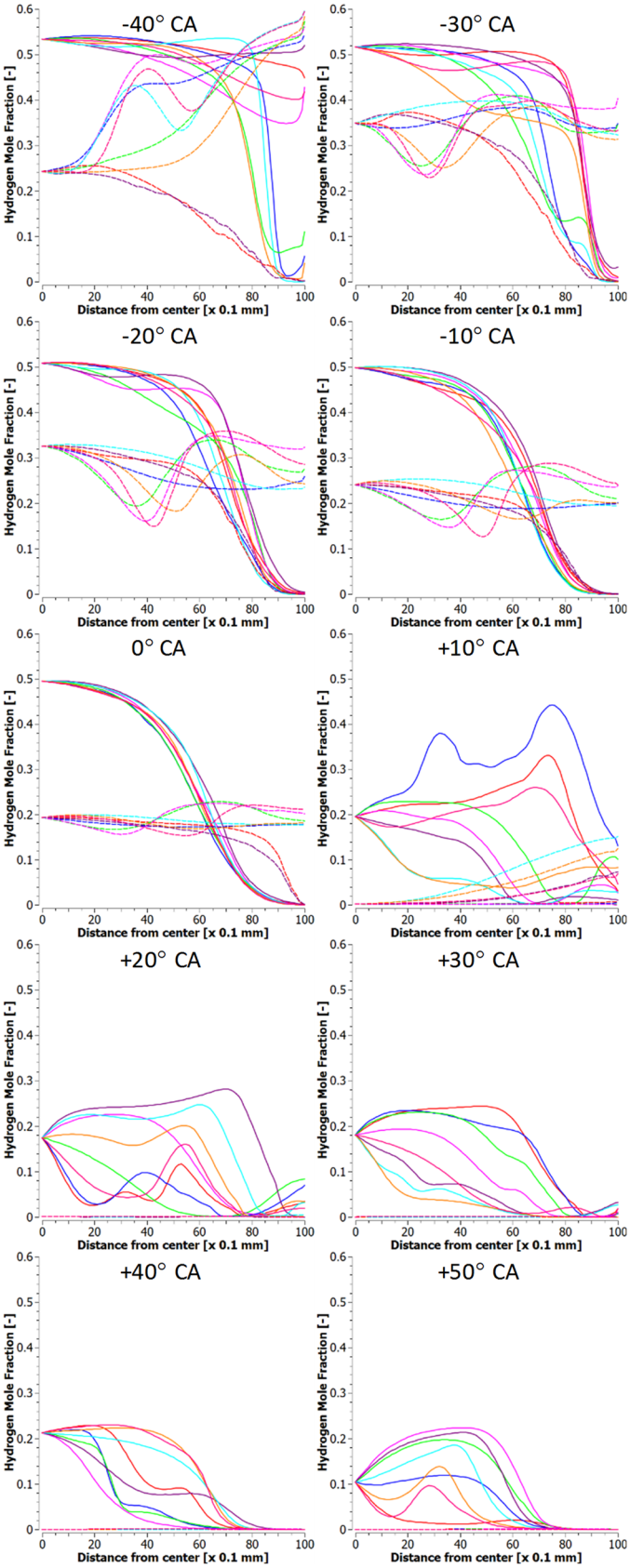

Figure 5.17: Transient evolution of hydrogen mole fraction at 10° intervals from -40 to +50° CA. Solid curves – vortex; dashed – non-vortex.

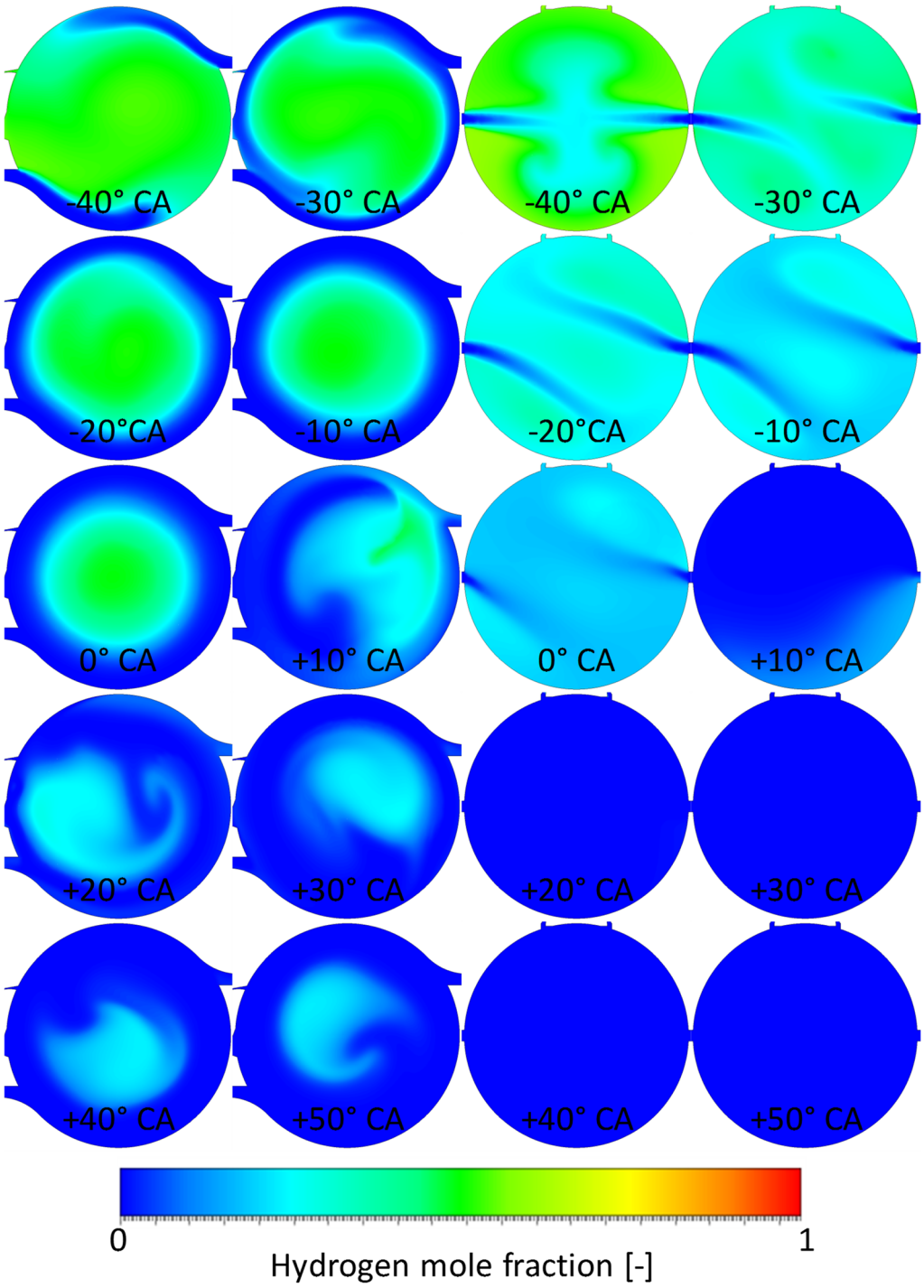

Figure 5.18: Transient iso-contour images showing hydrogen mole fraction at 10° intervals from -40 to +50° CA. Left 2 columns – vortex; right 2 columns – non-vortex.

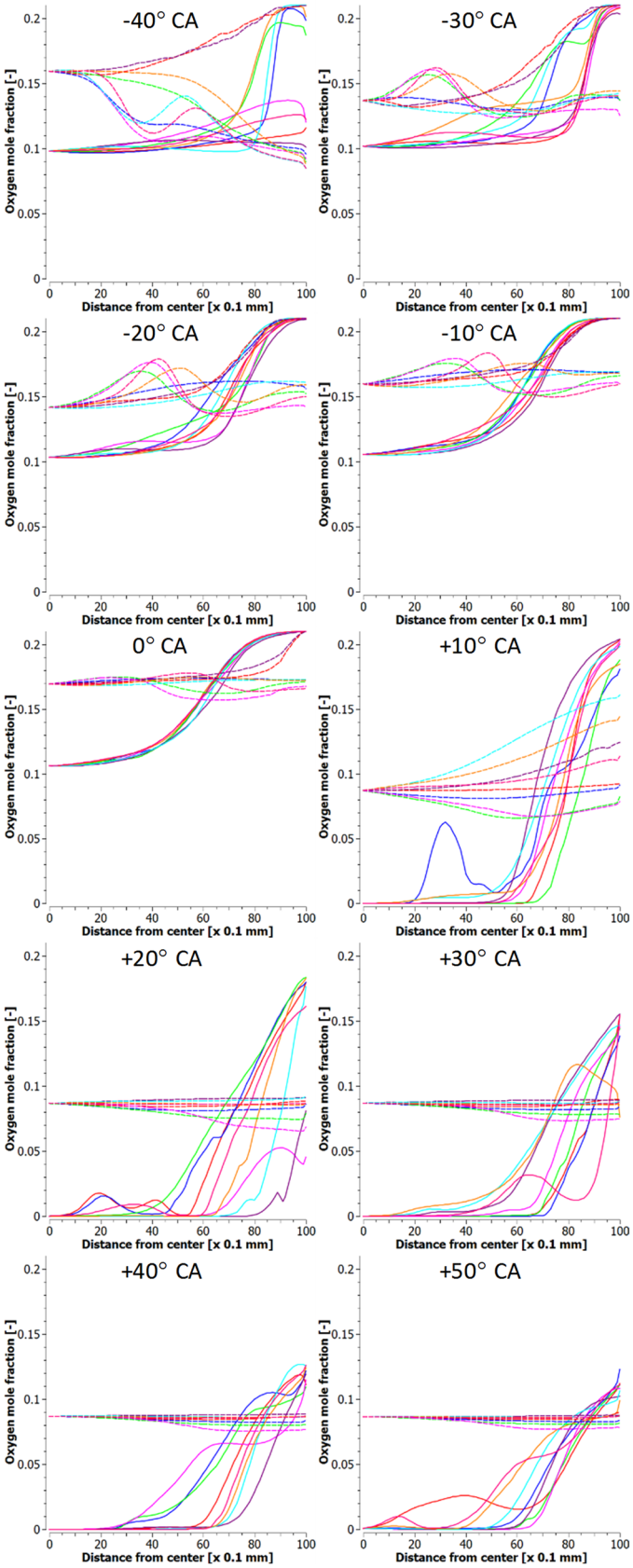

Figure 5.19: Transient evolution of oxygen mole fraction at 10° intervals from -40 to +50° CA. Solid curves – vortex; dashed – non-vortex.

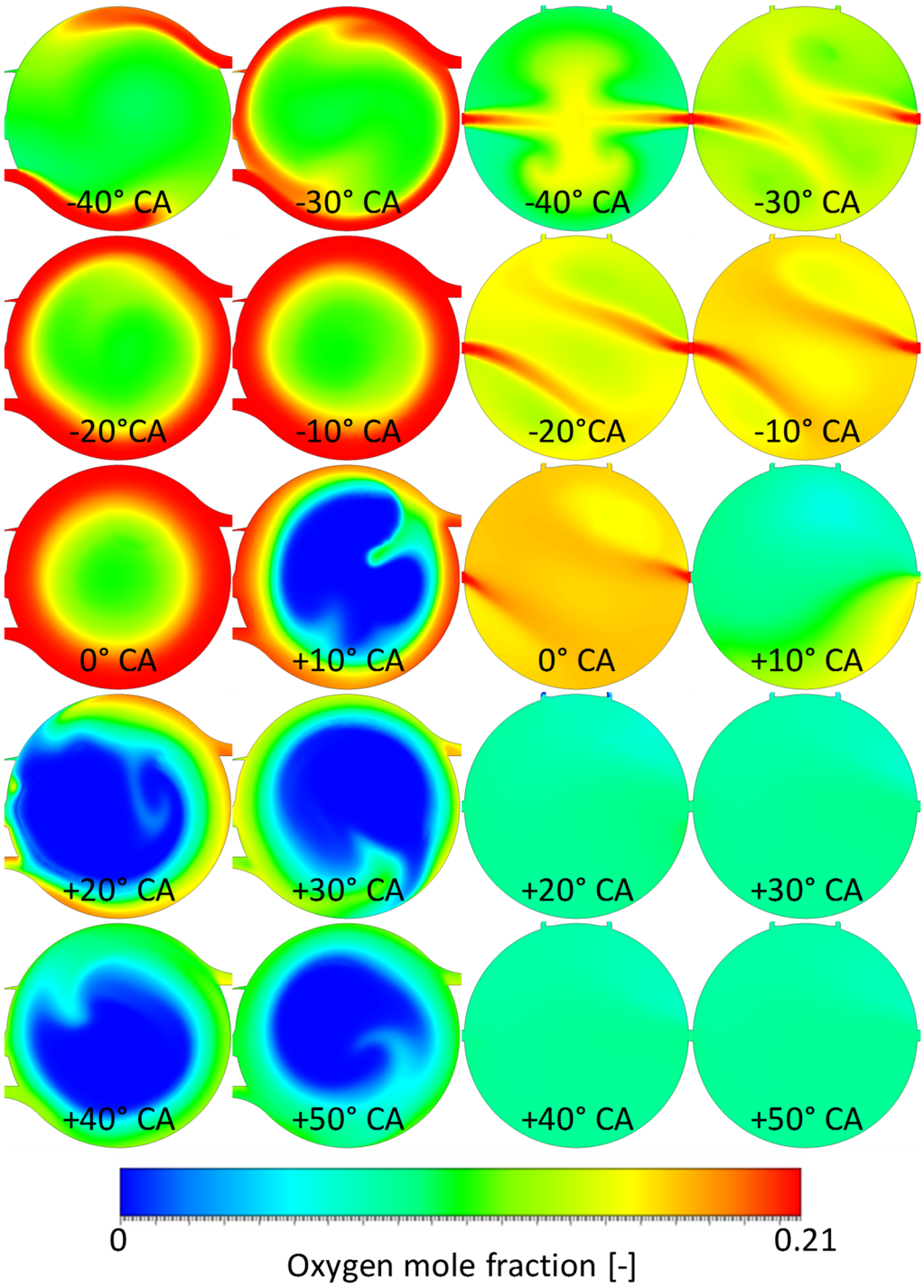

Figure 5.20: Transient iso-contour images showing oxygen mole fraction at 10° intervals from -40 to +50° CA. Left 2 columns – vortex; right 2 columns – non-vortex.

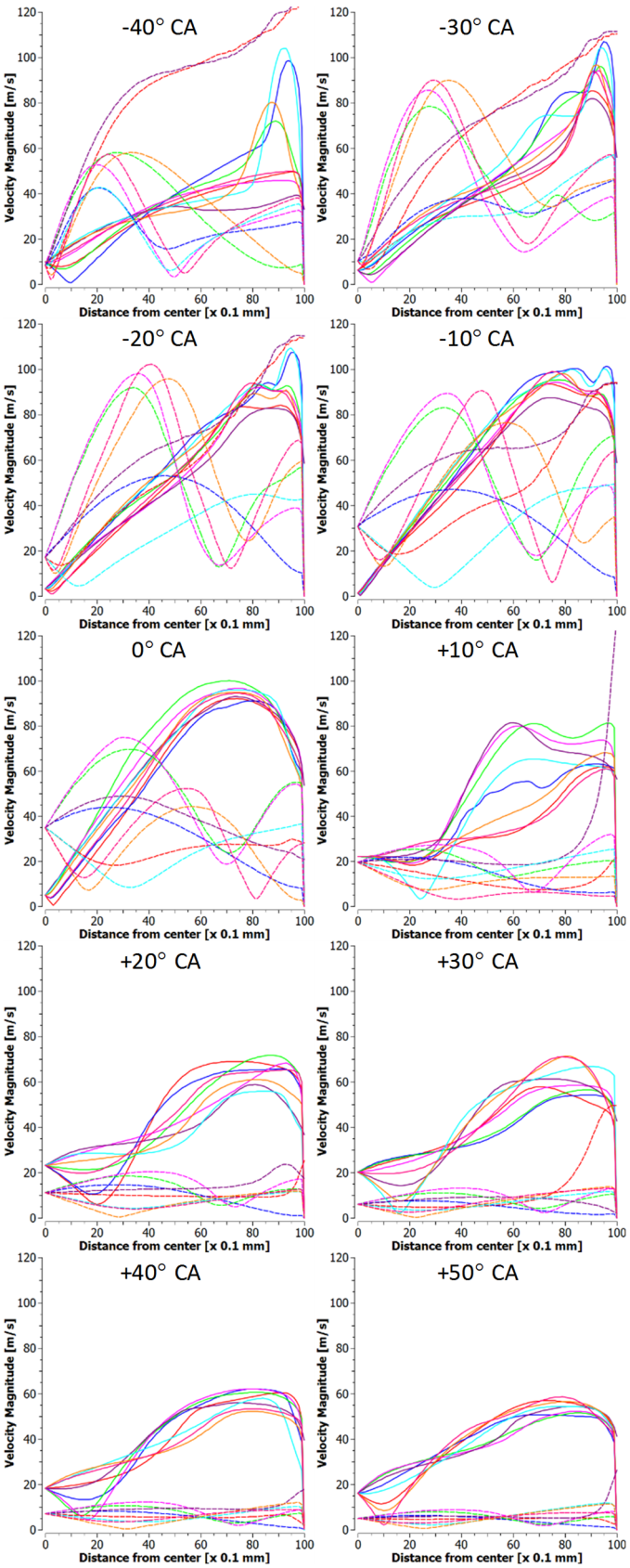

Figure 5.21: Transient evolution of velocity magnitude at 10° intervals from -40 to +50° CA. Solid curves – vortex; dashed – non-vortex.

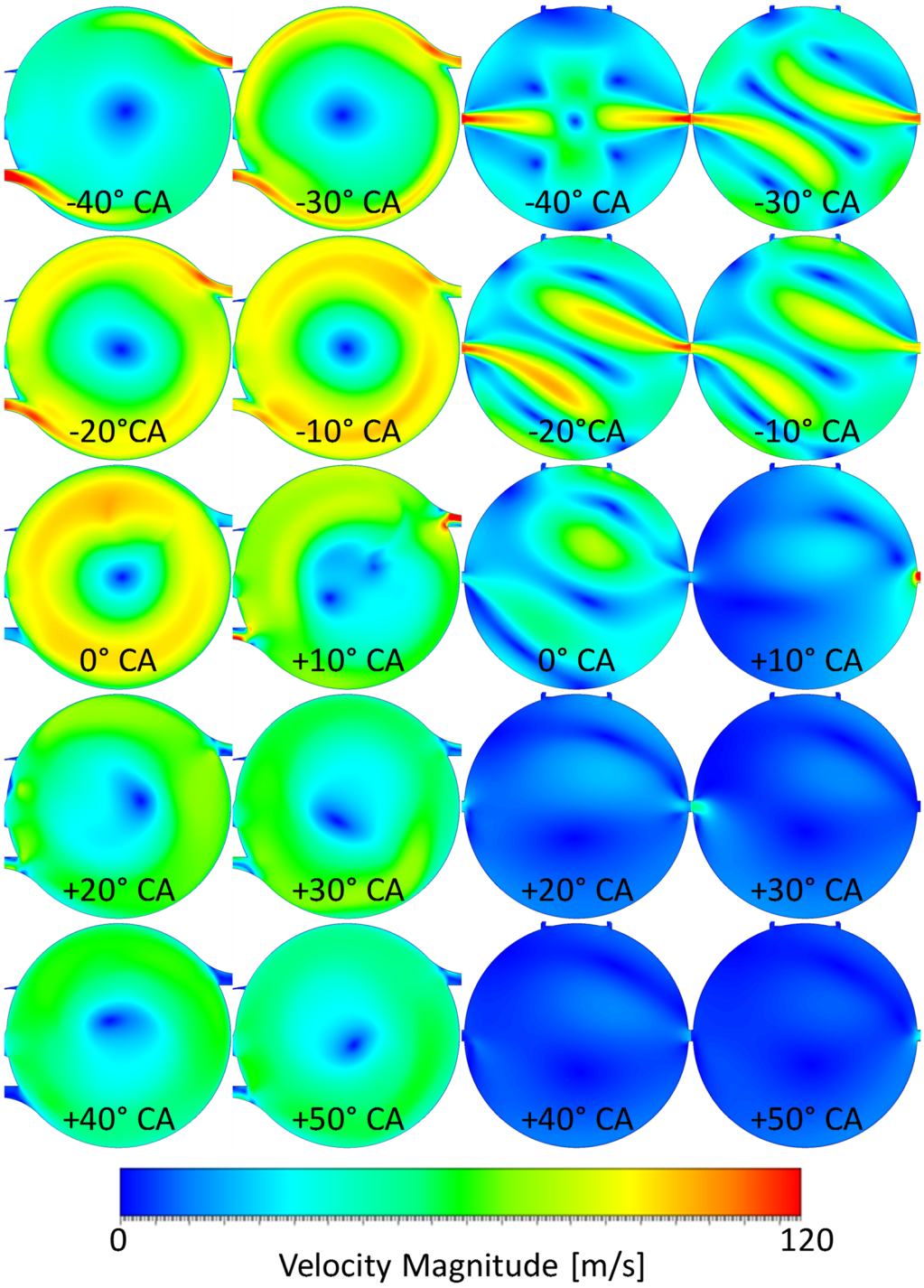

Figure 5.22: Transient iso-contour images showing velocity magnitude at 10° intervals from -40 to +50° CA. Left 2 columns – vortex; right 2 columns – non-vortex.

More tellingly, Figures 5.19 and 5.20 show that oxygen is substantially depleted in the center during and after combustion as expected, but a substantial fraction remains in the outer periphery. Here, combustion is suppressed and the dense relatively cold unreacted oxygen molecules are inhibited from traversing toward the center, while hydrogen, as seen in Figure 5.18 – completely within the hot burned zone – is simultaneously unable to migrate to the periphery as a result of centripetal body forces of the rotating charge counteracting against the different density gases. The structure of oxygen stratification is not disturbed in a large scale or destroyed due to mixing during combustion, indicating that the insulating air layer adjacent to the wall is substantially maintained.

The velocity plots and images are presented in Figures 5.21 and 5.22. At the end of the compression stroke, at 0° CA, the flow in the vortex chamber behaves macroscopically as a solid body rotation by the linear relationship from the center up to a radius of about 6 mm, as shown in Figure 5.21. Combustion disturbs the motion of the flow field –but after it is substantially complete, the flow can be seen to resume to a regular rotation but with decayed velocity magnitude. In the non-vortex case, there is no ordered motion as can be seen by the random distribution of velocity magnitude, and as is further evidenced by the plots of circumferential velocity in Figure 5.23 showing negative values, while that of the vortex design rises monotonically and linearly from the center over a large part of the radius.

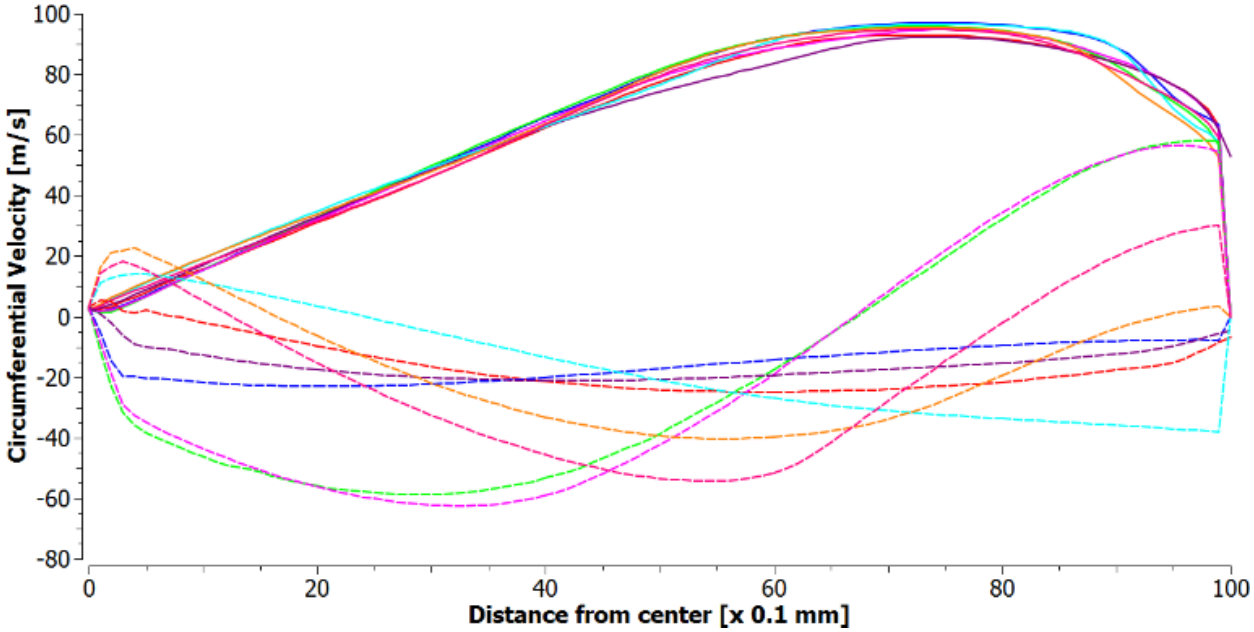

Figure 5.23: Circumferential velocity at moment before start of ignition (-0.5° CA). Solid curves – vortex; dashed curves – non-vortex.

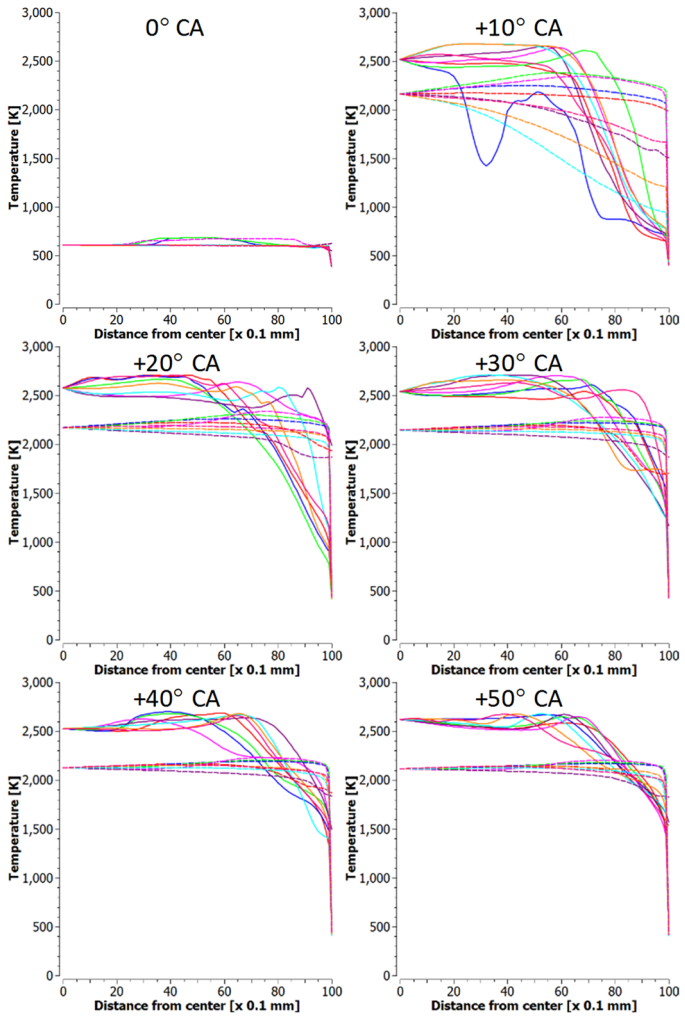

Figure 5.24: Transient evolution of gas temperature at 10° intervals from 0° to +50° CA. Solid curves – vortex; dashed – non-vortex.

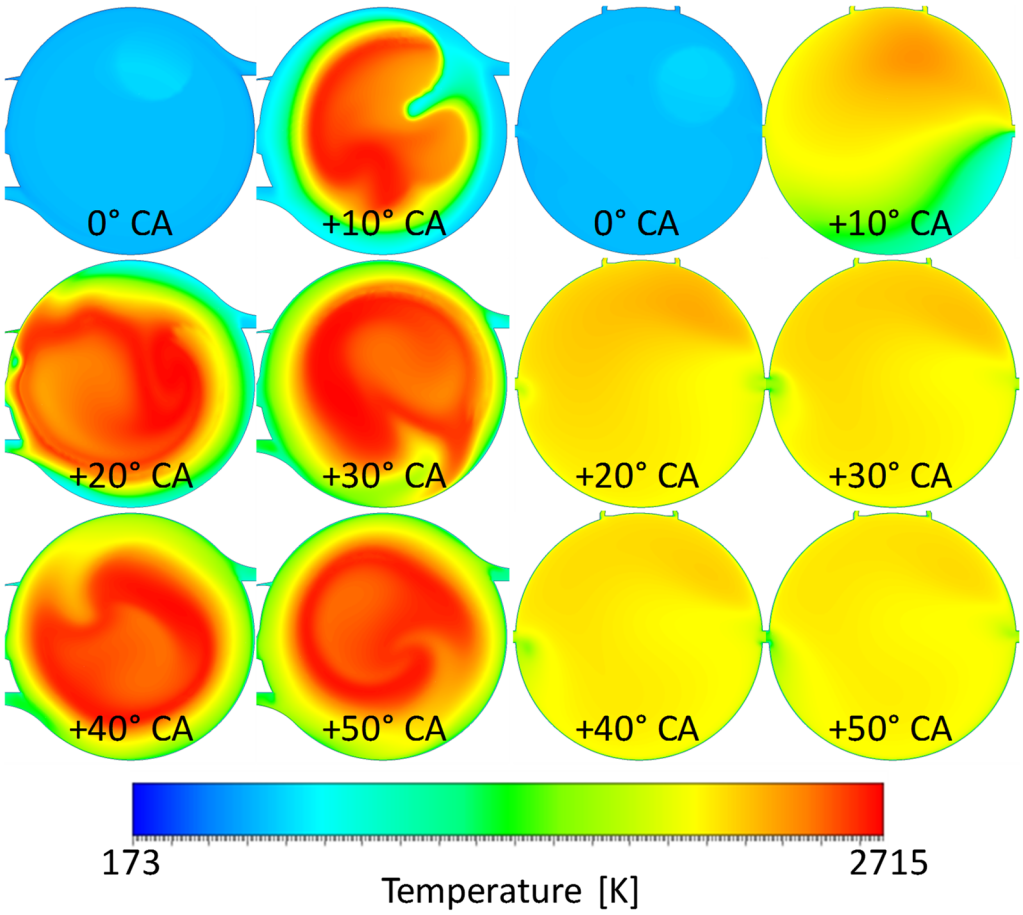

Figure 5.25: Transient iso-contour images showing gas temperature at 10° intervals from 0 to +50° CA. Left 2 columns – vortex; right 2 columns – non-vortex.

Figures 5.24 and 5.25 show the transient development of gas temperature. The vortex case has consistently higher temperatures near the center due to the higher equivalence ratio in this region. However, as time progresses, there is a noticeable curvature of the temperature profile, while that of the non-vortex case remains almost constant except very close to the wall. At +50° CA the near-wall temperatures of the vortex case are lower in all the polled locations than the non-vortex counterpart, as can be seen from a close-up view of the last 2 mm distance from the wall in Figure 5.26.

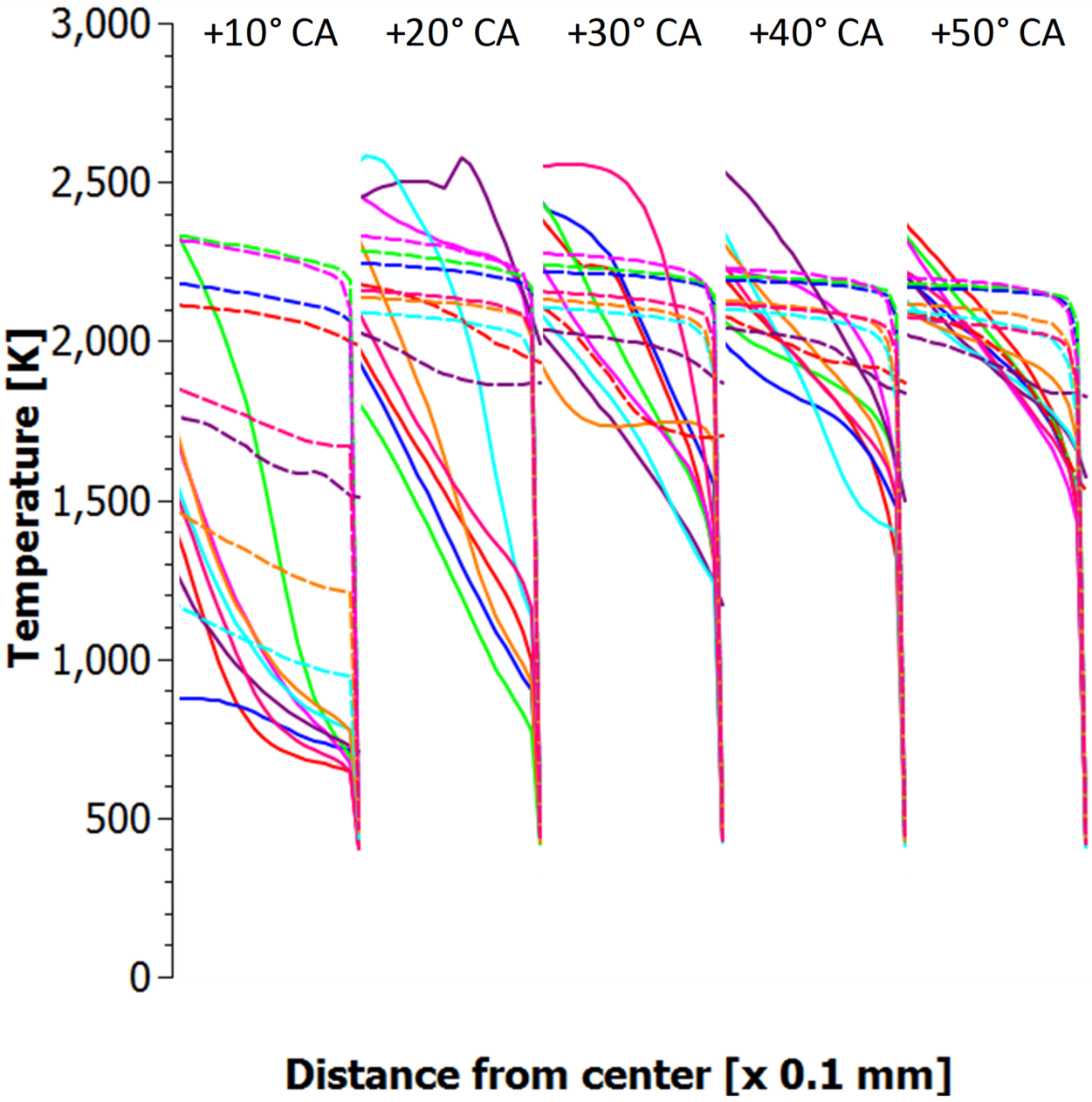

Figure 5.26: Close-ups of temperature profiles in the near-wall region at 10° intervals from +10° to +50° CA. Solid curves – vortex; dashed – non-vortex.

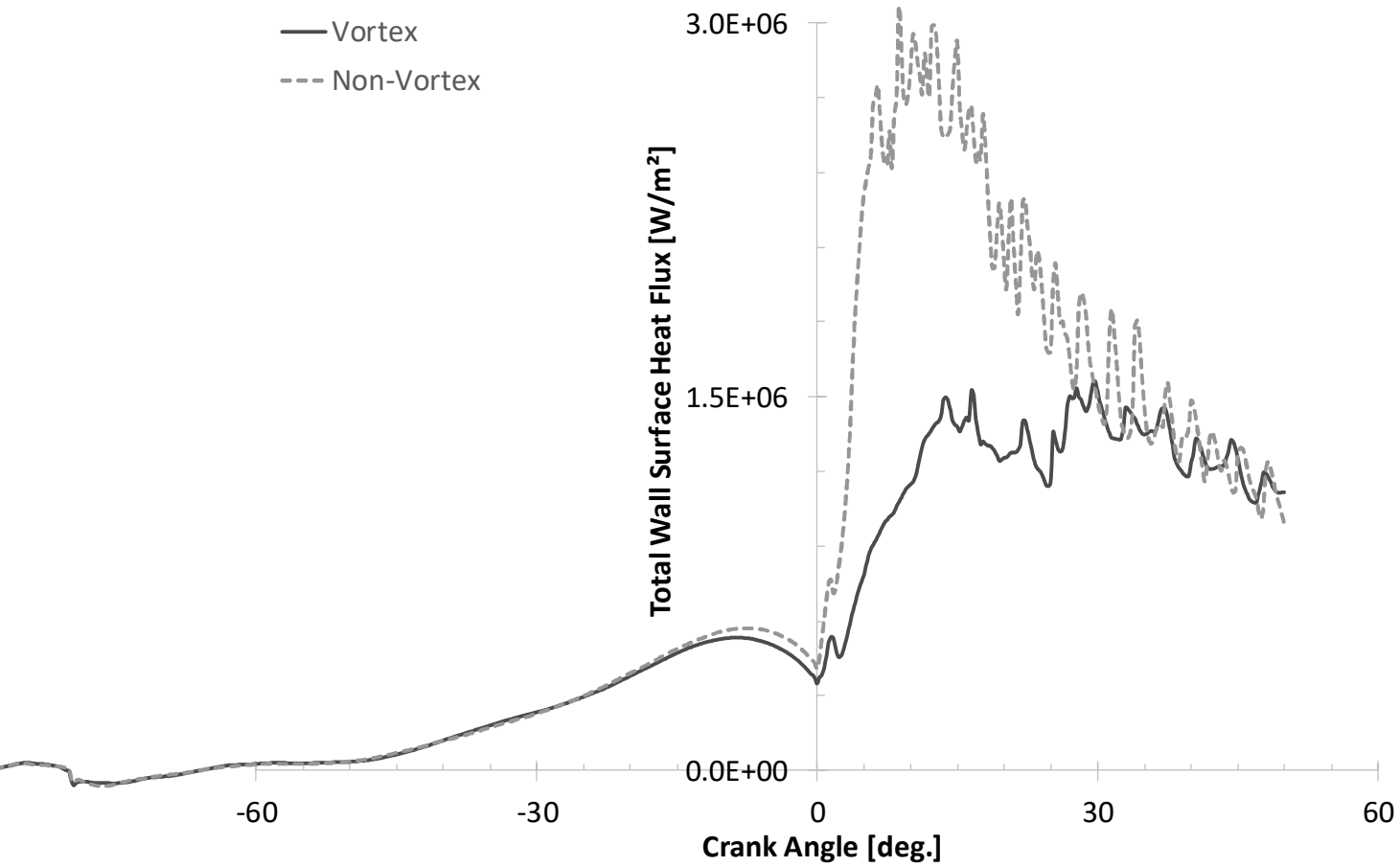

Figure 5.27: Comparison of area-weighted average total wall surface heat flux, vortex vs. non-vortex, -90° SOI, 10° CA injection duration.

The most important result is the total wall surface heat flux. Here the wall is modeled as made from aluminum of 5 mm thickness and having a constant surface temperature of 373.15 K throughout. Figure 5.27 shows that the area-weighted average for the vortex-stratified process yields a wall surface heat flux that rises more gradually and peaks about half that of the non-vortex case. Compare this with the 71% reduction estimated from the analytical calculation performed earlier, noting that this larger percentage reduction assumes that the burned gas temperatures remain equal, while Figure 5.24 shows that the vortex case has peak temperatures up to some 500 K higher to arrive at the 50% lower peak heat flux. Recalling that the chamber is modeled as a constant volume from TDC onwards, past the peak the non-vortex chamber heat flux shows a gradually declining trend that is not seen to the same degree with the vortex counterpart. Closer inspection reveals the cause to be contributed by a combination of two factors:

1. Decaying flow velocity, thus reducing the local convective coefficient as the combustion process proceeds;
2. Declining gas temperature at the thermal boundary layer, more pronounced globally in the non-vortex case due to heat transfer.

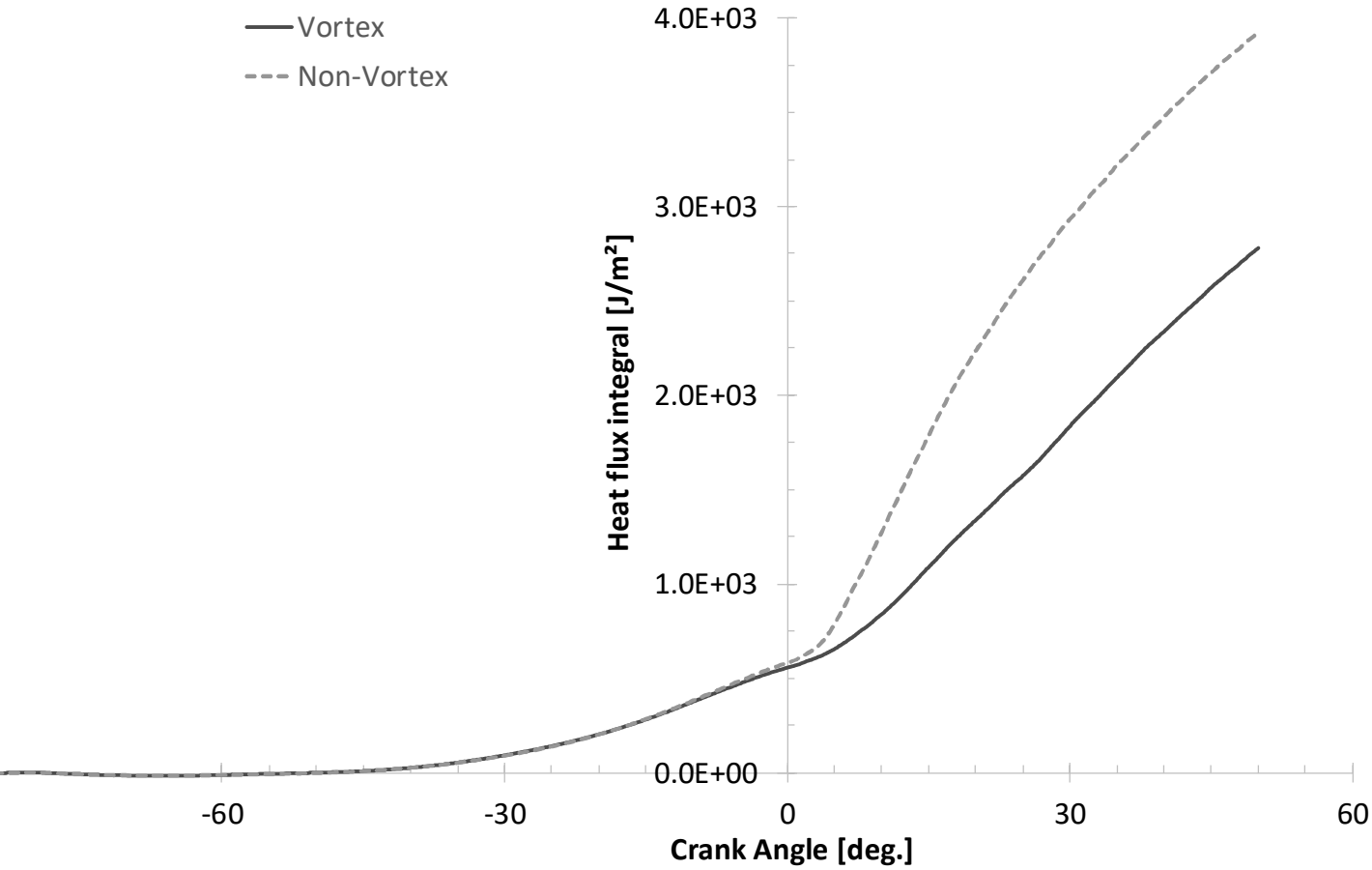

Figure 5.28: Comparison of heat flux integral or cumulative heat transfer, vortex vs. non-vortex, -90° SOI, 10° CA injection duration.

The preceding discussion compares the peak values of the heat flux, but it is the total cumulative or integral heat transfer that is ultimately responsible for diminishing the engine thermal efficiency. This is shown in Figure 5.28 and still shows a substantial reduction for the vortex approach.

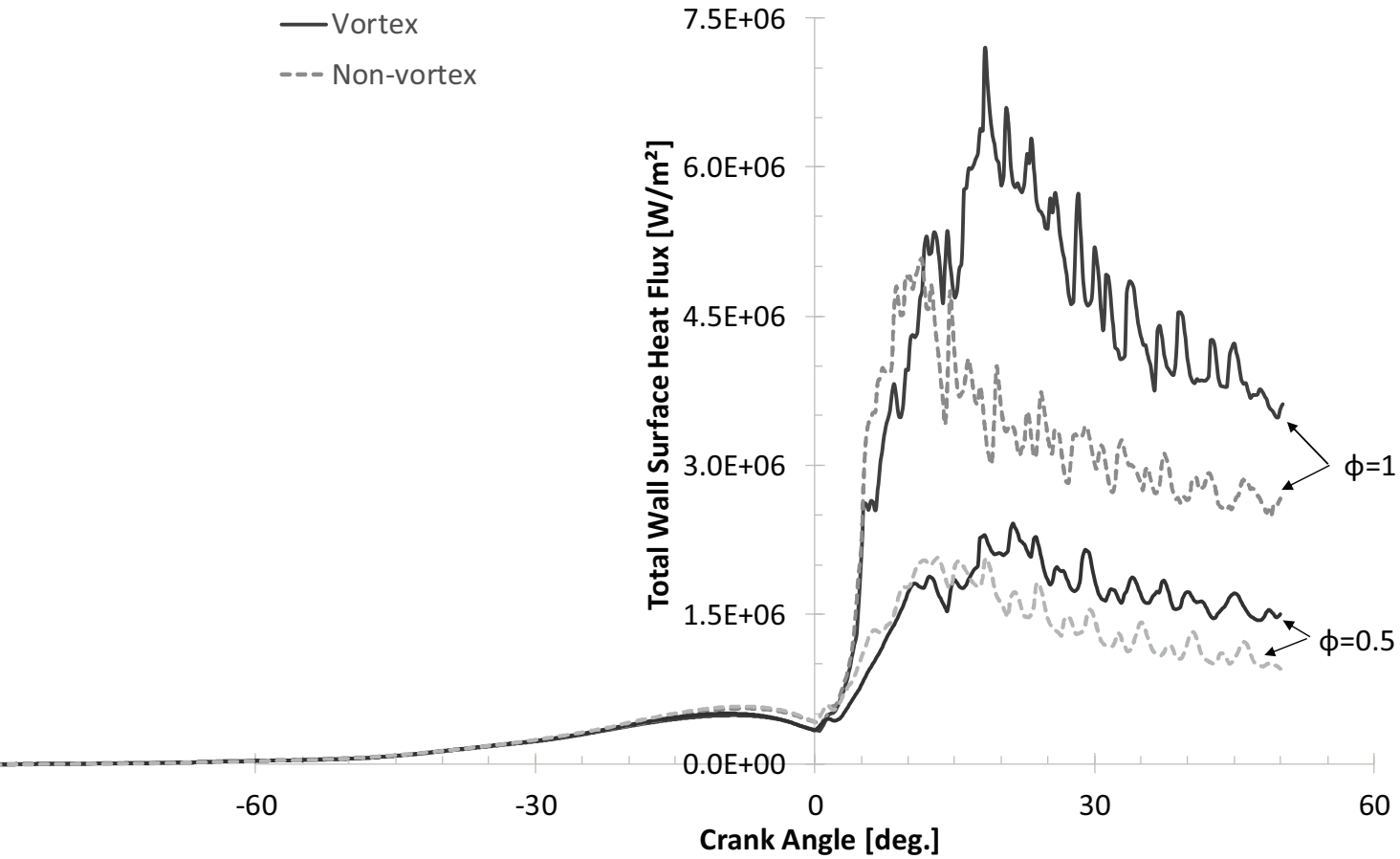

Figure 5.29: Comparison of area-weighted average total wall surface heat flux, vortex vs. non-vortex, homogeneous premixed charge, stoichiometric (φ =1) and φ =0.5.

In order to investigate the effect of flame-extent limitation further, both combustion chamber designs are considered with homogeneous (non-stratified) premixed mixtures of $\phi = 1$ and 0.5, the results of which are shown in Figure 5.29. In both cases, the premixed-vortex cases now show higher peak heat fluxes on equal hydrogen mole fraction bases – substantially so with stoichiometric mixtures – now that the flames are not imposed from being confined away from the wall and due to the flow velocity effect raising the heat transfer coefficient.

5.5 Summary

Numerical simulations demonstrate that a combustion chamber design that sets up a highly ordered, rapidly rotating vortex flow is effective to create a radially distinct but concentrically uniform charge stratification – confining the fuel-concentrated core in the center of the combustion chamber while leaving the periphery adjacent to the walls composed of non-

combusting, essentially pure air. This novel flow-induced flame-extent confinement field is found to reduce peak convective wall heat transfer losses by 50% compared to a combustion chamber design that actualize a homogeneous mixture without specific charge motion directionality. This order of magnitude is supported by predictions from an analytical solution of the convective heat transfer equation. Important visual phenomena of the mixture preparation and combustion processes have been qualitatively validated by correlating experimental schlieren observations in an optically accessible engine with counterpart density gradient or "pseudo-schlieren" images derived from CFD numerical models. The phenomenon of reduced wall heat flux by the here-introduced vortex approach is due to the combination of two effects:

1. Charge stratification during mixture preparation in the course of the compression stroke due to finite-time diffusion being outpaced by the replenishment of pure air at the periphery. Absent mixture stratification by means of imposed charge premixing, the high velocities of the vortex approach only counterproductively increase heat fluxes;
2. Limiting of the extent of flame propagation to some distance away from the wall by segregation of different-density reactants induced by body forces. Combustion is inhibited at the periphery and the flame is observed to curl radially inwards and burn the fuel until the available oxygen is depleted.

CHAPTER 6 DISCUSSION

6.1 Preface

The preceding chapters introduced an approach of reducing wall heat transfer losses via a combination of two phenomena – first by stratifying the charge mixture radially in the combustion chamber so that a fuel-concentrated core is confined in the center while the periphery adjacent to the walls is composed of essentially pure air so that this periphery does not participate in combustion; and second by further delaying or preventing the propagating flame front from reaching close to the walls by the action of very strong centripetal body forces that predisposes the hot and therefore less dense burning gas toward the centre. Both of these effects are achieved through a unique exploitation of gas diffusion and fluid dynamic properties, and have been realized in a reciprocating internal combustion engine; demonstrated and observed visually in a working prototype; analysed numerically using CFD; and the ultimate objective of reducing the wall heat transfer losses by this approach quantified. This work has merely introduced a new concept for improving the efficiency of internal combustion engines but in so doing has opened up new areas for future investigations; some of these are discussed in turn.

6.2 Outlook

The experimental portion in this work had originally intended to perform direct measurements of wall surface heat flux by means of a commercially purchased thermopile sensor as have been used in referenced works, for example by Demuynck et al (2009) [76]. This sensor was fitted to the combustion chambers. However, an unfortunate set of circumstances conspired together to make these measurements impossible. First, it was discovered that the data acquisition system employed was wholly inadequate for the task, in terms of sampling frequency and response time as a non-exclusive listing. The engine could be operated in firing mode for only a few seconds at a time in order to avoid damage of the uncooled engine being turned over at up to 5000 RPM. The start of the firing events and measuring period are triggered from the test cell control panel and orchestrated by the Simulink model controller, Digilent FPGA and OpalRT HiL described in Chapter 4. However, the response time from the triggered signal to

the beginning of acquisition exceeded the total fired time; therefore, not only was it impossible to obtain heat flux measurements, but also measurements of flow rates of hydrogen and air, and several channels of thermocouples and pressure transducers, which were also connected on the same data acquisition system. While significant efforts were spent to test and shake-down the system offline in advance, a considerable proportion of limited, fixed test-cell time devoted to debugging the system could only be performed with the engine in-place and running. In the course of time under prolonged fired runs that yielded no acceptable measurement data, the heat flux sensor itself became defective and no replacement spares were on-hand. After being faced with the realities of having to change the data acquisition system completely and purchase new sensors – all while having no scope for additional funding and test-cell time, the decision made was to abandon heat flux measurement. It is now a foregone conclusion why this is not included in this dissertation; however, there is scope for future work to perform an experimental comparison of wall heat fluxes between the vortex-stratified approach introduced in this dissertation and a conventional case representing current practice.

Future experimental investigations could also perform different optical diagnostic approaches. Many schlieren imaging variants have been devised over the years with the objective in most of these to extract quantitative data -- some of these approaches permit distinguishing the density gradient field in color or through a background-orientated method [103]; direct determination of the density field by diffraction interferometry [104]; or extracted from the gradient field via image processing [105]; and even performing velocimetry measurements without seeding particles [106]. Other approaches include laser-induced fluorescence (LIF) [107], particle image velocimetry (PIV) [108] and laser-Doppler anemometry (LDA) [109]. Employing these visualization methods will give additional insights to the mechanisms and dynamics of the vortex-stratified principle. Of particular interest is to validate the forced-segregation of hot low-density and colder, heavier gas species as reported by Lapsa and Dahm (2009) [63] and predicted in the CFD simulations in see Section 5.4.

Future numerical analyses should certainly be performed with 3-D engine models with deforming meshes for the piston and detailed modeling of injector lift. As computational costs are rapidly declining and high-performance computing (HPC) clusters are simultaneously

becoming increasingly accessible, more-detailed and higher-accuracy numerical analyses can foreseeably be performed, for example with Large-Eddy Simulation (LES) as the turbulence model instead of the less computationally intensive Reynolds-Averaged Navier-Stokes (RANS) approach used here [110], and combustion utilizing detailed reaction kinetics [111].

One of the observed shortcomings in the vortex-stratified concept was the residual presence of unburned hydrogen at the center of the combustion chamber. It is in part a victim of its own success, due to the setting up of a mixture substantially rich of stoichiometric at the center and the apparent effectiveness of the gravitational field in inhibiting the hot, low-density hydrogen at the centre from meeting the colder, denser oxygen-containing gas at the periphery and being consumed completely. Future work, performed either experimentally or numerically, can further optimize the combustion chamber geometry and employ, for example, direct injection of premixed hydrogen-air at a desired equivalence ratio; multiple injection strategies as proposed by Shudo and Oba (2009) [47]; or air-blast injections as proposed by Oppenheim [49] directed at the rotational centerline of the vortex flow, all in order to bring the equivalence ratio in the centre close to stoichiometric or as otherwise desired so as to maximize the combustion efficiency.

An important design challenge will be to realize the vortex-stratified combustion system without a divided chamber, that is, to achieve the same effects presented in this work in an open combustion chamber formed by the geometry of the piston, cylinder and head. This will permit realizing further gains in thermal efficiency of a similar magnitude as that achieved in direct-injection Diesel engines over indirect-injection schemes.

Hydrogen remains of high research interest for use in internal combustion engines because of the possibility of producing it from a wide variety of primary energy feedstocks, including renewable resources. The special problems posed by hydrogen combustion – one of which is higher wall transfer losses reducing the realizable potential thermal efficiency that inspired this work – can also be applied to other gaseous fuels; in fact, the vortex-stratified approach is ambivalent to the employed fuel. Nevertheless, the vortex-stratified principle could be applied with diverse gaseous fuels like natural gas, liquefied petroleum gas (LPG), biogas,

syngas, flare gas, landfill gas, etc. Due to the effectiveness to develop a fuel-rich core, the vortex-stratified principle can be highly advantageous for engines operating at extremely lean global fuel-air equivalence ratios and/or high dilution with inert or residual gas fractions, where ignitability is poor, and both calorific values and flame speeds are low.

In the longer term, there is potential of combining the vortex-stratified approach with non-conventional combustion processes such as partially premixed combustion (PPC) [83], reactivity-controlled compression ignition (RCCI) [84] and homogeneous-charge compression ignition (HCCI) [82], the latter of which would actually by definition cease to be strictly homogeneous if combined with vortex-stratification and revert to something more like PPC in name if not concept. The main attraction of the synergy between the abovementioned combinations include very low emissions of engine-out pollutants. Vortex-stratification could be particularly suitable with HCCI to address two major implementation problems associated with the latter:

1. Wall quenching leading to low combustion efficiency [112]: Highly dilute, low-temperature combustion is very sensitive to quenching due to the relatively cold walls. The vortex-stratified approach would limit the extent of the combustible mixture away from the walls allowing the mixture to autoignite at multiple locations while limiting the effects of adverse near-wall conditions;
2. Limited operating range and cyclic variability [113]: HCCI engines suffer from limited load and speed range and operating regions of high cyclic variability, particularly at lean mixture conditions. Vortex-stratification could first permit extending the lean, low-load limit by means of more robust autoignition of a locally richer mixture in the center. Secondly, the highly ordered rotating flow motion could exhibit greater cycle-to-cycle consistency, as well as more spatially and cyclically predictable distribution of equivalence ratio. Validation of this could be done in multi-cycle CFD simulation as done by Scarcelli et al (2016) [114].

CHAPTER 7 CONCLUSION

At the beginning of this dissertation, five research objectives were set; these have been fulfilled. With the primary goal of improving the thermal efficiency of hydrogen-fueled engines, a literature survey delved into research being done to achieve these high efficiencies and the encountered challenges for further improvement. It was found that the main factor complicit in constricting the thermal efficiency of hydrogen fueled engines is due to losses from heat transfer through the combustion chamber walls. This heat energy is ultimately rejected into the environment and is lost from being able to perform useful work by the engine. Several works in the literature have proposed different solutions of reducing this loss and others have quantified the potential impact for improved efficiency by some magnitude reduction of wall heat transfer losses. Along the lines of reducing the convective heat transfer losses to the surrounding walls during combustion, using techniques not before used in the domain of reciprocating internal combustion engines, this dissertation has contributed the conception of a novel vortex-stratified combustion process studied using hydrogen as the fuel.

This dissertation has explained the theoretical background of this approach; designed, constructed and tested a working experimental prototype; observed the stratified-vortex combustion process visually using the schlieren method in fired operation; and comparatively analyzed the results of thermodynamic measurements between two combustion chamber designs – one featuring a homogeneous mixture without specific charge motion directionality representing current spark ignited engine practice and another with the here-introduced vortex-stratified approach. Finally, a comparative, transient 2-D CFD analysis quantified a potential 50% reduction in the peak convective heat flux with the vortex-stratified process compared to the reference non-vortex design. The total cumulative heat transfer is also significantly reduced.

Future work being actively pursued include patenting the vortex-stratified combustion process and exploring applications such as for large gaseous fueled engines.

Tout au long de ces travaux de thèse doctorale, l'objectif principal a été d'améliorer l'efficacité thermique des moteurs à hydrogène. Dans un premier temps, une étude bibliographique a permis de déterminer les procédés capables d'offrir les meilleurs rendements mais également d'en comprendre leurs limites. Il est apparu que le principal phénomène limitant l'efficacité thermique des moteurs à hydrogène est dû à des pertes de chaleur aux parois de la chambre à combustion. Cette chaleur est ultimement dissipée au milieu environnant, diminuant ainsi l'énergie disponible pour que le moteur effectue un travail utile. Plusieurs études antérieures ont proposé diverses solutions afin de réduire ces pertes. D'autres travaux se sont attachés à quantifier l'impact potentiel de la réduction des transferts de chaleur sur l'amélioration du rendement du moteur. En se basant sur la réduction des pertes de chaleur par convection aux parois lors de la combustion, en utilisant des techniques novatrices dans le domaine des moteurs à combustion interne, cette thèse a contribué à la conception d'un nouveau procédé à combustion stratifiée par vortex utilisant l'hydrogène comme source de carburant.

Cette nouvelle configuration de moteur a tout d'abord été étudiée théoriquement, ensuite conçu, construit et enfin testé expérimentalement à l'aide d'un prototype. Des observations du procédé de combustion stratifiée par vortex ont été réalisées en utilisant la méthode de strioscopie. De plus, des études thermodynamiques ont été menées dans le but de comparer cette configuration à une chambre plus traditionnelle ou le mélange y est homogène. Enfin des simulations CFD 2-D en mode transitoire, ont permis d'évaluer une réduction potentielle à 50% pour le flux thermique convectif de pointe lorsque la configuration vortex-stratifiée est utilisée.

Les travaux futurs se poursuit activement comprennent breveter le processus de combustion vortex stratifié et d'explorer des applications telles que pour les gros moteurs de gaz.

REFERENCES

[1] Eichlseder, H., Klell, M., "Wasserstoff in der Fahrzeugtechnik – Erzeugung, Speicherung, Anwendung," Vieweg+Teubner Verlag, Wiesbaden, 2010.

[2] Furuhama, S., "Two-stroke hydrogen injection engine," Int J Hydrogen Energy, **4**(6):571-576, 1979.

[3] Furuhama, S., Kobayashi, Y., "A Liquid Hydrogen Car with a Two-Stroke Direct Injection Engine and LH2 Pump," Int J Hydrogen Energy, **7**(10):809-820, 1982.

[4] Furuhama, S., Kobayashi, Y., "Development of a Hot-Surface-Ignition Hydrogen Injection Two-Stroke Engine," Int J Hydrogen Energy, **9**(3):205-213, 1984.

[5] Wallner, T. et al., "Operating strategy for a hydrogen engine for improved drive-cycle efficiency and emissions behavior," Int J Hydrogen Energy, **34**(10):4617-4625, 2009.

[6] Grabner, P. et al., "Optimisation of a Hydrogen Internal Combustion Engine with Inner Mixture Formation," 1st International Symposium on Hydrogen Internal Combustion Engines, Graz, pp. 59-70, 2006.

[7] Verhelst, S., Sierens, R., "Hydrogen Engine-Specific Properties," Int J Hydrogen Energy **26**, pp. 987-990, 2001.

[8] Verhelst, S., Wallner, T., "Hydrogen-Fueled Internal Combustion Engines," Prog. Energy Combust. Sci., **35**(6):490–527, December 2009, doi:10.1016/j.pecs.2009.08.001.

[9] http://media.ford.com/article_display.cfm?article_id=23844 (accessed on June 15th, 2012).

[10]http://www.bmw.com/com/en/insights/technology/efficient_dynamics/phase_2/clean_energy/bmw_hydrogen_7.html (accessed on June 15th, 2012).

[11] Morgan, E., Lincoln, R., "Duty Cycle for Recreational Marine Engines," SAE Technical Paper 901596, 1990, doi:10.4271/901596.

[12] http://www.tc.gc.ca/publications/en/tp511/pdf/hr/tp511e.pdf(accessed on June 15th, 2012).

[13] Caley, D., Cathcart, G., "Development of a Natural Gas Spark Ignited Direct Injection Combustion System," NGV2006, Cairo, 2006, http://orbeng.com.au/download-document/332-2006-ngv.html (accessed on June 15th 2012).

[14] Ambler, M., Zocchi, A., "Development of the Aprilia DITECH 50 engine.," SAE Technical Paper 2001-01-1781, 2001, doi:10.4271/2001-01-1781.

[15] Blair, G. P., "Design and Simulation of Two-Stroke Engines," Society of Automotive Engineers, Warrendale, 1999.

[16] Heywood, J. B., Sher, E., "The Two-Stroke Cycle Engine: Its Development, Operation, and Design," Society of Automotive Engineers, Cambridge, 1999.

[17] Ghojel, J. I., "Review of the development and applications of the Wiebe function: A tribute to the contribution of Ivan Wiebe to engine research," International Journal of Engine Research, **11**(4):297-312, August 2010.

[18] Heywood, J. B., "Internal Combustion Engine Fundamentals," McGraw-Hill, New York, p. 840, 1988.

[19] White, C.M.; Steeper, R.R.; Lutz, A.E., "The Hydrogen-Fueled Internal Combustion Engine: A Technical Review," Int J Hydrogen Energy **31**(10):1292–1305, August 2006, doi:10.1016/j.ijhydene.2005.12.001.

[20] Murillo, S., Míguez, J.L., Porteiro, J., et al, "Viability of LPG Use in Low-Power Outboard Engines for Reduction in Consumption and Pollutant Emissions," Int. J. Energy. Res., **27**(5):467-480, April 2003, doi:10.1002/er.889.
[21] Yilmaz, M. et al., Heat transfer and friction characteristics in decaying swirl flow generated by different radial guide vane swirl generators, Energy Conversion and Management **44** (2003) pp. 283–300.
[22] Zhang, D., Turbulent Swirling Combustion of Premixed Natural Gas and Air, PhD dissertation, University of British Columbus, 1995.
[23] Scarcelli, R., Lean-Burn Operation for Natural Gas/Air Mixtures: The Dual-Fuel Engines, PhD Dissertation, Università degli Studi di Roma Tor Vergata, 2008.
[24] Hill, P.G., Zhang, D., The effects of swirl and tumble on combustion in spark-ignition engines, Progress in Energy and Combustion Science **20**(5), 1994, pp. 373-429, doi:10.1016/0360-1285(94)90010-8.
[25] Heywood, J. B., "Internal Combustion Engine Fundamentals," 1988, New York, McGraw-Hill.
[26] Oh, D., "Development and Transient Performance Simulation of a 2-Stage Turbocharged DI Otto Engine Concept," Master thesis, RWTH Aachen University, 2009.
[27] Ricardo, H.R., The High- Speed Internal Combustion Engine, 2nd Edition, Blackie & Son Limited, London, Chapter IV, pp. 95-128, 1931
[28] Heywood, J. B., "Internal Combustion Engine Fundamentals,", McGraw-Hill, New York, pp. 2-3, 1988
[29] "Key Events in the History of Air Quality in California," http://www.arb.ca.gov/html/brochure/history.htm, accessed on April 4, 2016.
[30] "Brief History," http://www.opec.org/opec_web/en/about_us/24.htm, accessed on April 4, 2016.
[31] Date, T., Yagi, S., Ishizuya, A., and Fujii, I., "Research and Development of the Honda CVCC Engine," SAE Technical Paper 740605, 1974, doi:10.4271/740605.
[32] Arcoumanis, C., Hull, D., and Whitelaw, J., "An Approach to Charge Stratification in Lean-Burn, Spark- Ignition Engines," SAE Technical Paper 941878, 1994, doi:10.4271/941878.
[33] Brandstetter, W., "The Volkswagen Lean Burn PC-Engine Concept," SAE Technical Paper 800456, 1980, doi:10.4271/800456.
[34] Weaving, J.H. (ed), "Internal Combustion Engineering: Science and Technology," Elsevier Applied Science, London, pp. 137-171, 1990.
[35] Hofbauer, P., Sator, K., "Advanced Automotive Power Systems - Part 2: A Diesel for a Subcompact Car," SAE Technical Paper 770113, 1977, doi:10.4271/770113.
[36] Georgi, B., Hunkert, S., Liang, J., and Willmann, M., "Realizing Future Trends in Diesel Engine Development," SAE Technical Paper 972686, 1997, doi:10.4271/972686.
[37] Escudier, M., "Confined Vortices in Flow Machinery," Annu. Rev. Fluid Mech., 1987(19):27-52).
[38] Munson, S. M., Sauer, J. A., Rocholl, J. D., et al., "Development of a Low-Cost Vortex-Cooled Thrust Chamber Using Hybrid Fabrication Techniques," 47th AIAA/ASME/SAE/ASEE Joint Propulsion Conference & Exhibit, 31 July - 03 August 2011, San Diego, California, AIAA 2011-5835.
[39] Lewellen, W. S., "A Review of Confined Vortex Flows," NASA Contractor Report 1772, National Aeronautics and Space Administration, Washington, D. C., July 1971.

[40] Kerrebrock, J. L., Meghreblian, R. V., "Vortex Containment for the Gaseous-Fission Rocket," Journal of the Aerospace Sciences, **28**(9), September 1961.
[41] Eichlseder, H., Wallner, T., Freymann, R., Ringler, J., "The Potential of Hydrogen Internal Combustion Engines in a Future Mobility Scenario," SAE Technical Paper 2003-01-2267, 2003, doi:10.4271/2003-01-2267.
[42] Wimmer, A., Wallner, T., Ringler, J., Gerbig, F., "H2-Direct Injection – A Highly Promising Combustion Concept," SAE Technical Paper 2005-01-0108, 2005, doi:10.4271/2005-01-0108.
[43] Shudo, T., "Improving thermal efficiency by reducing cooling losses in hydrogen combustion engines," Int J Hydrogen Energy **32**(17):4285–4293, 2007, doi:10.1016/j.ijhydene.2007.06.002.
[44] Eichlseder, H., Grabner, P., Gerbig, F., Heller, K., "Advanced Combustion Concepts and Development Methods for Hydrogen IC Engines , FISITA 2008 World Automotive Congress, F2008-06-103, 2008, Munich, Germany.
[45] Michl, J., Schenk, M., Rottengruber, H., Huhn, W., "Thermal Boundary Conditions in a Stoichiometric Operating Hydrogen Engine," FISITA 2008 World Automotive Congress, F2008-06-110, 2008, Munich, Germany.
[46] Shudo, T., Nabetani, S., Nakajima, Y., "Analysis of the degree of constant volume and cooling loss in a spark ignition engine fuelled with hydrogen," International Journal of Engine Research, **2**(1):81-92, February 2001, doi:10.1243/1468087011545361.
[47] Shudo T., Oba S., "Mixture distribution measurements using laser induced breakdown spectroscopy in hydrogen direct injection stratified charge," Int J Hydrogen Energy **34**(5):2488-2493, March 2009, doi:10.1016/j.ijhydene.2009.01.012.
[48] Grabner, P., Eichlseder, H., Gerbig, F., Gerke, U., "Optimisation of a Hydrogen Internal Combustion Engine With Inner Mixture Formation," 1st International Symposium on Hydrogen Internal Combustion Engines, September 28-29, 2006, Graz, Austria.
[49] Oppenheim, A., "Prospects for Combustion in Piston Engines," SAE Technical Paper 2002-01-0999, 2002, doi:10.4271/2002-01-0999.
[50] Heitland, H., Rinne, G., Wislocki, K., "Can the Best Fuel Economy of Today's Engines Still Be Improved?" SAE Technical Paper 981912, 1998, doi:10.4271/981912.
[51] Norton, D. G., Vlachos, D. G., "Combustion characteristics and flame stability at the microscale: a CFD study of premixed methane/air mixtures," Chemical Engineering Science **58**(21):4871–4882, November 2003, doi:10.1016/j.ces.2002.12.005.
[52] Toulson, E., Schock, H., Attard, W., "A Review of Pre-Chamber Initiated Jet Ignition Combustion Systems," SAE Technical Paper 2010-01-2263, 2010, doi:10.4271/2010-01-2263.
[53] Brandstetter, W., Decker, G., Reichel, K., "The Water-Cooled Volkswagen PCI-Stratified Charge Engine," SAE Technical Paper 750869, 1975, doi:10.4271/750869.
[54] Brandstetter, W., „Über neuere Arbeiten am VW-PCI- und VW-PCV-Schichtladeverfahren," MTZ **38**(7/8):327-330, 1977.
[55] Brandstetter, W., "The Volkswagen Lean Burn PC-Engine Concept," SAE Technical Paper 800456, 1980, doi:10.4271/800456.
[56] Peterson, R. C., Alkidas, A. C., "A Visual Study of Divided-Chamber Diesel Combustion Using a Rapid Compression Machine," Combustion and Flame **53**(1–3):65-81, November 1983, doi:10.1016/0010-2180(83)90007-X.

[57] Arcoumanis, C., Hull, D., Whitelaw, J., “An Approach to Charge Stratification in Lean-Burn, Spark- Ignition Engines,” SAE Technical Paper 941878, 1994, doi:10.4271/941878.

[58] Socolofsky S. A., Jirka, G. H., Mixing in Rivers: Turbulent Diffusion and Dispersion, Book chapter from “Environmental Fluid Mechanics Part I: Mass Transfer and Diffusion”, Lecture script from Institut für Hydromechanik, Universität Karlsruhe, 2002.

[59] Petersen, B., Ghandhi, J., “High-resolution turbulent scalar field measurements in an optically accessible internal combustion engine,” Exp Fluids **51**:1695–1708, 2011, doi:10.1007/s00348-011-1178-z

[60] Golombok, M., Chewter, L., “Centrifugal Separation for Cleaning Well Gas Streams,” Ind. Eng. Chem. Res. **43**(7):1734–1739, 2004, doi:10.1021/ie030691i.

[61] Golombok, M., Morley, C., “Thermodynamic Factors Governing Centrifugal Separation of Natural Gas,” Chemical Engineering Research and Design **82**(4): 513–516, April 2004, doi:10.1205/026387604323050227.

[62] Golombok, M., Klaas, B., “Removal of CO2 from a Gas Stream Using an Experimental Centrifuge,” Ind. Eng. Chem. Res. **44**(13), pp. 4721–4725, 2005, doi: 10.1021/ie0501327.

[63] Lapsa, A. P., Dahm, W. J. A., “Hyperacceleration effects on turbulent combustion,” Proc. of the Combustion Institute **32**(2):1731–1738, 2009, doi:10.1016/j.proci.2008.05.038.

[64] Dumitrache, A., Frunzulica, F., Ionescu, T. C., “Mathematical Modelling and Numerical Investigations on the Coanda Effect,” In Nonlinearity, Bifurcation and Chaos - Theory and Applications, edited by Awrejcewicz, J., Hagedorn P., 2012, accessed 2015/02/01, http://cdn.intechopen.com/pdfs-wm/40430.pdf, doi: 10.5772/50403.

[65] Oh D., Plante J., “A Highly Efficient Small-Displacement Marine Two-Stroke H2-DI Engine With Low Emissions,” ASME. J. Eng. Gas Turbines Power **135**(8):082001-082001-10, 2013, doi:10.1115/1.4023752.

[66] Technical Data for Alicat M-Series Mass Flow Meters, http://www.alicat.com/documents/specifications/Alicat_Mass_Meter_Specs.pdf, accessed 2016/02/24.

[67] Namazian, M., Hansen, S., Lyford-Pike, E., Sanchez-Barsse, J. et al., "Schlieren Visualization of the Flow and Density Fields in the Cylinder of a Spark-Ignition Engine," SAE Technical Paper 800044, 1980, doi:10.4271/800044.

[68] Salazar, V., Kaiser, S., “Influence of the Flow Field on Flame Propagation in a Hydrogen-Fueled Internal Combustion Engine,” SAE Int. J. Engines, **4**(2):2376-2394, 2011, doi:10.4271/2011-24-0098.

[69] Weinrotter, M., Wintner, E., Iskra, K., Neger, T. et al., “Optical Diagnostics of Laser-Induced and Spark Plug-Assisted HCCI Combustion,” SAE Technical Paper 2005-01-0129, 2005, doi:10.4271/2005-01-0129.

[70] Baritaud, T., “High Speed Schlieren Visualization of Flame Initiation in a Lean Operating S.I. Engine,” SAE Technical Paper 872152, 1987, doi:10.4271/872152.

[71] Meier, F., Köhler, J., Stolz, W., Bloss, W. et al., “Cycle-Resolved Hydrogen Flame Speed Measurements with High Speed Schlieren Technique in a Hydrogen Direct Injection SI Engine,” SAE Technical Paper 942036, 1994, doi:10.4271/942036.

[72] Spicher, U., Kröger, H., Ganser, J., "Detection of Knocking Combustion Using Simultaneously High-Speed Schlieren Cinematography and Multi Optical Fiber Technique," SAE Technical Paper 912312, 1991, doi:10.4271/912312.

[73] http://www.photron.com/datasheet/FASTCAM_SA-X2.pdf, accessed 2016/02/24.

[74] Luminus PT121 Product Datasheet, http://www.mouser.com/pdfdocs/Luminus_PT121Specifcation_PDS1384_Rev08E3.pdf, accessed 2016/02/24.

[75] Kaiser, S. A., Salazar, V. M., Hoops, A. A., "Schlieren measurements in the round cylinder of an optically accessible internal combustion engine," Applied Optics, **52**(14): 3433-3443, 2013, doi:10.1364/AO.52.003433.

[76] Demuynck, J., Raes, N., Zuliani, M., et al. "Local heat flux measurements in a hydrogen and methane spark ignition engine with a thermopile sensor," Int J Hydrogen Energy **34**(24):9857-9868, December 2009, doi:10.1016/j.ijhydene.2009.10.035.

[77] Watts, P., Heywood, J. B., "Simulation Studies of the Effects of Turbocharging and Reduced Heat Transfer on Spark-Ignition Engine Operation," SAE Technical Paper 800289, 1980, doi:10.4271/800289.

[78] Kamo, R., Bryzik, W., Glance, P., "Adiabatic Engine Trends-Worldwide," SAE Technical Paper 870018, 1987, doi:10.4271/870018.

[79] Oppenheim, A., Kuhl, A., Packard, A., Hedrick, J. et al., "Model and Control of Heat Release in Engines," SAE Technical Paper 960601, 1996, doi:10.4271/960601.

[80] Borman, G., Nishiwaki, K., "Internal combustion engine heat transfer," Progress in Energy and Combustion Science **13**(1):1–46, 1987, doi:10.1016/0360-1285(87)90005-0.

[81] Pischinger, R., "The Importance of Heat Transfer to IC Engine Design and Operation," ICHMT Digital Library, 1988, pp. 445-466, doi: 10.1615/ICHMT.1988.20thAHT.400.

[82] Caton, J. A., "The thermodynamic characteristics of high efficiency, internal-combustion engines," Energy Conversion and Management **58**: 84–93, June 2012, doi:10.1016/j.enconman.2012.01.005.

[83] Fridriksson, H. S., Hajireza, S., Tunér, M., et al., "A CFD Investigation of Heat Transfer in a Diesel Fueled PPC Engine Applying Design of Experiments," Proc. ASME 2012 Internal Combustion Engine Division Fall Technical Conference, Vancouver, BC, Canada, September 23–26, 2012, ICEF2012-92059, pp. 747-756, doi:10.1115/ICEF2012-92059.

[84] Hendricks, T. L., Splitter, D. A., Ghandhi, J. B., "Experimental investigation of piston heat transfer under conventional diesel and reactivity-controlled compression ignition combustion regimes," International Journal of Engine Research, September 2014, **15**(6):684-705, doi: 10.1177/1468087413512310.

[85] LeFeuvre, T., Myers, P., Uyehara, O., "Experimental Instantaneous Heat Fluxes in a Diesel Engine and Their Correlation," SAE Technical Paper 690464, 1969, doi:10.4271/690464.

[86] Alkidas A.C., Myers J.P., "Transient Heat-Flux Measurements in the Combustion Chamber of a Spark-Ignition Engine," ASME. J. Heat Transfer **104**(1):62-67, 1982, doi:10.1115/1.3245069.

[87] Drell I.L., Belles F.E., "Survey of hydrogen combustion properties," Technical Report 1383, National Advisory Committee on Aeronautics, 1958.

[88] Das, L.M., "Hydrogen-oxygen reaction mechanism and its implication to hydrogen engine combustion," Int. J. Hydrogen Energy, **21**(8):703-715, August 1996, doi:10.1016/0360-3199(95)00138-7.

[89] Demuynck, J., De Paepe, M., Verhaert I., et al., "Heat loss comparison between hydrogen, methane, gasoline and methanol in a spark-ignition internal combustion engine," Energy Procedia **29**:138–146, 2012, doi:10.1016/j.egypro.2012.09.018.

[90] Blanc, M. V., Guest, P. G., von Elbe, G., et al., "Ignition of Explosive Gas Mixtures by Electric Sparks. I. Minimum Ignition Energies and Quenching Distances of Mixtures of Methane, Oxygen, and Inert Gases," The Journal of Chemical Physics **15**(798), 1947, doi: 10.1063/1.1746337.

[91] Harris, M. E., Grumer, J., von Elbe, G., et al., "Burning velocities, quenching, and stability data on nonturbulent flames of methane and propane with oxygen and nitrogen: Application of theory of ignition, quenching, and stabilization to flames of propane and air," Third Symposium on Combustion and Flame and Explosion Phenomena, **3**(1):80–89, 1948, doi:10.1016/S1062-2896(49)80010-9.

[92] Friedman, R., Johnston, W. C., "The Wall-Quenching of Laminar Propane Flames as a Function of Pressure, Temperature, and Air-Fuel Ratio," J. Appl. Phys. **21**:791-795, 1950, doi:10.1063/1.1699760.

[93] Friedman, R., Johnston, W. C., "Pressure Dependence of Quenching Distance of Normal Heptane, Iso-Octane, Benzene, and Ethyl Ether Flames," J. Chem. Phys. **20**:919, 1952, doi:10.1063/1.1700600.

[94] Heindl, R., Eichlseder, H., Spuller, C., Gerbig, F. et al., "New and Innovative Combustion Systems for the H2-ICE: Compression Ignition and Combined Processes," SAE Int. J. Engines **2**(1):1231-1250, 2009, doi:10.4271/2009-01-1421.

[95] Scarcelli, R., Wallner, T., Matthias, N., Salazar, V. et al., "Numerical and Optical Evolution of Gaseous Jets in Direct Injection Hydrogen Engines," SAE Technical Paper 2011-01-0675, 2011, doi:10.4271/2011-01-0675.

[96] Scarcelli, R., Wallner, T., Matthias, N., Salazar, V. et al., "Mixture Formation in Direct Injection Hydrogen Engines: CFD and Optical Analysis of Single- and Multi-Hole Nozzles," SAE Int. J. Engines **4**(2):2361-2375, 2011, doi:10.4271/2011-24-0096.

[97] Lin, W., "Large-Eddy Simulation of Premixed Turbulent Combustion Using Flame Surface Density Approach," PhD dissertation, University of Toronto, 2010.

[98] Sukumaran, S., Kong, S. C., "Numerical study on mixture formation characteristics in a direct-injection hydrogen engine," Int J Hydrogen Energy **35**(15):7991–8007, 2010, doi:10.1016/j.ijhydene.2010.05.090.

[99] Le Moine J., Senecal P. K., Kaiser S.A., et al., "A Computational Study of the Mixture Preparation in a Direct–Injection Hydrogen Engine," ASME. J. Eng. Gas Turbines Power **137**(11):111508-111508-5, 2015, doi:10.1115/1.4030397.

[100] "Propagation of the Flame Front," accessed March 29, 2016, https://www.sharcnet.ca/Software/Ansys/16.0/en-us/help/flu_th/flu_th_sec_zimont_flame.html

[101] Peters, N., "Turbulent Combustion," Cambridge University Press, Cambridge, England. 2000.

[102] "Enhanced Wall Treatment ε-Equation (EWT-ε)," accessed August 4, 2016, https://www.sharcnet.ca/Software/Ansys/16.2.3/en-us/help/flu_th/flu_th_sec_ewt_eps.html

[103] Hargather, M. J., Settles, G. S., "A comparison of three quantitative schlieren techniques," Optics and Lasers in Engineering **50**(1):8–17, January 2012, doi:10.1016/j.optlaseng.2011.05.012.

[104] Kumar, R., Chhachhia, D. P., Aggarwal A. K., "Folding mirror schlieren diffraction interferometer," Applied Optics, **45**(26):6708-6711, 2006, doi:10.1364/AO.45.006708.

[105] Dalziel, S. B., Hughes, G. O., Sutherland, B. R., “Whole-field density measurements by ‘synthetic schlieren’,” Experiments in Fluids **28**(4):322-335, 2000, doi:10.1007/s003480050391.

[106] Hargather, M. J., Settles, G. S., "Recent developments in schlieren and shadowgraphy," 27th AIAA Aerodynamic Measurement Technology and Ground Testing Conference, 28 June - 1 July 2010, Chicago, Illinois, AIAA 2010-4206.

[107] O'Connor, J.,Musculus, M., “Optical Investigation of the Reduction of Unburned Hydrocarbons Using Close-Coupled Post Injections at LTC Conditions in a Heavy-Duty Diesel Engine,” SAE Int. J. Engines **6**(1): 379-399, May 2013, doi:10.4271/2013-01-0910.

[108] Soid, S.N., Zainal, Z.A., “Spray and combustion characterization for internal combustion engines using optical measuring techniques – A review,” Energy, **36**(2):724-741, February 2011, doi:10.1016/j.energy.2010.11.022.

[109] Bertsch, M., Schreer, K., Disch, C., Beck, K. W., et al., “Investigation of the Flow Velocity in the Spark Plug Gap of a Two-Stroke Gasoline Engine using Laser-Doppler-Anemometry,” SAE Int. J. Engines **5**(1):34-41, January 2012.

[110] Hamzehloo, A., Aleiferis, P., “Computational Study of Hydrogen Direct Injection for Internal Combustion Engines,” SAE Technical Paper 2013-01-2524, 2013, doi:10.4271/2013-01-2524.

[111] Wong, Y.K., Karim, G. A., “A kinetic examination of the effects of the presence of some gaseous fuels and preignition reaction products with hydrogen in engines,” Int J Hydrogen Energy, **24**(5):473–478, 1999, doi:10.1016/S0360-3199(98)00097-4.

[112] Kong, S. C., Reitz, R. D., “Numerical study of premixed HCCI engine combustion and its sensitivity to computational mesh and model uncertainties,” Combustion Theory and Modelling, **7**(2):417-433, 2003, doi:10.1088/1364-7830/7/2/312.

[113] Hellström, E., Stefanopoulou, A., Vavra, J., Babajimopoulos, A., et al., “Understanding the Dynamic Evolution of Cyclic Variability at the Operating Limits of HCCI Engines with Negative Valve Overlap,” SAE Int. J. Engines **5**(3):995-1008, 2012, doi:10.4271/2012-01-1106.

[114] Scarcelli, R., Sevik, J., Wallner, T., Richards, K., et al., “Capturing Cyclic Variability in EGR Dilute SI Combustion Using Multi-Cycle RANS,” ASME J. Eng. Gas Turbines Power, GTP-16-1079 (accepted manuscript), 2016, doi:10.1115/1.4033184.